



UNIVERSITY OF
LIVERPOOL

**A Study of Homogeneous Hydrogenation of CO₂ to
Formic Acid and Formic Acid Dehydrogenation**

Thesis submitted in accordance with the requirements of the
University of Liverpool for the degree of Doctor in Philosophy

By

Zhijun Wang

May 2016

ACKNOWLEDGEMENTS

Foremost, I would like to express my sincere gratitude to my advisor Prof. Jianliang Xiao for the continuous support of my Ph. D study and research, for his patience, motivation, enthusiasm, and immense knowledge. His guidance helped me in all the time of research and writing of this thesis. I could not have imagined having a better advisor and mentor for my Ph. D study.

My sincere thanks also go to my co-advisor Prof. Can Li from Dalian Institute of Chemical Physics (DICP), who has enlightened me the first glance of research. I am grateful for his support, encouragement, insightful discussions and advice. I truly feel privileged to be a member of his group.

Besides my advisors, I would like to particularly thank Dr. Shengmei Lu from DICP for her selfless help and for the stimulating discussions. In addition, her beautiful personality has influenced me in many ways. I would like to show my gratitude to Dr. Xin Zhou who worked in DICP previously for her kind help on computational studies. I also thank Dr. Chao Wang from Shaanxi Normal University for his help on thesis preparation.

It is hard to thank everyone who helped me and describe all the moments that touched me deeply in such a limited page, but still I would like to thank my fellow labmates in Xiao group: Dr. Xiaofeng Wu, Dr. Jianjun Wu, Dr. Jen Smith, Dr. Jonathan Barnard, Dr. Weijun Tang, Dr. Ho Yin Li, Dr. Angela Gonzalez de Castro, Dr. Dinesh Talwar, Edward Booth, Thomas White and Ziyu Wang, for the experimental help in lab, for the helpful discussions and suggestions, for the time we worked together and for all the fun we have had in the past years. Also I thank my labmates and friends in Can Li group: Dr. Jun Li, Dr. Yan Liu, Dr. Chunmei Ding, Dr. Rengui Li, Dr. Jijie Wang, Dr. Jingxiu Yang, Dr. Wengang Guo, Mingpan

Cheng, Bao Zhang, Ping Cheng, Bo Yuan, Ping Chen and Xianghui Liu.

Thanks to all the staff and technicians in the chemistry department of University of Liverpool and DICP, who have helped me a lot both at work and in personal life.

Last but not least, I would like to thank my family for their endless love and support, without which I wouldn't have achieved anything. I am grateful to have Xinchun Mao as my best friend and partner who helped me enormously.

ABSTRACT

The concentration of CO₂ in the atmosphere continues to increase due to an escalating rate of fossil fuel combustion, causing ever mounting concern about climate change. Meanwhile CO₂ is an abundant, safe and renewable C1 source. Thus transformation of CO₂ to value-added chemicals is of great significance and has been extensively investigated in the past decades. Homogeneous hydrogenation of CO₂ to formic acid (FA) especially has drawn significant attention, not only because FA itself has various applications including FA fuel cell, but also because FA can be a good hydrogen storage medium. The hydrogenation of CO₂ using such as solar-generated H₂ to produce FA, which is readily transportable, and the dehydrogenation of FA to release H₂ provide a decent strategy for hydrogen storage via CO₂ recycling.

However, it remains a challenge for the efficient hydrogenation of CO₂ to FA and FA dehydrogenation under mild conditions, especially for the aqueous phase reaction. Bearing these in mind, this work focus on the development of homogeneous catalysts for this reversible transformation and the main results are summarized as follows:

1. Cyclometallated [IrCp*(N[^]C)Cl] complexes (N[^]C = 2-aryl imidazoline ligand) have been synthesized as the catalyst for the homogeneous hydrogenation of CO₂ to formate, and satisfactory reactivity (TOF: 57330 h⁻¹, TON: 102200) was achieved at 80 °C in a mixture solution of MeOH/H₂O. Water has been found to play an important role in this reaction and the catalysts with hydrophilic ligands show much higher activity in the hydrogenation of CO₂ than those with hydrophobic ligands.

2. Considering the electronic property of the ligand and catalyst water solubility, water-soluble iridium complexes $[\text{IrCp}^*(N,N')\text{Cl}]\text{Cl}$ bearing conjugated N,N' -diimine ligands were subsequently synthesized and applied to CO_2 hydrogenation. This catalyst is capable of efficiently hydrogenating CO_2 to produce FA directly in water without any additives under mild reaction conditions. At $80\text{ }^\circ\text{C}$, the reaction turnover frequency (TOF) exceeds 13000 h^{-1} at 5.0 MPa of H_2/CO_2 (1:1).

3. FA dehydrogenation to H_2 and CO_2 is studied using the iridium catalyst $[\text{IrCp}^*(N,N')\text{Cl}]\text{Cl}$ in water without any additives, affording a TOF of 487500 h^{-1} at $90\text{ }^\circ\text{C}$ and a turnover number (TON) of 2400000 with *in situ* prepared catalyst at $80\text{ }^\circ\text{C}$, the highest values reported for FA dehydrogenation to date.

4. In addition, the FA dehydrogenation is shown to be catalyzed by $[\text{RhCp}^*\text{Cl}_2]_2$ in the FA/ NEt_3 azeotrope and is found to be accelerated by the addition of simple halide ions, especially I.

Key words: CO_2 hydrogenation, formic acid, formic acid dehydrogenation, iridium catalysts, homogeneous catalysis

TABLE OF CONTENTS

ACKNOWLEDGEMENTS	I
ABSTRACT.....	III
TABLE OF CONTENTS.....	V
ABBREVIATIONS	VIII
Chapter 1 Introduction - Recent Development in Homogeneous Hydrogenation of CO ₂ to Formic Acid and Formic Acid Dehydrogenation.....	1
1.1 Current Research Status of CO ₂ Chemistry	2
1.2 Recent Development on Homogeneous Hydrogenation of CO ₂ to Formic Acid/Formate	4
1.2.1 Hydrogenation of CO ₂ to formate in organic solvent	7
1.2.2 Hydrogenation of CO ₂ to FA/formate using scCO ₂ as solvent	9
1.2.3 Aqueous hydrogenation of CO ₂ to formate.....	10
1.2.4 Hydrogenation of CO ₂ to FA	16
1.3 Brief Introduction of Hydrogen Energy	17
1.4 Recent Development on Homogeneous FA Dehydrogenation	19
1.4.1 FA dehydrogenation in organic solution with additives	20
1.4.2 FA dehydrogenation in organic solution without additives	24
1.4.3 Aqueous dehydrogenation of FA with additives.....	25
1.4.4 Aqueous dehydrogenation of FA without additives.....	26
1.5 Conclusions and Objectives of This Thesis	27
1.5.1 Literature summary	27
1.5.2 Thesis objectives	28
Chapter 2 Hydrogenation of CO ₂ to Formate Catalyzed by Cyclometallated Ir-N [^] C Complexes.....	30
2.1 Introduction.....	31
2.2 Hydrogenation of CO ₂ to Formate with Ir-N [^] C Complex	32
2.2.1 Initial catalyst screening.....	32
2.2.2 Optimization of reaction conditions.....	34

2.2.3 Further development of catalyst.....	37
2.3 Summary	45
2.4 Experimental Section	46
2.4.1 General information	46
2.4.2 Synthesis and characterization of ligands and complexes	46
2.2.3 General procedure for CO ₂ hydrogenation	50
2.2.4 Contact angle measurement	51
Chapter 3 Hydrogenation of CO ₂ to FA Catalyzed by Ir- <i>N,N'</i> Diimine Catalysts	52
3.1 Introduction.....	53
3.2 Hydrogenation of CO ₂ to FA with Ir- <i>N,N'</i> Complex in Water	54
3.2.1 Ir-catalyzed CO ₂ hydrogenation in water without base	54
3.2.2 Reaction Mechanism Study	57
3.2.3 Thermodynamics of the base-free aqueous hydrogenation of CO ₂	64
3.3 Hydrogenation of CO ₂ to Formate with Ir- <i>N,N'</i> Complex.....	66
3.4 Summary	71
3.5 Experimental Section	71
3.5.1 General information	71
3.5.2 Synthesis and characterization of ligands and complexes	72
3.5.3 Procedure for catalytic hydrogenation of CO ₂ in water	76
3.5.4 UV-Vis absorption measurement.....	77
Chapter 4 Formic Acid Dehydrogenation Catalyzed by Ir- <i>N,N'</i> diimine Catalysts.....	78
4.1 Introduction.....	79
4.2 FA Dehydrogenation with Ir- <i>N,N'</i> Diimine Complex in Water	80
4.2.1 FA dehydrogenation reaction.....	80
4.2.2 Reaction mechanism study.....	82
4.2.3 Catalytic stability test.....	87
4.3 Summary	89
4.4 Experimental Section	89
4.4.1 General information	89

4.4.2 Procedure for catalytic dehydrogenation of FA	89
4.4.3 Calculation of TON and TOF	90
4.4 Gas composition analysis.....	91
Chapter 5 Iodide-Promoted Dehydrogenation of FA on a Rhodium Complex.....	94
5.1 Introduction.....	93
5.2 [RhCp*Cl ₂] ₂ Catalyzed FA Dehydrogenation	94
5.2.1 FA dehydrogenation in the presence of additives	94
5.2.2 Kinetics of FA dehydrogenation.....	95
5.2.3 The structure of active catalysts.....	100
5.2.4 Proposed reaction mechanism.....	104
5.2.5 Catalytic stability test.....	105
5.3 Summary	106
5.4 Experimental Section	107
5.4.1 General information	107
5.4.2 Synthesis and characterization of ligands and complexes	107
5.4.3 <i>In situ</i> ¹ H NMR analysis	107
Chapter 6 Conclusions and Perspectives	110
6.1 Conclusions.....	110
6.2 Deficiencies.....	111
6.3 Perspectives.....	111
Notes and References.....	113
Appendixes	130
Appendix A.....	130
Appendix B	131
Appendix C	136
Appendix D.....	140

ABBREVIATIONS

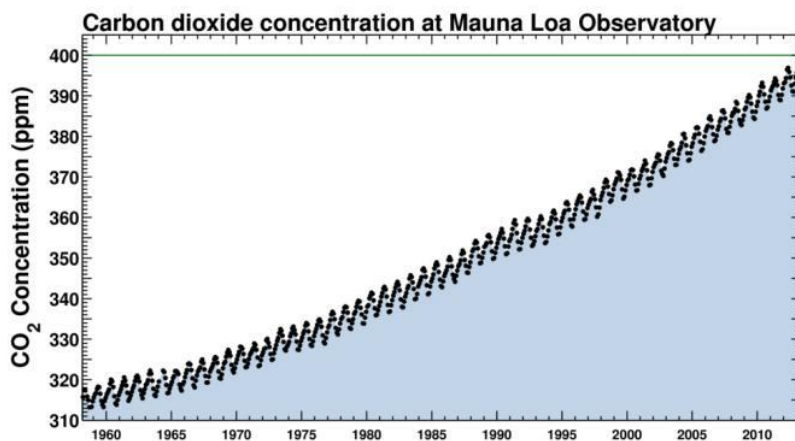
4DHBP	4,4'-dihydroxy-2,2'-bipyridine
Abs	absorbance
AcO	acetoxy
bpy	bipyridine
CCS	carbon capture and storage
Cp*	pentamethylcyclopentadienyl
cod	1,5-cyclooctadiene
DBU	1,8-diazabicycloundec-7-ene
DCM	dichloromethane
DMF	dimethylformamide
DMOA	dimethyloctylamine
dmpe	1,2-bis(dimethylphosphino)-ethane
DMSO	dimethyl sulfoxide
dppe	1,2-Bis(diphenylphosphino)ethane
EMIMCl	1-ethyl-3-methylimidazolium chloride
ESI	electrospray ionization
Et ₃ N	triethylamine
FA	formic acid
FID	flame ionization detector
F/T	Formic acid/triethylamine azeotrope
GC	gas chromatography
h	hour
HOMO	highest occupied molecular orbital
HRMS	high resolution mass spectroscopy

IL	ionic liquid
KIE	kinetic isotope effect
LA	Lewis acid
LUMO	lowest unoccupied molecular orbital
m	min
NBD	norbornadiene
NHC	N-heterocyclic carbenes
NMR	nuclear magnetic resonance
PEM	proton exchange membrane
PMe ₃	trimethylphosphine
PPh ₃	triphenylphosphine
ppm	parts per million
PTA	1,3,5-triaza-7-phosphaadamantane
RDS	rate determining step
s	second
SIE	solvent isotope effect
TCD	thermal Conductivity Detector
THBPM	4,4',6,6'-tetrahydroxy-2,2'-bipyrimidine
THF	tetrahydrofuran
TOF	Turnover frequency
TON	Turnover number
tppts	tris(3-sulfonatophenyl)phosphine
tppps	3-sulfonatophenyldiphenylphosphine
UV-Vis	ultraviolet–visible spectroscopy

Chapter 1 Introduction - Recent Development in Homogeneous Hydrogenation of CO₂ to Formic Acid and Formic Acid Dehydrogenation

1.1 Current Research Status of CO₂ Chemistry

The global atmospheric CO₂ level has been increasing continuously since the industrial revolution in the 19th century due to the excessive consumption of fossil fuel (coal, petroleum, natural gas), which has disequibrated the natural carbon cycle. The concentration of CO₂ in the atmosphere has reached unprecedented level of over 400 ppm recently (Scheme 1.1) from 280 ppm when it was before the year 1800,^[1] causing ever increasing concern about climate change as CO₂ is one of the main green-house gases.

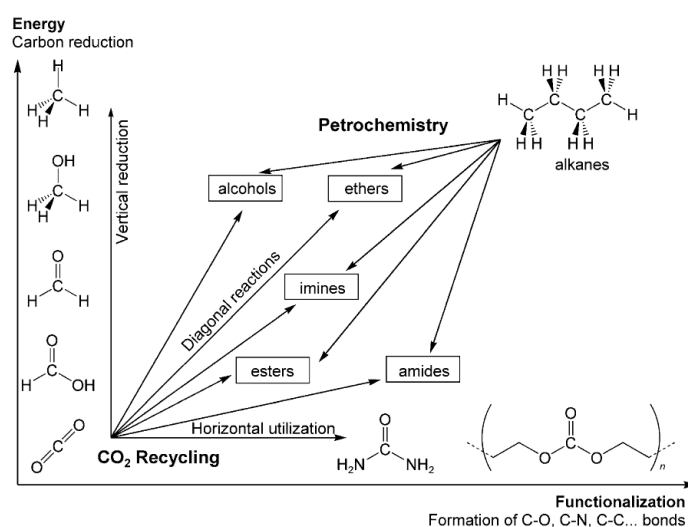


Scheme 1.1 Atmosphere CO₂ concentration during the past 50 years. Copyright: Scripps Institution of Oceanography, UC San Diego.

Currently, there are mainly two strategies to cut down CO₂ emissions: on the one hand, the CO₂ capture and storage (CCS) as well as the utilization of CO₂ as a renewable and environmentally friendly source of carbon can directly reduce the atmospheric CO₂ concentration;^[2-5] on the other hand, improving the energy utilization efficiency and developing sustainable clean energy such as hydrogen can ultimately reduce the CO₂ emissions.^[6-8] Both have become hot research topics and have been intensively studied. At present, the large-scale CO₂ capture technology is growing mature at the main energy and chemical industry points,^[9] and

the subsequent processing of CO₂ for utilization has become the key step. CO₂ can be utilized physically and chemically. For the physical utilization, besides the CO₂ storage process, it can be used as an oil displacement agent and a green extraction solvent at its supercritical phase, and in food industry and agriculture. However, these processes only recycle the CO₂ instead of diminishing it, especially considering the tremendous CO₂ emission per year, and thus can't fundamentally solve the CO₂ problems.

The chemical utilizations of CO₂ focus on the conversion of CO₂ to value-added chemicals and fuels that will not only reduce CO₂ emissions in areas where geologic storage may not be an optimal solution but also replace fossil source with CO₂ as an abundant, non-toxic, cheap, environmentally benign and renewable C1 resource, thus enabling CO₂ into the carbon cycle rather than an increasing waste.



Scheme 1.2 Transformations of utilizing CO₂ as alternatives to petrochemicals (Taken from ref. 10).

As shown in Scheme 1.2, the chemical utilization of CO₂ mainly includes two fashions distinguished by the oxidation state of carbon. Firstly, the CO₂ recycling approaches don't involve the change of the central carbon's oxidation state and no

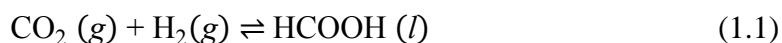
related energy storage process occurs. Examples are the synthesis of urea, carbonates, and poly/cyclic-carbonates from CO₂.^[4, 11-14] Secondly, the CO₂ reduction approaches refer to the stepwise hydrogenation of CO₂ to formic acid, formaldehyde, methanol, methane and their derivatives such as polyols, carboxylic acids, amides, esters and ethers.^[15, 16] During the reduction process, the oxidation state of central carbon decreases, realizing energy storage. The CO₂ reduction not only offers a convenient synthesis strategy utilizing CO₂ as building block but also has great significance from the viewpoint of sustainable fuel production; thus it has gained more and more attention during the past decades.

CO₂ reduction is generally difficult because CO₂ possesses the highest oxidation state of carbon, and is thermodynamically stable and kinetically inert. The standard formation heat of CO₂ is -394.38 kJ/mol, and the C=O bond energy is 749 kJ/mol. Therefore the reactions that generate reduced forms of CO₂ always require energy input and oxygen acceptors,^[16-22] such as H₂, silane, borane and carbanion, etc. Because H₂ can be easily obtained from water nowadays and the corresponding reduction process gives varieties of valuable products without generating much waste, the CO₂ hydrogenation technology has become one of the core technologies of CO₂ reduction and has been widely studied.

1.2 Recent Development on Homogeneous Hydrogenation of CO₂ to Formic Acid/Formate

Formic acid (FA) is the main product in homogeneous hydrogenation of CO₂. Only a few examples give CO, methanol and even methane as products; but the reactivity and selectivity are low.^[23-25] Hydrogenation of CO₂ to FA is endergonic in the gas phase (eqn. 1.1), but exergonic in the aqueous phase (eqn. 1.2); thus solvent affects this reaction greatly. For instance, this reaction has been investi-

gated in a wide variety of organic solvents, ionic liquids, water and supercritical CO₂. Moreover, most of the currently reported homogeneous catalytic systems need the addition of base to enhance the productivity because base can consume the generated FA and thus shift the equilibrium forward (eqn. 1.3).



$$\Delta G^\theta = 32.8 \text{ kJ/mol}$$



$$\Delta G^\theta = - 4 \text{ kJ/mol}$$



$$\Delta G^\theta = - 35.4 \text{ kJ/mol}$$

The synthesis of FA/formate by the hydrogenation of CO₂ was first discovered by Farlow and Adkins in 1935 using Raney nickel as the catalyst.^[26] The first homogeneously catalyzed example was reported by Inoue et al. in 1976.^[27] Extensive studies have been done afterwards to develop catalysts based on Rh, Ru, Pd, Ir, Fe, Co complexes and so on, for the hydrogenation of CO₂ to FA. The catalytic metal center, along with the coordinating ligands which could regulate the electronic and steric structure of the metal center, determines the reactivity and selectivity of the hydrogenation of CO₂. Ligands shown to be active towards the hydrogenation of CO₂ include phosphine ligands, pincer type ligands (PNP, PCP, PNN, etc.), N-heterocyclic carbene ligands and *N,N*-chelated ligands (pyridine and pyrimidine derivatives). The resulting state-of-the-art homogeneous catalyst systems developed during the past decades have been adequately summarized in the literature.^[17] Several reports have stated that catalysts with electron donating ligand are beneficial for the hydrogenation of CO₂.^[28-30] But beyond that, there's no rule to follow with respect to the influence of ligand structures on the

Table 1.1 Hydrogenation of CO₂ to formate/FA^a

Catalyst precursor	Solvent	Additive	P(H ₂ /CO ₂) /MPa	T /°C	Time /h	TON	TOF ^b /h ⁻¹	Ref
RuH ₂ (PPh ₃) ₄	C ₆ H ₆	NEt ₃ /H ₂ O	2.5/2.5	rt	20	87	4	27
Co(P1) ₂ H	THF	Verkade's base	0.05/0.05	21	<1	2000	3400	31
RuH(Cl)(CO)(P2)	DMF	DBU	3/1	120			1100000	32
RuH ₂ (PMe ₃) ₄	scCO ₂	NEt ₃	8.5/12	50		3700	1400	40
RuCl ₂ (PMe ₃) ₄	scCO ₂	NEt ₃	8.5/12	50		7200	1040	41
[Rh(cod)(methallyl)]/ PBu ₄ tppms	scCO ₂	EMIM HCO ₂	5/5	50	20	1970	>295	43
RhCl(tppts) ₃	H ₂ O	NHMe ₂	2/2	rt	12	3440	290	44
[RuCl ₂ (tppms) ₂] ₂	H ₂ O	NaHCO ₃	6/3.5	80	0.03		9600	46
RuCl ₂ (PTA) ₄	H ₂ O	NaHCO ₃	6/0	80			345	49
IrH ₃ (P3)	H ₂ O/THF	KOH	4/4	200	2	300000	150000	52
IrH ₃ (P3)	H ₂ O/THF	KOH	4/4	120	48	3500000	73000	52
IrH ₃ (P4)	H ₂ O	KOH	2.8/2.8	185	24	348000	14500	57
FeH ₂ (CO)(P2)	H ₂ O/THF	NaOH	0.67/0.33	80	5	790	156	58
IrI ₂ (AcO)(bis-NHC)	H ₂ O	KOH	3/3	200	75	190000	2500	59
[Cp*Ir(6DHBP)(OH ₂)] ²⁺	H ₂ O	KHCO ₃	0.5/0.5	120	8	12 500	(25200)	30
[Cp*Ir(6DHBP)(OH ₂)] ²⁺	H ₂ O	NaHCO ₃	0.05/0.05	25	33	330	(27)	30
[(Cp*IrCl) ₂ (THBPM)] ²⁺	H ₂ O	KHCO ₃	0.05/0.05	25	336	7200	(65)	67
[(Cp*IrCl) ₂ (THBPM)] ²⁺	H ₂ O	KHCO ₃	2/2	50	8	153000	(15700)	67
[Cp*Ir(N2)(OH ₂)] ²⁺	H ₂ O	KHCO ₃	0.05/0.05	25	24	190	65	69
[Cp*Ir(N2)(OH ₂)] ²⁺	H ₂ O	NaHCO ₃	0.5/0.5	50	24	28000	(3060)	69
[Rh(NBD)(PMe ₂ Ph) ₃] BF ₄	wet THF	-	4.6/4.6	40	72		2.7	72
[(Cp*Ir(4,4'-OMe-bpy) (OH ₂)] ²⁺	citrate buffer	-	5.5/2.5	40			27	74
RuCl ₂ (PTA) ₄	H ₂ O	-	15/5	60		74		75
RuCl ₂ (PTA) ₄	DMSO	-	15/5	40		749		75

^a: Insignificant digits are rounded; ^b: The data in the parentheses are initial TOFs.

hydrogenation activity, with each type of the above mentioned ligands showing good examples of hydrogenation at certain reaction conditions.

For industrial production, which is the long-term goal of CO₂ hydrogenation research, mild reaction conditions, simple catalytic systems and green solvents are always desired. Thus this section will focus on the recent development on homogeneous hydrogenation of CO₂ to FA/formate, highlighting the most efficient catalytic systems under typical reaction conditions (Table 1.1), e.g. non-aqueous/aqueous systems and basic/base-free reaction systems.

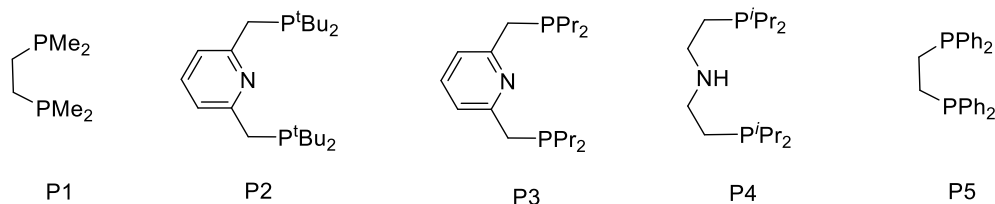
1.2.1 Hydrogenation of CO₂ to formate in organic solvent

In most of the currently reported homogeneous catalyst systems, base is needed to enhance the hydrogenation of CO₂ to formate because: i) base consumes the generated FA and thus thermodynamically shifts the equilibrium forward; ii) base has been found to accelerate the H₂ heterolysis during the catalytic cycle, therefore kinetically promoting the catalytic activity.

The landmark work by Inoue et al. in 1976 using triphenylphosphine (PPh₃) complexes of Ru, Rh, Ir, etc., created the new research field of homogeneous hydrogenation of CO₂ to FA.^[27] The reaction was carried out using a mixture of 2.5 MPa CO₂ and 2.5 MPa H₂ in benzene containing a catalyst, a small amount of water and a base (amine) at room temperature, and a turnover frequency (TOF) of 4 h⁻¹ and turnover number (TON) of 87 after 20 h were obtained.

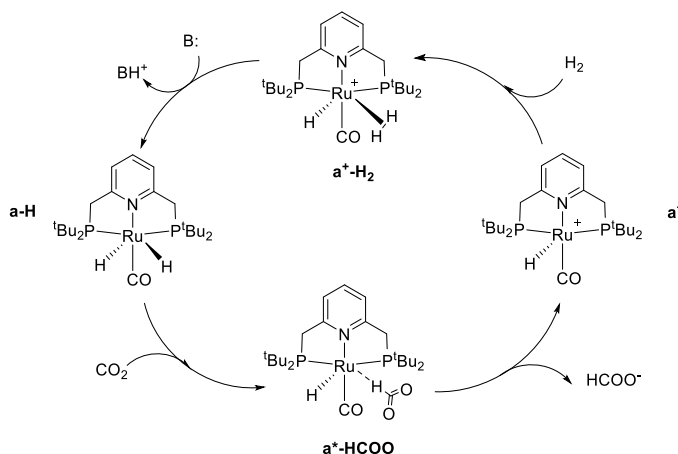
In 2013, Linehan et al. reported a Co complex, Co(dmpe)₂H (dmpe: 1,2-bis(dimethylphosphino)-ethane, P1, Scheme 1.3), for the hydrogenation of CO₂ in THF.^[31] In the presence of a very strong base, Verkade's base, at room temperature, the high TOFs of 3400 h⁻¹ and 74000 h⁻¹ were achieved under 0.1 MPa and 2.0 MPa of CO₂/H₂ (1:1), respectively. One drawback of this catalytic reaction is the requirement of Verkade's base (pK_a = 33.6) for regeneration of

$\text{Co}(\text{dmpe})_2\text{H}$ from $[\text{Co}(\text{dmpe})_2(\text{H})_2]^+$.



Scheme 1.3 Examples of the phosphine and pincer ligands used for the hydrogenation of CO_2

Very recently, Pidko et al. developed a highly stable temperature-switchable Ru-based system for the reversible hydrogenation of CO_2 that exhibits unprecedented rates for H_2 loading and release under mild conditions.^[32] Using DMF as a solvent, DBU as a base at $120\text{ }^\circ\text{C}$ and $4.0\text{ MPa H}_2/\text{CO}_2$ (3/1), the Ru-PNP complex $[\text{RuH}(\text{Cl})(\text{CO})(\text{P2})]$ (P2, Scheme 1.3) provided a TOF as high as 1100000 h^{-1} , which represents one of the highest values reported to date. Based on the kinetic studies (Scheme 1.4), CO_2 insertion (**a-H** to **a*-HCOO**) is postulated to be the rate determining step (RDS), which implies that the strength of the base promoter does not influence the reaction rate but it has a substantial effect on the reaction thermodynamics.



Scheme 1.4 Proposed catalytic cycle for the hydrogenation of CO_2 with Ru-PNP catalyst
(Based on ref. 32).

Moreover, other catalytic systems have also been reported for CO₂ hydrogenation to formate in organic solvents like DMSO, methanol, toluene, diglyme, and ethanol.^[33-39]

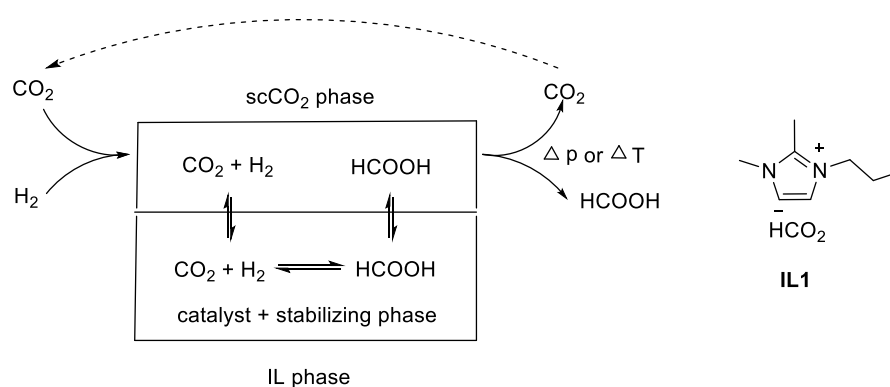
1.2.2 Hydrogenation of CO₂ to FA/formate using scCO₂ as solvent

Supercritical CO₂ (scCO₂) could act as both reactant and solvent, and leads to better mass transport and heat transfer properties as well as high solubility of H₂.

In the 1990's, Noyori and Jessop et al. carried out the hydrogenation of CO₂ in scCO₂ mainly using ruthenium phosphine complexes as catalyst, and the reaction needs additives such as amine and methanol.^[40] Later, Jessop et al. developed a remarkable catalytic system with [RuCl(OAc)(PMe₃)₄] (TOF up to 95000 h⁻¹) in scCO₂.^[41] The study also revealed an accelerating effect on the rate of the hydrogenation reaction by utilizing appropriate amine and alcohol adducts. While Lewis bases are required for formate generation by CO₂ hydrogenation, the role of alcohol is not well-known. Alcohols may not generate carbonic acids, but it could be involved as a proton donor and hydrogen-bond donor.^[41, 42]

In 2012, Leitner et al. proposed a new concept that applies continuous-flow hydrogenation of scCO₂ to produce pure formic acid in a single process unit as shown in Scheme 1.5.^[43] They first identified a suitable combination of catalysts and ionic liquid (IL) matrices in batch reactions using triethylamine (NEt₃) as base and IL as the stationary phase, and achieved high initial TOF using a ruthenium catalyst [Ru(cod)(methallyl)₂]/PBu₄TPPMS (cod = 1,5-cyclooctadiene, TPPMS = monosulfonated triphenylphosphine). When using **IL1** containing intrinsic anion basicity as the liquid phase, a TON of 1970 and a TOF of 295 h⁻¹ were obtained in a continuous-flow system. FA extraction from the nonvolatile amine-functionalized IL was found to be the limiting factor under the continuous-flow conditions. Anyhow, free FA can be collected via the integrated product

separation, which is eventually required for most applications.



Scheme 1.5 Process for the direct continuous-flow hydrogenation of CO_2 to free FA based on a two-phase system (Redraw from ref. 43).

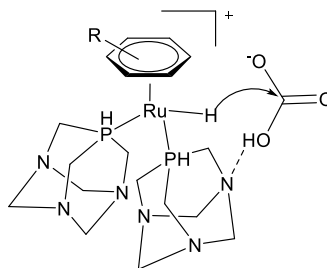
1.2.3 Aqueous hydrogenation of CO_2 to formate

As a green solvent, water has been explored as solvent for various catalytic reactions. In particular, aqueous phase hydrogenation of CO_2 has been explored extensively, and sometimes the limitation is the solubility of catalyst in water.

In 1993, Leitner et al. first reported water-soluble rhodium-phosphine complexes that can catalyze the hydrogenation of CO_2 to formate in water/amine mixtures. Among the catalysts examined, $\text{RhCl}(\text{tppts})_3$ (tppts: tris(3-sulfonatophenyl)phosphine) exhibited a high TON of 3440 at room temperature and 4.0 MPa of H_2/CO_2 .^[44] Later Joó et al. carried out the hydrogenation reaction in aqueous solutions with inorganic base, such as NaHCO_3 , using a series of rhodium and ruthenium complexes including $[\text{RuCl}_2(\text{tppms})_2]_2$ (tppms: 3-sulfonatophenyldiphenylphosphine), $[\text{RhCl}(\text{tppms})_3]$, and $[\text{RuCl}_2(\text{PTA})_4]$ (PTA: 1,3,5-triaza-7-phosphaadamantane).^[45-48]

Laurency et al. reported reaction mechanisms of iridium and ruthenium catalysts incorporating the water-soluble PTA ligand.^[49-51] They demonstrated the formation of $[\eta^6\text{-(C}_6\text{H}_6\text{)RuH(PTA)}_2]^+$ as the major hydride species, and proposed a

mechanism involving hydride transfer to bicarbonate as shown in Scheme 1.6. TOFs of 237 and 409 h⁻¹ were obtained at 70 and 80 °C, respectively, with 10.0 MPa of H₂ and 1 M HCO₃⁻.^[50]

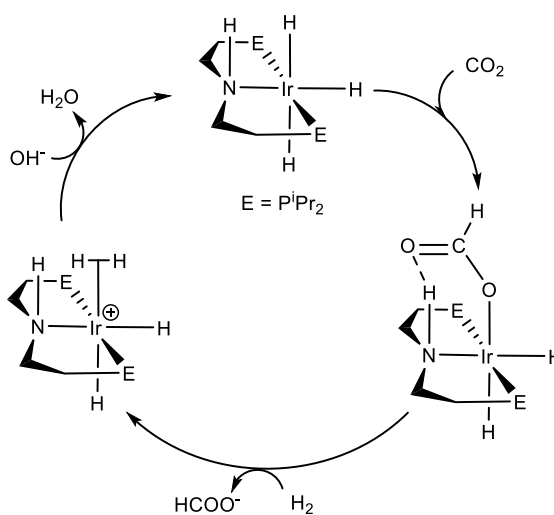


Scheme 1.6 Possible catalyst and substrate interaction during the hydrogenation of HCO₃⁻ in aqueous solution (Taken from ref. 50).

In 2009, Nozaki and co-workers synthesized a new Ir(III) trihydride complex bearing a PNP pincer ligand, [IrH₃(P3)] (P3, Scheme 1.3), for CO₂ hydrogenation in basic aqueous solution, and achieved the highest activity to that date at high temperature and high pressure.^[52, 53] The use of THF as a co-solvent was necessary due to the low water solubility of the complex. This catalyst exhibited a TOF of 150000 h⁻¹ at 200 °C and a TON of 3500000 at 120 °C over a period of 48 h under 8 MPa of H₂/CO₂ (1/1) in H₂O/THF (5/1). This excellent catalytic performance soon attracted considerable attention, and led to related research, including the previously mentioned Pidko's work. Pincer ligands are known as multi-dentate ligands that strongly bind to a metal center preventing dissociation of the ligand from the metal.^[54-56] The idea that an alkylphosphine-based pincer ligand would be an efficient electron donor may be beneficial for the hydrogenation of CO₂. Another inspiration comes to the importance of ligand tautomerization, e.g. the aromatization/dearomatization of the pincer ligand in Nozaki's work.

In 2011, Hazari and co-workers reported an air-stable, water-soluble catalyst, [IrH₃(P4)] (P4, Scheme 1.3), for the hydrogenation of CO₂.^[57] The iridium complex contains an NH group in the secondary coordination sphere. This hydrogen

bond donor, upon reaction with CO₂, facilitated the formation of the stable complex [Ir(OCHO)(H)₂(P4)] (Scheme 1.7), which was effective for CO₂ hydrogenation with a maximum TON of 348000 and TOF up to 18780 h⁻¹. Their DFT calculations indicated that CO₂ insertion was more thermodynamically favorable by means of stabilization of an N–H–O hydrogen bond through an outer-sphere interaction.

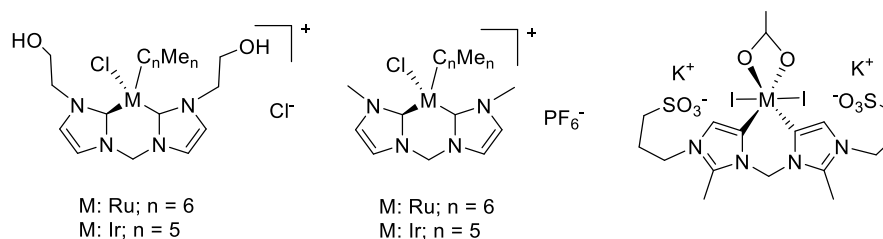


Scheme 1.7 Proposed mechanism for CO₂ hydrogenation using IrH₃(P4). (Taken from ref. 57)

With regard to using an earth-abundant metal instead of a noble transition metal with a pincer ligand, Milstein and coworkers focused attention on the active iron complex trans-[FeH₂(CO)(P2)] (P2, Scheme 1.3) which was capable of hydrogenating CO₂ with a TON of up to 790 and a TOF of up to 160 h⁻¹ at 80 °C under low pressure (0.6–1.0 MPa) in H₂O/THF (10/1).^[58]

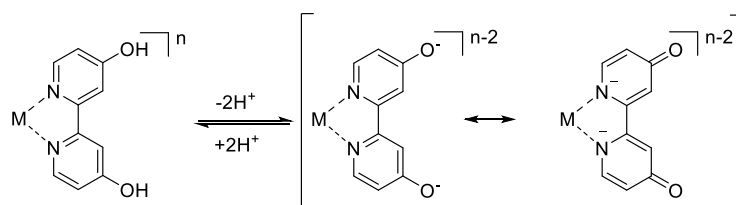
Peris et al. performed extensive studies of water-soluble Ru and Ir complexes using bis-NHC (N-heterocyclic carbenes) ligands (Scheme 1.8).^[59-61] A high TON of 190000 was achieved with complex [IrI₂(AcO)(bis-NHC)] (Scheme 1.8, right), at 200 °C under 6.0 MPa of H₂/CO₂ (1/1) in 75 h. Chelating-NHC ligands can impart a high thermal stability to the metal complexes and lead to high catalytic activity of the complex due to their electron donor character. Incorporating sul-

fonate or hydroxy substituents into the carbon side chains improves the water solubility of the complexes, and their catalytic performance for the aqueous hydrogenation of CO₂ was considerably improved.



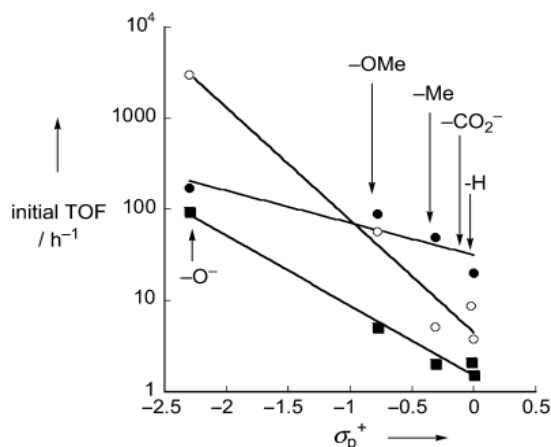
Scheme 1.8 Peris's NHC complexes for CO₂ hydrogenation in water^[59-61]

In the last decade, Himeda's group has published elegant work on aqueous hydrogenation of CO₂ using molecular complexes with aromatic *N,N'*-chelated ligands. Inspired by the idea of electron-donating ligand being beneficial for CO₂ hydrogenation, they designed and synthesized a series of half-sandwich complexes [(C_nMe_n)M(4,4-R₂-bpy)Cl]⁺ (n = 5, 6; M = Ir, Rh, Ru; R = OH, OMe, Me, H; bpy = bipyridine) by introducing different electron-donating groups to the bpy ligand of the prototype catalyst [(C_nMe_n)M(bpy)Cl]Cl, and applied them for the hydrogenation reaction.^[62-65] The proton-responsive hydroxy-substituted bpy ligands are deprotonated upon increasing the solution pH beyond pH 5 to 6.^[65] Deprotonation of the OH group ($\sigma^+ = -0.92$) generates a much stronger oxyanion electron donor ($\sigma^+ = -2.30$) because of the effect of its "keto" resonance structure (Scheme 1.9).



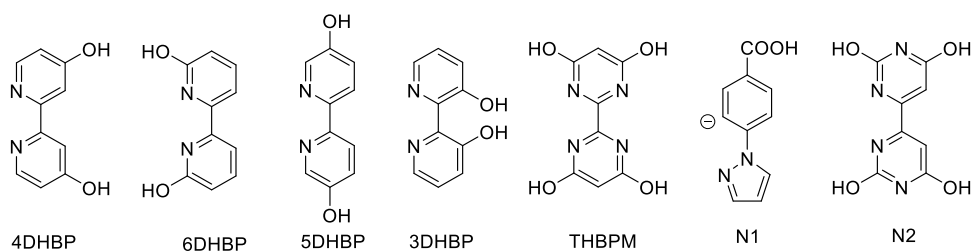
Scheme 1.9 Acid–base equilibrium between hydroxy form and oxyanion form, and the resonance structures of oxyanion form (Taken from ref. 63).

The Hammett plots show a good correlation between the initial TOFs and the σ_p^+ values of the substituents for the Ir, Rh, and Ru complexes (Scheme 1.10). The initial TOF of 5100 h^{-1} of the hydroxyl substituted complex $[\text{Cp}^*\text{Ir}(\text{4DHBP})\text{Cl}]\text{Cl}$ (4DHBP, Scheme 1.11) is over 1000 times higher than that of the unsubstituted analogue $[\text{Cp}^*\text{Ir}(\text{bpy})\text{Cl}]\text{Cl}$ (4.7 h^{-1}) under the same conditions ($80 \text{ }^\circ\text{C}$, 1.0 MPa , $\text{CO}_2/\text{H}_2 = 1$), further demonstrating the importance of electron-donating ligand. A high TOF of 42000 h^{-1} and TON of 190000 using $[\text{Cp}^*\text{Ir}(\text{4DHBP})\text{Cl}]\text{Cl}$ was obtained at $120 \text{ }^\circ\text{C}$ and 6.0 MPa . This catalyst even converts CO_2 to formate at ambient temperature ($25 \text{ }^\circ\text{C}$) and pressure (0.1 MPa) in 1 M NaHCO_3 aqueous solution with the TOF of 7 h^{-1} .



Scheme 1.10 Correlation between initial TOFs and σ_p^+ values of substituents (R) for CO_2 hydrogenation: M = Ir (\circ), Rh (\bullet), Ru (\blacksquare) (Taken from ref. 63).

The Fukuzumi group also reported a proton-responsive catalyst $[\text{Cp}^*\text{Ir}(\text{N1})(\text{OH}_2)]^+$ (N1, Scheme 1.11) that efficiently produces formate in 2.0 M KHCO_3 aqueous solution (pH 8.8) with the TOF of 6.8 h^{-1} and TON of 100 (20 h) at $30 \text{ }^\circ\text{C}$ and 0.1 MPa of H_2 .^[66] While most catalysts required some pressure of CO_2 in basic aqueous solution, this complex can hydrogenate HCO_3^- .

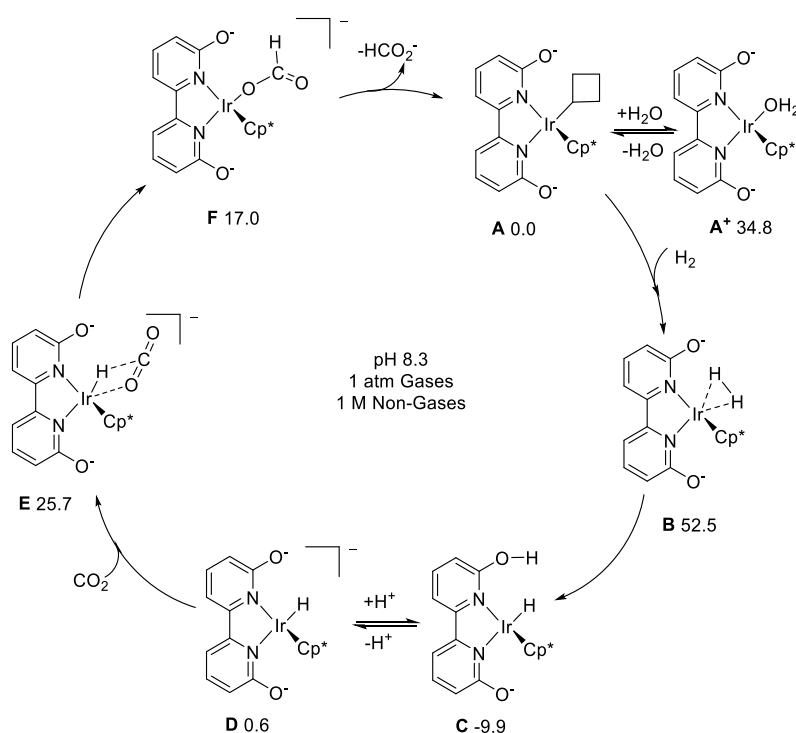


Scheme 1.11 Proton-responsive ligands used for CO₂ hydrogenation

In the context of constructing a second-coordination-sphere effective ligand, which is inspired by the hydrogen bond in hydrogenase, the collaboration between the Himeda and Fujita groups has led to a series of half-sandwich IrCp* complexes with ligands including nDHBP, THBPM, N2 (n = 3-6, Scheme 1.11) as catalysts for CO₂ hydrogenation and FA dehydrogenation under mild conditions in water. The bioinspired complexes [Cp*Ir(6DHBP)(OH₂)]²⁺, [Cp*Ir(N2)(OH₂)]²⁺, and [(Cp*IrCl)₂(THBPM)]²⁺ bearing pendant OH groups exhibit significantly improved catalytic activity in CO₂ hydrogenation (Table 1.1).^[30, 62, 65, 67-71]

During their investigation, they found that [Cp*Ir(6DHBP)(OH₂)]²⁺ (TOF: 8050 h⁻¹) showed much higher activity than [Cp*Ir(4DHBP)(OH₂)]²⁺ (TOF: 5100 h⁻¹) under the same conditions. Because the electron-donating ability of the hydroxyl group at the *para* and *ortho* positions should be similar, Himeda et al. proposed that the additional rate enhancement arises from the proximity of the hydroxyl groups in 6DHBP to the metal center and a possible cooperative effect in the activation of the substrate. Experimental and computational studies on the reaction mechanism indicate that the heterolysis of H₂ is the RDS and the adjacent oxyanions, formed from deprotonated hydroxyl groups under basic conditions, act as pendant bases and assist the heterolysis of H₂ (Scheme 1.12, **A** to **D**). The calculations also suggested that CO₂ insertion into the Ir-H bond is stabilized by a weak hydrogen bond between the hydrido ligand and deprotonated pendant base

(Scheme 1.12, E).



Scheme 1.12 Proposed mechanism for the CO_2 hydrogenation by $[\text{Cp}^*\text{Ir}(\text{6DHBP})(\text{OH}_2)]^{2+}$. Computed free energies at pH 8.3 are indicated in units of kJ mol^{-1} relative to 1M **A** in aqueous solution and 0.1 MPa H_2 and CO_2 gases. The calculated change in free energy around the cycle is $-42.0 \text{ kJ mol}^{-1}$ (Redraw from ref. 30).

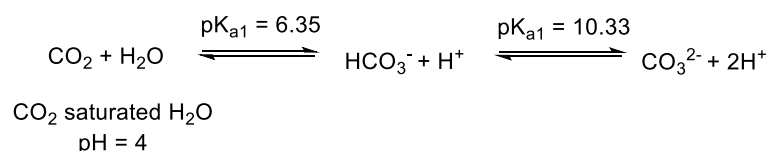
1.2.4 Hydrogenation of CO_2 to FA

Base is needed in most of the currently reported catalyst systems. On the contrary, without adding base, hydrogenating CO_2 will produce FA directly and few catalytic systems are found to be effective.

In 1992, Nicholas et al. reported that the complex $[\text{Rh}(\text{NBD})(\text{PMe}_2\text{Ph})_3]\text{BF}_4$ (NBD: norbornadiene) serves as a precatalyst for the hydrogenation of CO_2 to FA at moderate temperatures in THF solution, however with TON of only 10-60/day.^[72]

Ogo and Fukuzumi et al. proposed that between pH 6-9 the real substrate for the hydrogenation reaction was not CO_2 but bicarbonate ion (HCO_3^-), because

CO₂ dissolved in H₂O shows pH-dependent equilibrium between HCO₃⁻ (pK_{a1} = 6.35 at 25 °C) and CO₃²⁻ (pK_{a2} = 10.33) (Scheme 1.13). They performed the CO₂ hydrogenation in an acidic buffer (pH = 3) using the bipyridine-derived aqua iridium/ruthenium complexes as catalysts, and were able to achieve FA without adding base, with best TOF of 27 h⁻¹ at 40 °C and 8.0 MPa.^[73, 74]



Scheme 1.13 CO₂ hydrolysis in water^[73]

In 2014, Laurency et al. described the direct hydrogenation of CO₂ into FA using RuCl₂(PTA)₄ (PTA = 1,3,5-triaza-7-phosphaadamantane) as catalyst, in aqueous solution and in DMSO without any additives.^[75] In water, at 40 °C, 0.2 M FA can be obtained under 20 MPa; however, in DMSO the same catalyst affords 1.9 M FA. In both solvents the catalysts can be reused multiple times without a decrease in activity.

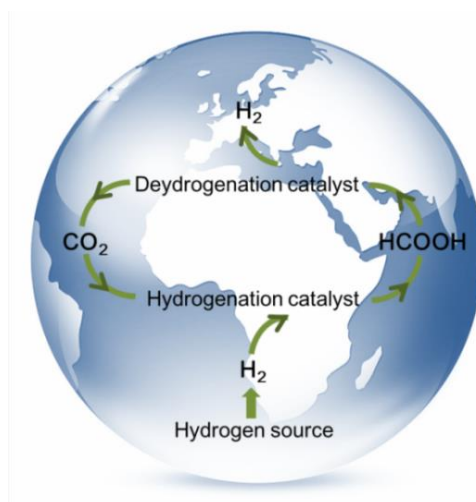
1.3 Brief Introduction of Hydrogen Energy

As mentioned in Section 1.1, a second strategy to reduce the atmospheric CO₂ content is using renewable energy source. Moreover, it is probably the final solution for both the energy crisis and environmental problem human beings are currently facing. Hydrogen is an ideal candidate as an energy carrier for mobile fuel cell applications, as it does not have any adverse effects on the environment, and is thus expected to be a promising energy vector for the near future. Nowadays, solar-generation of hydrogen is being intensely studied, e.g. photocatalysis hydrogen production^[76-79] and electrolysis of water.^[80-83]

Despite the potential for production of solar-generated hydrogen, the problems

of storage and transport is often considered to be a bottleneck for realization of the hydrogen economy. Among different hydrogen storage material systems, hydrogen adsorption on porous materials, including carbonaceous materials, zeolites, and metal-organic frameworks, yields low hydrogen uptake per unit of weight in ambient conditions.^[84-88] Meanwhile, metal hydrides systems suffer from high weight and cost concerns; moreover, high temperatures are often required to release hydrogen.^[89-93] Thus the search for safe and effective liquid-phase hydrogen storage material, e.g. ammonia borane, hydrous hydrazine, cycloalkanes, nitrogen-substituted heterocycles, methanol and formic acid, is receiving much attention.^[94]

Therefore, among the value-added products of CO₂ reduction, FA is of great significance for it can also be employed as hydrogen carrier (Scheme 1.14). Although theoretically FA is not a perfect hydrogen storage medium due to its relatively small hydrogen content (4.4 wt %), it is currently still one of the best among liquid storage and transport media for H₂ due to its non-toxicity and excellent stability.

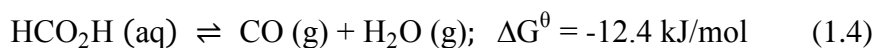


Scheme 1.14 Demonstration of hydrogen energy storage using FA

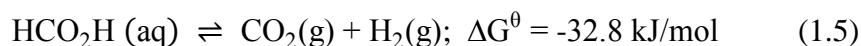
1.4 Recent Development on Homogeneous FA Dehydrogenation

In a typical hydrogen storage system using FA as the hydrogen storage material, the dehydrogenation of FA is indispensable as a companion reaction to CO₂ hydrogenation.^[95, 96] The decomposition of FA has been reported with both homogeneous^[67, 97-102] and heterogeneous catalysts.^[103, 104] The heterogeneous decomposition of FA usually requires high temperature, and thus loses reaction selectivity and causes CO contamination by FA dehydration (eqn. 1.4), which is poisonous to the catalyst in the proton exchange membrane (PEM). For practical utilization, the CO content is generally required to be less than 10 ppm. Compared with the heterogeneous dehydrogenation of FA, homogeneous catalysis of FA dehydrogenation has been less studied, although FA has been widely used as a hydrogen donor in transfer hydrogenation in the field of organic synthesis.^[105-107] After the pioneering work on FA dehydrogenation using homogeneous catalysts was reported by Coffey in 1967,^[108] which gave TOF and TON of 8900 h⁻¹ and 11000 for FA dehydrogenation in acetic acid using IrH₃(PPh₃)₃ as catalyst, not much research interest in this research topic was attracted.^[18] However in the past several years, the discovery of highly active homogeneous catalysts for FA dehydrogenation under mild conditions has stimulated renewed interest in FA as an H₂ carrier.

FA dehydration:



FA dehydrogenation:



In this section, recent progress on FA dehydrogenation will be introduced, highlighting the most efficient catalytic systems under various reaction conditions. Although the dehydrogenation of FA is thermodynamically favorable (eqn. 1.5), the addition of base or other additives is widely employed. Since FA dehydro-

generation is the reverse reaction of the hydrogenation of CO₂, a catalyst could be effective to both reactions and this section is relevant to section 1.2.

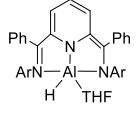
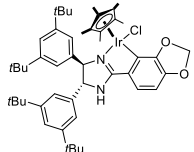
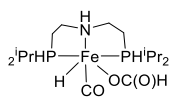
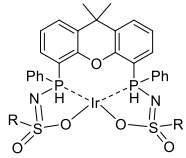
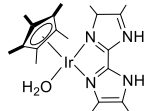
1.4.1 FA dehydrogenation in organic solution with additives

In 2008, Beller et al. reported the dehydrogenation of a FA/triethylamine (FA/Et₃N) azeotropic mixture, which evolved H₂ and CO₂ exclusively, using ruthenium-based catalysts with triphenylphosphine-type ligands.^[109] The high initial TOF of 2700 h⁻¹ (initial 20 min) and a TON of 890 (2 h) at 40 °C were obtained with the commercially available ruthenium complex [RuCl₂(PPh₃)₃]. The effects of different phosphine ligands, amines, and ruthenium complexes on catalytic activity and durability were then investigated,^[110] and a better combination of [RuCl₂(C₆H₆)₂] with a bidentate phosphine ligand P5 (Scheme 1.3) was identified. Because the presence of an amine is beneficial for hydrogen production, loss of the amine by volatilization led to a decrease in reaction rate. Thus using a less volatile amine, DMOA (dimethyloctylamine), resulted in the highest TON of 1000000 for 1080 h at 25 °C.^[111] During the course of the reaction, the CO concentration did not exceed 2 ppm.

Later, based on this catalytic system, Wills reported dehydrogenation of FA/amine mixtures with [RuCl₂(DMSO)₄].^[112, 113] Although CO (190–440 ppm) was detected by GC, a high TOF of 18 000 h⁻¹ was observed at 120 °C. They also reported long-term operation under continuous flow conditions. Gas production rates as high as 1.5 L min⁻¹ and total gas production of 462 L were obtained during 6 h.

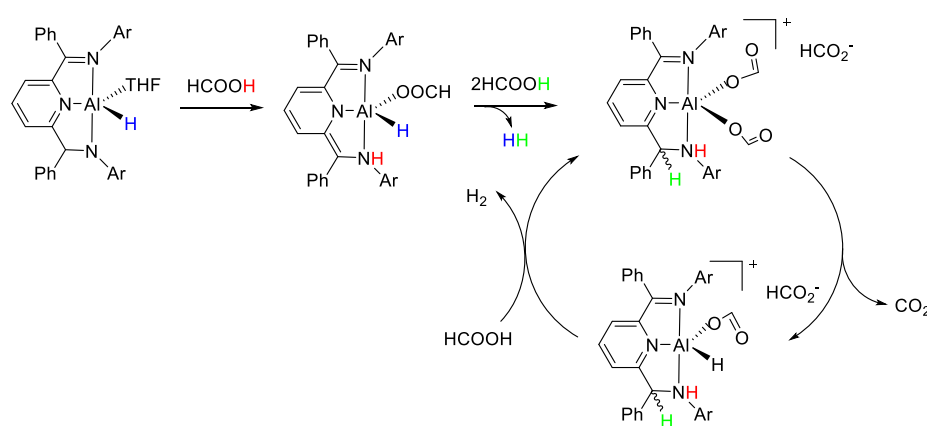
Milstein et al. applied iron-based PNP pincer complex [(P2)Fe(H)₂(CO)] (P2, Scheme 1.3) as catalysts for the dehydrogenation of FA.^[114] The reaction in dioxane in the presence of 50 mol % Et₃N at 40 °C led to a total TON of 100000 in 10 days. The poor activity in water is likely due to the low solubility of the catalyst.

Table 1.2 Dehydrogenation of formate/FA^a

Catalyst precursor	Solvent	Additive	T/ °C	Time	TON	Initial TOF/h ⁻¹	CO ^b / ppm	Ref
IrH ₃ (PPh ₃) ₃	AcOH		118		>11000	8900	n.d.	108
[RuCl ₂ (PPh ₃) ₃]	DMF	NEt ₃	40	2 h	890	2700	n.d.	109
[RuCl ₂ (C ₆ H ₆) ₂]/dppe		DMOA	25	45 d	1000000	1000	<2	111
RuCl ₂ (DMSO) ₄		NEt ₃	120	>2.5 h	25000	18000	200	112
[(P2)Fe(H) ₂ (CO)]	dioxane	NEt ₃	40	10 d	100000		650	114
	THF	NEt ₃	65	1 h	2200	5200	n.d.	115
		NEt ₃	40			147000	n.d.	116
[RuH(Cl)(CO)(P2)]	DMF	NEt ₃	90	2 h	326500	257000	n.d.	32
	DMF	NEt ₃	90	2 h	1060000	250000	n.d.	32
	dioxane	LiBF ₄	80	9.5 h	984000	197000	<0.5%	117
Fe(BF ₄) ₂ /PP ₃	Propylene carbonate		80	19 h	92400	9425	<20	118
	dioxane		85	<10 m	>250	3300	(<10)	120
[Ru(OH ₂) ₆](tos) ₂ /tppts	H ₂ O	HCO ₂ Na	120	90 h	>40000	460	n.d.	122
[Cp*Ir(OH ₂)(bpm)Ru(bpy) ₂](SO ₄)	H ₂ O	HCO ₂ Na	25	20 m	140	430	n.d.	125
[Cp*Ir(OH ₂)(N1)]	H ₂ O	HCO ₂ K	25	10 m		1880	n.d.	66
[(Cp*IrCl ₂)(THBPM)] ²⁺	H ₂ O	HCO ₂ Na	90	7 h	165000	228000	n.d.	67
[Cp*Ir(4DHBP)Cl] ⁺	H ₂ O		90	1.5 h	14000		n.d.	127
[(Cp*IrCl ₂)(THBPM)] ²⁺	H ₂ O		60	4 h	20000	12000	n.d.	67
	H ₂ O		80	0.5 h	34000	10000	n.d.	128

^a: Insignificant digits are rounded; ^b: n.d.: not detected (or not reported)

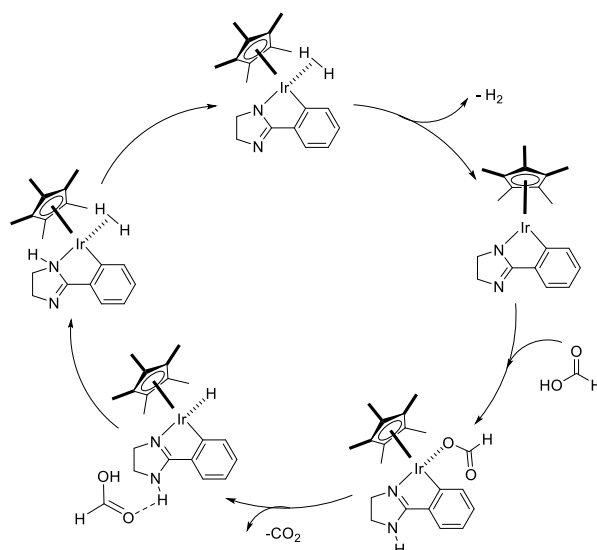
Berben et al. reported that aluminum pincer complexes with the-phenyl-substituted bis(imino)pyridine ($^{\text{Ph}}\text{I}_2\text{P}$) ligands showed the high initial TOF of 5200 h^{-1} in $\text{Et}_3\text{N}/\text{THF}$ at $65 \text{ }^\circ\text{C}$ without CO production.^[115] They characterized each of the elementary steps in the catalytic cycle. The complex $(^{\text{Ph}}\text{I}_2\text{P})\text{Al}(\text{THF})\text{H}$ reacted with 3 equiv. of HCO_2H to afford the doubly protonated species as a resting state. They proposed that the β -hydride elimination from the doubly protonated form affords an Al-H intermediate, which smoothly releases H_2 upon protonation (Scheme 1.15).



Scheme 1.15 Proposed mechanism for FA dehydrogenation by $(^{\text{Ph}}\text{I}_2\text{P})\text{Al}(\text{THF})\text{H}$ (based on ref. 115)

In 2013, our group (Xiao) reported that the $\text{N}^{\wedge}\text{C}$ cyclometallated iridium(III) complexes derived from 2-aryl imidazoline ligands were found to be excellent catalysts for the decomposition of FA together with NEt_3 to give H_2 and CO_2 under mild conditions with no CO formation.^[116] The fine tuning of catalyst structure led to a high TOF of 147000 h^{-1} at $40 \text{ }^\circ\text{C}$. The presence of the remote γ -NH unit in the ligand was shown to be essential for catalytic activity, without which no reaction occurs. Mechanistic studies suggest that the dehydrogenation is rate-limited by the step of hydride protonation, which is made feasible by the γ -NH unit on the imidazoline ring *via* an unusual form of long-range metal–ligand

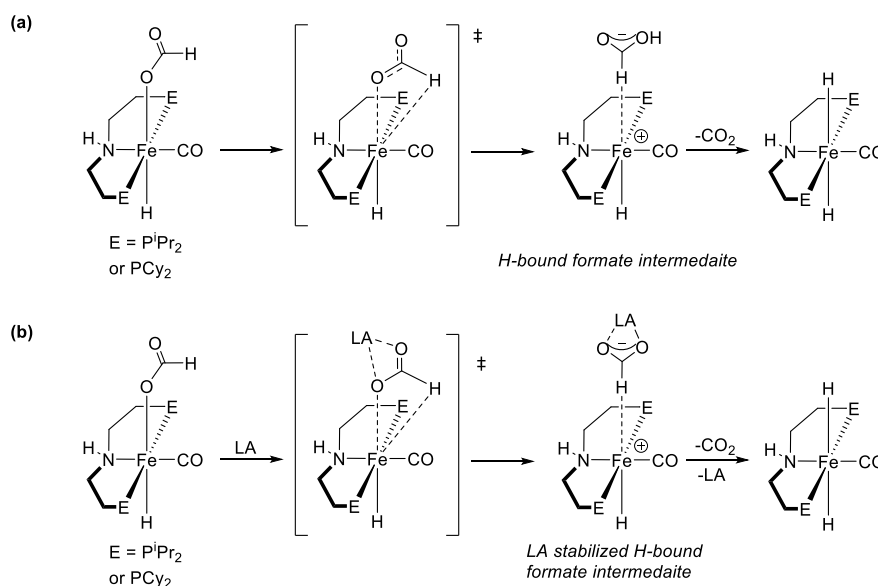
bifunctional catalysis involving FA-assisted proton hopping (Scheme 1.16).



Scheme 1.16 Proposed catalytic cycle for the dehydrogenation of HCO₂H (Taken from ref. 116).

As mentioned previously, the PNP-pincer complex [RuH(Cl)(CO)(P2)] reported by the Pidko group is highly active for CO₂ hydrogenation as well as the FA dehydrogenation in DMF/Et₃N. A high TOF of 257000 h⁻¹ and TON of 1063000 (for 5 h) were achieved with continuous addition of FA at 90 °C in separate experiments.^[32] The loss of volatile Et₃N at 90 °C is a major problem for this system.

Hazari and Schneider et al. reported Lewis acid (LA) assisted FA dehydrogenation catalyzed by iron-based PNP pincer complexes [(^RPN^HP)Fe(CO)H(Cl)] (^RPN^HP = HN[CH₂CH₂(PR₂)]₂; R = ⁱPr or Cy, Scheme 1.17) in dioxane without the need for an external base.^[117] The presence of LA cocatalysts provided the high TOF of 196700 h⁻¹ and TON of 1000000 in 9.5 h in dioxane at 80 °C. Unfortunately, CO (less than 0.5%) was detected in the produced gas mixture. Scheme 1.17 shows the LA assisted decarboxylation of a key iron formate intermediate.



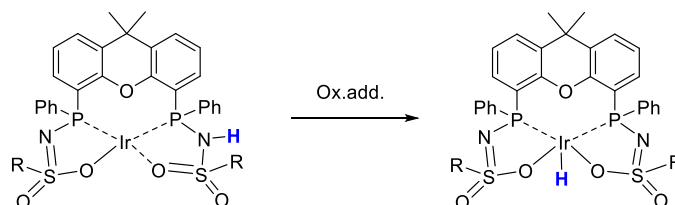
Scheme 1.17 Proposed pathway for decarboxylation in the absence (a) and presence (b) of a LA. (Redraw from ref. 117)

1.4.2 FA dehydrogenation in organic solution without additives

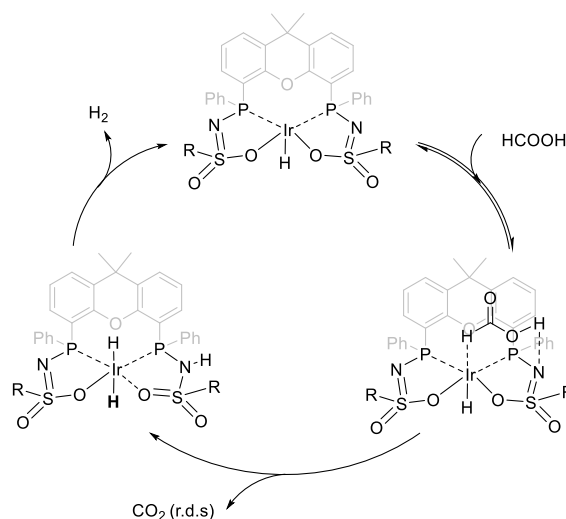
In 2011, Beller et al. reported an active iron catalyst system for the liberation of H₂ from FA. Applying 0.005 mole % of Fe(BF₄)₂ · 6H₂O and P(CH₂CH₂PPh₂)₃ to a solution of FA in propylene carbonate, with no further additives or base, affords TOF up to 9425 per hour and a TON of more than 92000 at 80 °C.^[118] Subsequently, they reported the results of a detailed investigation of the effect of various ligands, metal salts, solvent, and additives (e.g., chloride, fluoride, formate).^[119] The addition of water resulted in a decrease in catalytic activity.

Reek et al. reported the base-free FA dehydrogenation using an iridium complex bearing a phosphine-functionalized sulfonamide (bisMETAMORPhos) ligand, the anionic form of which can function as an internal base.^[120, 121] The system produced CO-free H₂ with the TOF of 3270 h⁻¹ in dioxane at 85 °C. The initial Ir(I) complex underwent a slow proton transfer from the neutral ligand arm to the metal, resulting in the formation of the active Ir(III)–H complex (Scheme

1.18). The bifunctional ligand allowed the direct hydride transfer from FA to the Ir center rather than the common β -hydride elimination. It also facilitated the release of hydrogen (Scheme 1.19).



Scheme 1.18 Formation of active species for complex Ir(bisMETAMORPhos) *via* internal proton transfer. (Redraw from ref. 120)



Scheme 1.19 Proposed mechanism for the cooperative dehydrogenation of FA. (Redraw from ref. 120)

1.4.3 Aqueous dehydrogenation of FA with additives

In 2008, Laurency et al. reported an aqueous system of $\text{HCO}_2\text{H}/\text{HCO}_2\text{Na}$ for FA dehydrogenation using a ruthenium catalyst with a water-soluble phosphine ligand, for example, tppts (tris(3-sulfonatophenyl)phosphine).^[122, 123] The TOF of 460 h^{-1} was observed at $120 \text{ }^\circ\text{C}$ without the use of an organic amine, but instead a small amount of HCO_2Na was used for the activation of the catalyst. Constant hydrogen generation with total TON > 40000 was achieved by continuous addition of FA.

The Fukuzumi group has made early effort on aqueous dehydrogenation of FA using water soluble iridium/ruthenium complexes. In 2008, they reported FA dehydrogenation with half-sandwich complexes bearing bidentate 2,2'-bipyridine derivatives.^[124] With the addition of HCO₂Na, the system gave a TON of 30 in 2 h at pH 3.8 and 20 °C. They also reported a water soluble heterodinuclear iridium–ruthenium complex [Cp*Ir(OH₂)(bpm)Ru(bpy)₂](SO₄)₂ (bpm: 2,2'-bipyrimidine), which gave an initial TOF of 426 h⁻¹ at room temperature in HCO₂H/HCO₂Na (pH 3.8).^[125] More recently, they demonstrated the dehydrogenation of FA using a *C,N*-cyclometalated iridium complex bearing a proton-responsive carboxylic acid (N1, Scheme 1.11), which was also applied for the hydrogenation of CO₂ as previously mentioned, and a maximum TOF of 1880 h⁻¹ was obtained at pH 2.8 and 25 °C.^[66]

The iridium complexes with aromatic *N,N'* ligands developed based on the collaboration between the Himeda and Fujita groups not only catalyze the hydrogenation of CO₂ as described in section 1.2, but also are effective catalysts for the dehydrogenation of FA.^[67, 126] [(Cp*IrCl)₂(THBPM)]²⁺ catalyses the release of H₂ and CO₂ (1:1) from aqueous HCO₂H/HCO₂Na mixture with a TOF of 228000 h⁻¹ at 90 °C and TON of 308000 at 80 °C, the highest TOF and TON reported by then.^[67]

1.4.4 Aqueous dehydrogenation of FA without additives

In 2009, Himeda demonstrated the efficient evolution of CO-free hydrogen by the decomposition of FA using an iridium catalyst with 4DHBP (Scheme 1.11) as a ligand in H₂O.^[127] A high catalytic activity (TOF: 14000 h⁻¹ at 90 °C) and an almost complete consumption of FA were obtained without any additives. Furthermore, it was found that hydrogen could be generated even at elevated pressures.

The iridium catalyst [(Cp*IrCl)₂(THBPM)]²⁺ reported by Hull, Himeda and Fu-

jita et al. can also dehydrogenate FA in water without the addition of base, albeit giving a lower TOF of 12000 h^{-1} at $60 \text{ }^\circ\text{C}$.^[67]

In 2014, Wang, Himeda and coworkers reported an iridium-biimidazole complex for the FA dehydrogenation, giving a TOF of 34000 h^{-1} at $80 \text{ }^\circ\text{C}$, which was the highest TOF reported for FA dehydrogenation in water without bases or additives by then.^[128]

1.5 Conclusions and Objectives of This Thesis

1.5.1 Literature summary

Homogeneous hydrogenation of CO_2 to FA/formate and the dehydrogenation of FA/formate have been explored for decades, and they are gaining more and more attention from the beginning of this century due to both energy and environmental concerns. Because the hydrogenation of CO_2 is reversible, generally a catalyst which is effective for CO_2 hydrogenation can also catalyze the dehydrogenation of FA, although it may be more effective for one direction than the other.^[32, 66, 67, 129, 130]

Dozens of homogeneous catalyst systems based on metal complexes of Ir, Ru, Rh, Fe, Co, etc. have appeared for CO_2 hydrogenation and FA dehydrogenation, and the catalytic reactivity has been improved dramatically. For example, as described in section 1.2.3, Nozaki and co-workers reported the iridium trihydride complex $[\text{IrH}_3(\text{P}3)]$ for CO_2 hydrogenation to exhibit a TOF of 150000 h^{-1} at $200 \text{ }^\circ\text{C}$ and a TON of 3500000 at $120 \text{ }^\circ\text{C}$ over a period of 48 h under 8.0 MPa of H_2/CO_2 (1/1) in $\text{H}_2\text{O}/\text{THF}$ (5/1). Pidko et al. reported that $[\text{RuH}(\text{Cl})(\text{CO})(\text{P}2)]$ provided a TOF as high as 1100000 h^{-1} for the hydrogenation of CO_2 in DMF using DBU as a base at $120 \text{ }^\circ\text{C}$ and 4.0 MPa of H_2/CO_2 (3/1). For the dehydrogenation of FA/formate, Pidko's catalyst $[\text{RuH}(\text{Cl})(\text{CO})(\text{P}2)]$ also gives a high TOF of

257000 h⁻¹ and TON of 1063000 (for 5 h) at 90 °C in DMF/ Et₃N. These reports represented the best results by the time the objective of this thesis was set and some remain the highest to date.

The above mentioned results have been obtained in organic solvents. Other groups, like those of Laurenczy, Beller, Fukuzumi, Himeda and Fujita, have made effort to accomplish the hydrogenation of CO₂ and FA dehydrogenation in more environmentally benign solution, i.e. water, under milder conditions, and good reactivity has been achieved. Particularly, Fujita et al. reported the pH sensitive iridium complex [(Cp*IrCl)₂(THBPM)]²⁺ for this reversible reaction with remarkable TONs and TOFs. At high pH (2 M KHCO₃), CO₂ hydrogenation rates of 70 h⁻¹ (25 °C and 0.1 MPa) and 53800 h⁻¹ (80 °C and 5.0 MPa) were observed. At low pH, [(Cp*IrCl)₂(THBPM)]²⁺ can decompose FA or formate to give CO-free H₂ and CO₂, and a high TOF of 228000 h⁻¹ at 90 °C and TON of 308000 at 80 °C were obtained in 1M HCO₂H/HCO₂Na (1:1, pH 3.5).

Apart from the solvent problem, both CO₂ hydrogenation and FA dehydrogenation frequently rely on the addition of additives, such as bases and LA, which is against the principle of atom economy. The drawbacks of these catalytic systems are obvious: i) the employment of ungreen organic solvents; ii) the cost due to the addition of additives and product separation. At present, only a few catalytic systems have been reported to be active for CO₂ hydrogenation and FA dehydrogenation in water without bases or additives.^[67, 73-75, 127, 128] However, the reactivity is rather low.

1.5.2 Thesis objectives

From the viewpoint of practical application, simple and highly effective catalytic system is always desired. However there's still a great gap between lab research and industry production and the development of efficient homogeneous catalyst

remains necessary and challenging. Targeting at the current problems, the main objective of this thesis is to develop efficient homogeneous catalyst systems for the hydrogenation of CO₂ to FA and the FA dehydrogenation under mild and environmentally benign conditions. The key issue is the catalyst development and especially the design of ligands, which involves several factors, such as electronic property and water solubility, etc.

Based on the literature research and our group's previous work on hydrogenation/transfer-hydrogenation (Xiao),^[116, 131-134] this thesis focuses on the homogeneous catalytic hydrogenation of CO₂ and FA dehydrogenation using different metal complexes, and the study is carried out in the following aspects:

- (1) Chapter 2 reports homogeneous hydrogenation of CO₂ to formate catalyzed by N[^]C cyclometallated half-sandwich iridium catalysts;
- (2) In chapter 3, new ligand type is exploited and base-free aqueous hydrogenation of CO₂ has been realized using iridium catalysts with non-aromatic *N,N'* diimine ligands;
- (3) Chapter 4 applies this Ir-*N,N'* diimine catalyst to the FA dehydrogenation, and delightfully the highest TOF and TON values ever reported under similar conditions were achieved;
- (4) Chapter 5 presents the study of FA dehydrogenation using commercially available catalyst [RhCp*Cl₂]₂ in the presence of simple halide ions.

**Chapter 2 Hydrogenation of CO₂ to Formate Catalyzed by
Cyclometallated Ir-N[^]C Complexes**

2.1 Introduction

Homogeneous hydrogenation of CO₂ into formate/FA is an ideal way to utilize CO₂ and to store H₂; but it has been a long-standing challenge for the activation of CO₂. In CO₂ molecule, the C=O bond length is around 116.3 pm, which falls in between the C=O bond in carbonyl compounds of ca 123 pm and the triple C≡O bond of 112.8 pm. Thus CO₂ has partial triple bond character and is difficult to be activated. The catalyst library for the homogeneous hydrogenation of CO₂ to formate has been growing progressively since the first one, [RhCl(PPh₃)₃], was reported in 1976 by Inoue et al.^[27] Dozens of transition-metal complexes based on ruthenium,^[40-42, 75] rhodium,^[72, 135] iridium,^[30, 52, 57, 62, 70, 136] iron,^[35, 58, 137] cobalt^[31, 36] and nickel^[138] have been reported to exhibit activity for this reaction. However most of these catalyst systems show high activity only at harsh conditions such as high temperature and high pressure, which is unfavorable from the practical point of view. A number of catalysts can work under mild conditions but with moderate reactivity.^[30-32, 45, 69, 73, 74, 135] For example, Fujita et al. reported a dinuclear iridium complex with a bipyrimidine ligand for CO₂ hydrogenation to formate, giving a TOF of 15700 h⁻¹ and a TON of 153000 at 50 °C under the pressure of 4.0 MPa in 2 M KHCO₃ aqueous solution.^[67] Therefore, developing catalysts for mild and efficient hydrogenation of CO₂ to formate is still challenging.

In the early years, the research of Jessop and Sakaki et al. had indicated that the strong electron-donating ability of the ligand, e.g. phosphine ligands, leads to high activity of such a complex in CO₂ hydrogenation.^[28, 29] A few more reports subsequently followed. Peris et al. performed CO₂ hydrogenation using water-soluble Ru and Ir complexes bearing bis-NHC (*N*-heterocyclic carbenes) ligands, and high catalytic activity was obtained due to the electron donor character of the

NHC ligand.^[61] Himeda and Fujita et al. reported a series of half-sandwich iridium bipyridine complexes $[\text{Cp}^*\text{Ir}(4,4'-(\text{R})_2\text{-bpy})(\text{OH}_2)]\text{SO}_4$ and $[\text{Cp}^*\text{Ir}(6,6'-(\text{R})_2\text{-bpy})(\text{OH}_2)]\text{SO}_4$ ($\text{R} = \text{OH}, \text{OMe}, \text{Me}, \text{H}$) by introducing different electron-donating groups to the bpy ligand. For the hydrogenation of CO_2 using these complexes as catalyst, they also found that stronger electron-donating substituents lead to higher reaction rates.^[63]

$\text{N}^{\wedge}\text{C}$ cyclometallated metal complexes have been shown to be excellent catalysts for the reduction of $\text{C}=\text{O}$ bond.^[139, 140] The Xiao group has been working on hydrogenation/transfer hydrogenation for many years, and have reported that $\text{N}^{\wedge}\text{C}$ cyclometallated $[\text{Cp}^*\text{IrCl}]$ imido complexes derived from acetophenone imines are exceptionally active catalysts for the reduction of imines.^[131-134] The $\text{N}^{\wedge}\text{C}$ bidentate ligand is expected to be more electron-donating compared with the bipyridine type $\text{N}^{\wedge}\text{N}$ ligand; thus the $\text{N}^{\wedge}\text{C}$ cyclometallated $[\text{Cp}^*\text{IrCl}]$ complex could be effective catalyst for the hydrogenation of CO_2 .

More importantly, inspired by the hydrogenation/transfer hydrogenation work and the observation of gas evolution during the transfer hydrogenation reaction using the 5:2 FA/ Et_3N azeotrope (F/T) as hydrogen source with the cyclometallated iridium complex, the Xiao group has designed a type of $\text{N}^{\wedge}\text{C}$ cyclometallated iridium(III) complexes bearing phenylimidazoline ligands and found that they are excellent catalysts for the dehydrogenation of FA,^[116] giving TOF of up to 147000 h^{-1} at $40 \text{ }^\circ\text{C}$ in F/T azeotrope. These results prompted us to investigate the hydrogenation of CO_2 using this type of cyclometallated iridium complexes.

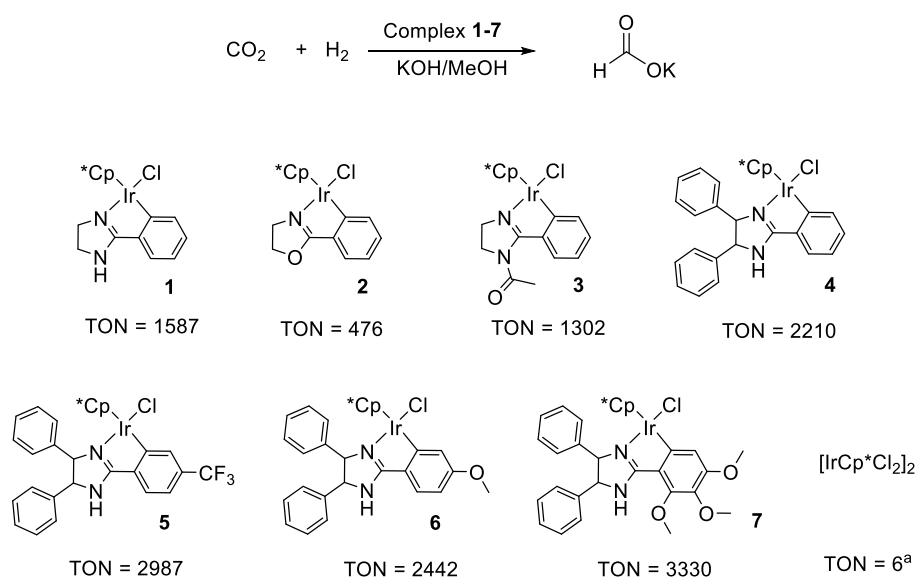
2.2 Hydrogenation of CO_2 to Formate with Ir- $\text{N}^{\wedge}\text{C}$ Complex

2.2.1 Initial catalyst screening

The CO_2 hydrogenation work started from screening of iridium catalysts formed

from $[\text{IrCp}^*\text{Cl}_2]_2$ and phenylimidazoline-type ligands, complexes **1-7**, which have been used for FA dehydrogenation^[116] and transfer hydrogenation^[141] previously. The hydrogenation reactions were carried out in a KOH/MeOH solution at 4.5 MPa of CO_2/H_2 (2:1) and 80 °C for 16 h, and the results are summarized in Scheme 2.1. ^1H NMR spectra confirmed the product to be potassium formate exclusively (Appendix, Scheme A.1). The amount of produced formate was determined by ^1H NMR using sodium *p*-toluenesulfonate as internal standard (Appendix, Scheme A.1).

Under the given reaction conditions, no reactivity was detected without catalyst. The iridium dimer $[\text{IrCp}^*\text{Cl}_2]_2$ itself hardly shows any activity (TON = 6, Scheme 2.1) for the hydrogenation of CO_2 , which indicates the importance of the ligand, comparing with complexes **1-7**.



Scheme 2.1 Hydrogenation of CO_2 using N^{C} cyclometallated iridium complexes **1-7**.

Reaction conditions: complex **1-7** (3.0 μmol), 1.0 M KOH MeOH solution (10.0 mL), 4.5 MPa CO_2/H_2 (1:2), 80 °C, 16 h. Reactions were carried out in a stainless steel autoclave (100 mL) with a glass inner. ^a: 5.0 μmol of $[\text{IrCp}^*\text{Cl}_2]_2$.

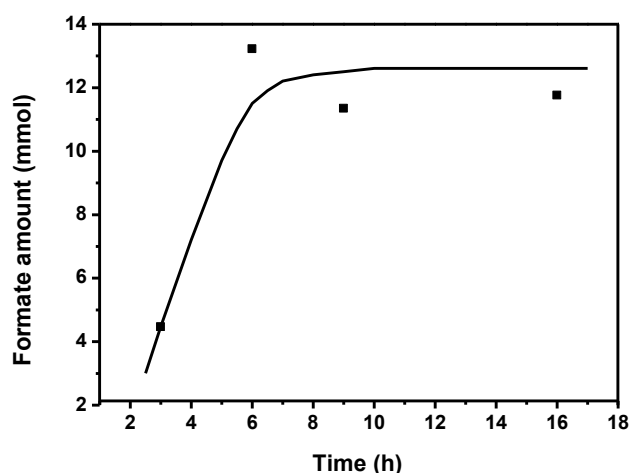
Ligand structure influences the catalytic activity greatly. Complexes **1-3** gave

TONs of 1587, 476, and 1302, respectively, for the hydrogenation of CO₂ to formate. Changing the imidazoline ring of the 2-imidazolyl ligand in complex **1** to the oxazoline ring (precatalyst **2**) and replacing the NH proton in the 2-imidazolyl ligand with acetyl group (precatalyst **3**) both led to less active catalysts, suggesting that the γ -NH unit on the N[^]C ligand facilitates this reaction. It is noteworthy that complexes **2** and **3** both show no reactivity towards FA dehydrogenation,^[116] whilst they can hydrogenate CO₂. This result implies that the CO₂ hydrogenation reaction and FA dehydrogenation reaction may undergo different reaction pathways using these cyclometallated Ir-N[^]C catalysts, especially considering the huge difference in reaction conditions, or the former is easier to occur.

By introducing bulky substituents onto the ligand, complex **4** shows increased TON (2210) compared with **1**, which is consistent with the FA dehydrogenation result.^[116] Complex **5** with electron withdrawing group on the phenyl ring and complex **6** with electron donating group on the phenyl ring both increase the reactivity, giving TONs of 2987 and 2442, respectively. These results indicate that the substituent's electron property doesn't influence the reaction rate in a simple way or it may have no influence at all, which is unexpected. One possible explanation is that the substituent on the phenyl ring is not much involved in the HOMO/LUMO of the iridium complex (*vide infra*). When complex **7** with three methoxy groups on the ligand was applied for the hydrogenation of CO₂, a much higher TON of 3330 was obtained. The following reaction condition optimizations were performed using complex **7** as catalyst.

2.2.2 Optimization of reaction conditions

The reaction was studied under various reaction times, and Scheme 2.2 shows that the reaction rate slows down in about 6 h. Thus for experimental convenience, the subsequent hydrogenation reactions were conducted either for 6 h or 16 h.



Scheme 2.2 Formate production from CO₂ hydrogenation at different reaction time.

Reaction conditions: complex **7** (3.0 μmol), 1.0 M KOH/MeOH solution (10.0 mL), 4.5 MPa CO₂/H₂ (1:2), 80 °C. Reactions were carried out in a stainless steel autoclave (100 mL) with a glass inner.

Table 2.1 Base screening for the hydrogenation of CO₂ to formate^a

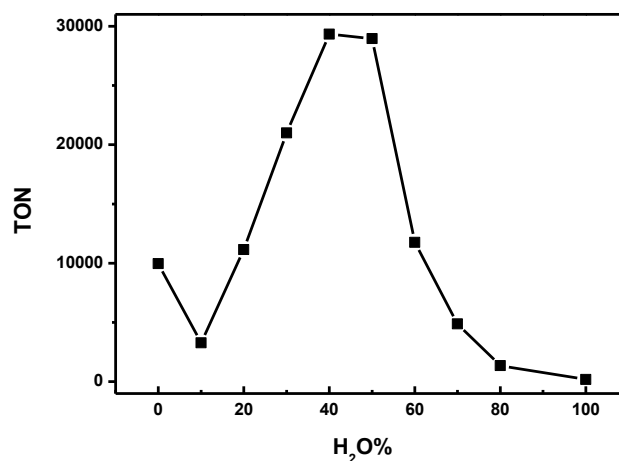
Entry	Base (2 M)	Solution	Formate (mmol)	TON
1	LiOH	MeOH 10.0 mL	10.20	3399
2	NaOH	MeOH 10.0 mL	13.35	4450
3	KOH	MeOH 10.0 mL	12.76	4255
4	CsOH	MeOH 6.5 mL + H ₂ O 3.5 mL	19.64	6545
5	KOH	MeOH 6.5 mL + H ₂ O 3.5 mL	16.50	5500

^a: Reaction conditions: complex **7** (3.0 μmol), 4.5 MPa CO₂/H₂ (1:2), 80 °C, 6 h. Reactions were carried out in a stainless steel autoclave (100 mL) with a glass inner.

Different bases (2 M) were then screened for the iridium catalyzed CO₂ hydrogenation as shown in Table 2.1. Entries 1-3 show the superior performance of NaOH (TON: 4450) and KOH (TON: 4255) compared with LiOH (TON: 3399). Since CsOH was purchased as a water solution, the hydrogenation reaction was conducted in a mixture solution of water and methanol. The TON further in-

creased to 6545 and the reaction approached approximately full conversion in terms of the amount of base used (Table 2.1, entry 4). The higher TON could be due to water playing some role in this reaction. When again using KOH as the base, a TON of 5500 (Table 2.1, entry 5) was attained in the mixture solution of MeOH/H₂O (6.5/3.5 mL), which is higher than that of the reaction carried out in pure methanol. Thus the impact of water on the hydrogenation reaction was investigated next.

With different volume ratios of MeOH/H₂O (total 10.0 mL), the hydrogenation of CO₂ was studied using complex **7** and the cheaper base KOH. The catalyst loading was lowered to 0.5 μmol to avoid high conversion. As displayed in Scheme 2.3, the TON for formate generation varies greatly with different ratios of MeOH/H₂O, with TON reaching the highest value (29325) when the ratio is around 1:1.



Scheme 2.3 TON of formate production from CO₂ hydrogenation in MeOH/H₂O solution. Reaction Conditions: complex **7** (0.5 μmol), 1.0 M KOH/MeOH/H₂O mixture solution (total volume 10.0 mL), 4.5 MPa CO₂/H₂ (1:2), 80 °C, 16 h. Reactions were carried out in a stainless steel autoclave (100 mL) with a glass inner.

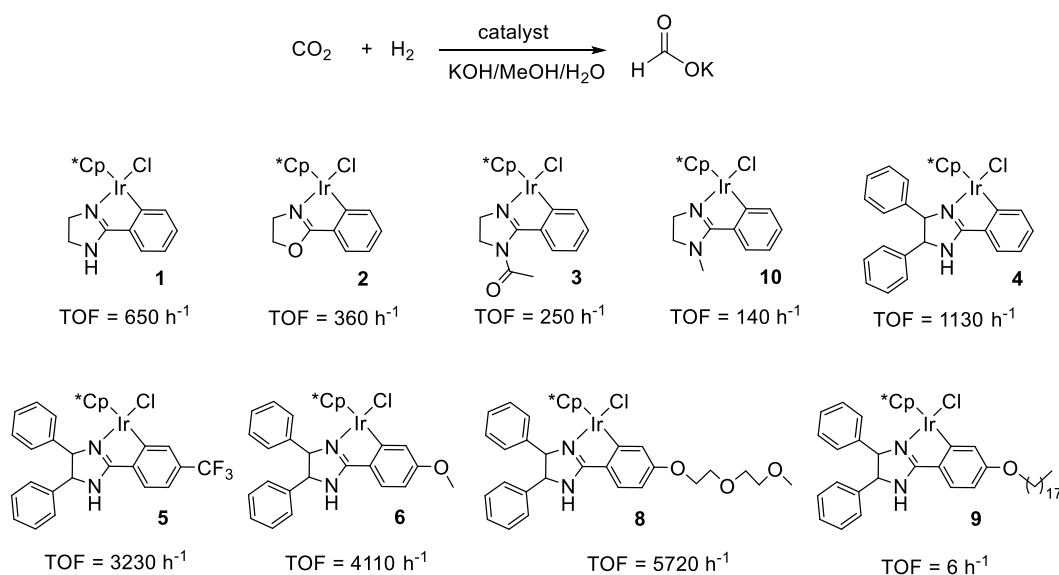
The effect of water in homogeneous hydrogenation of CO₂ has been noted and

investigated.^[18, 27, 28, 75, 142] In organic solvents, small amount of added water can enhance the reaction rates,^[72] and its function was assumed to be stabilizing the transition state through an H-bonding interaction between the coordinated water molecule and the oxygen of the approaching CO₂ in the insertion step of CO₂ to metal hydride. In basic aqueous solution, a kinetic isotopic effect (KIE) study with a proton-responsive iridium complex for CO₂ hydrogenation to formate demonstrates the involvement of water in the rate-determining step to accelerate the heterolysis of H₂.^[69] Thus the hydrogenation of CO₂ may be more favorable in water. However these cyclometallated Ir-N[^]C complexes are not soluble in water. Effort was subsequently made to increase the water solubility of catalysts and more studies were performed.

2.2.3 Further development of catalyst

In the MeOH/H₂O (1:1) mixture solution of KOH, some previously screened complexes and newly developed catalysts were tested again for CO₂ hydrogenation reaction, but at a lower temperature of 40 °C (Scheme 2.4). ¹H NMR spectra also confirmed the product to be potassium formate exclusively (Appendix, Scheme A.2). The amount of produced formate was detected by ion chromatography and no reactivity was detected without catalyst. In this section, TOF was adopted to describe the activity of the catalysts.

Complexes **1-3** and **10** give TOFs of 650 h⁻¹, 360 h⁻¹, 250 h⁻¹ and 140 h⁻¹, respectively. Moreover, replacing the NH proton in the 2-imidazolynyl ligand with either electron withdrawing acetyl group (precatalyst **3**) or electron donating methyl group (precatalyst **10**) both led to less active catalysts compared with complex **1**. The conclusion is similar as discussed in section 2.2.1, which is that the γ -NH unit on the N[^]C ligand shows its superiority for this reaction but is not indispensable.

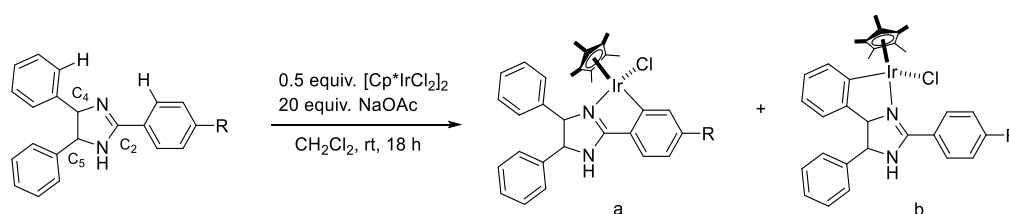


Scheme 2.4 Hydrogenation of CO₂ using cyclometallated Ir-N^{^C} complexes **1-6** and **8-10**. Reaction conditions: 0.2 μmol of complex, 1.0 M KOH/MeOH/H₂O (1:1) solution (10.0 mL), 5.0 MPa CO₂/H₂ (1:1), 40 °C, 1 h. Reactions were carried out in a stainless steel autoclave (300 mL) with a glass inner.

Under such reaction conditions, complexes **4-6** show better performance than **1**, giving TOFs of 1130 h⁻¹, 3230 h⁻¹ and 4110 h⁻¹, respectively. This TOF difference also suggests that no unambiguous conclusion can be drawn concerning the relationship between the electronic property of substituent and the catalytic reactivity. Noteworthy is that, the TOF value of 4110 h⁻¹ obtained with complex **6** bearing a relatively hydrophilic methoxy group on the ligand is considerably higher than that of complex **5**, in the mixture solution of MeOH/H₂O, encouraging us to incorporate hydrophilic ligand into the cyclometallated Ir-N^{^C} complexes.

Since water as solvent plays an important role in this reaction and these complexes are water-insoluble, complex **8** and **9** based on the backbone of complex **6** were designed to investigate the ligand hydrophilicity effect on reactivity. Complex **8** and **9** were synthesized using the same method as complex **6**, and each of them consists of two inseparable regioisomers, **8a/8b** and **9a/9b**, resulting from

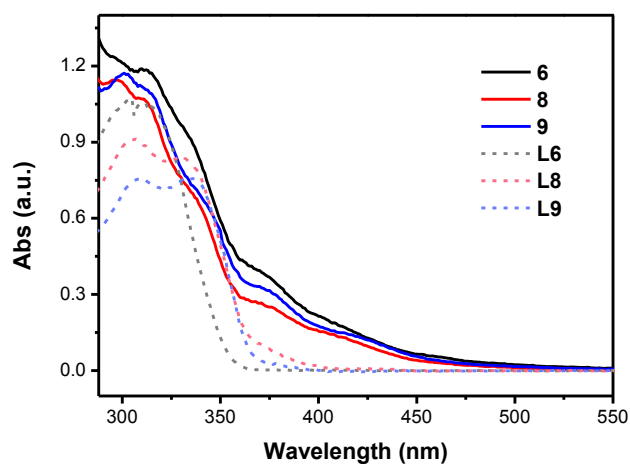
the competing cyclometallation of the C₂ and C₄ phenyl rings in the NaOAc-mediated cyclometallation reaction (Scheme 2.5; for characterizations, see experimental section). As expected, complex **8** with a poly ethylene glycol type substituent (-O(CH₂CH₂O)₂CH₃) on the cyclometallated aryl ring shows a higher TOF of 5720 h⁻¹ compared with complex **6**. In contrast, complex **9** with a long alkyl chain (-O(CH₂)₁₇CH₃) on the cyclometallated aryl ring hardly shows any activity under the otherwise identical conditions. These results indicate that catalyst with hydrophilic ligand show better catalytic activity than catalyst with hydrophobic ligand.



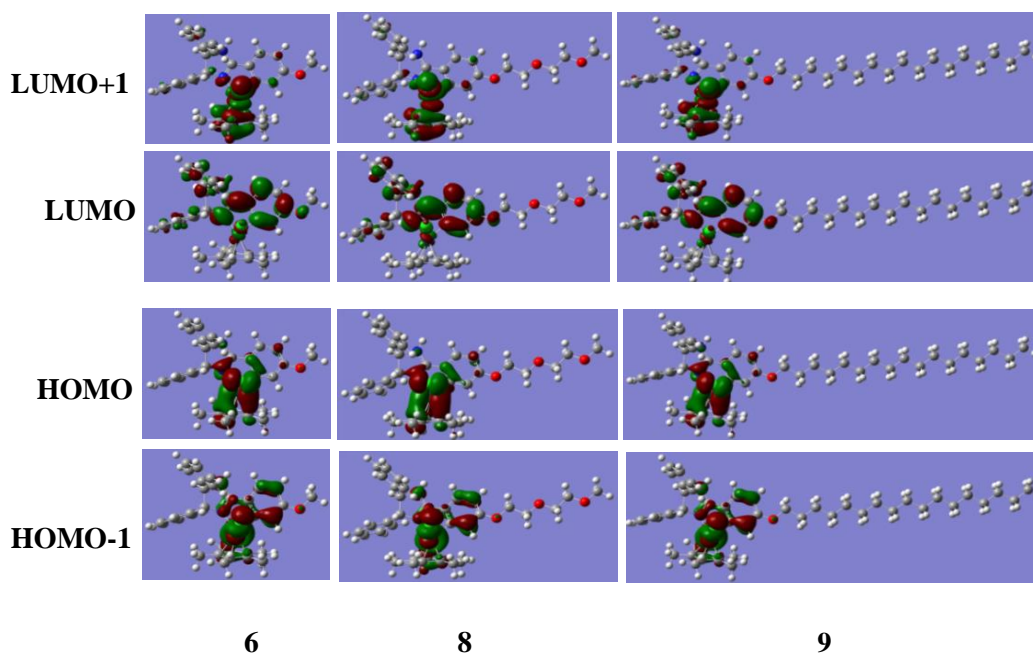
Scheme 2.5 Synthesis of complex **8** and **9**

The reason for the significant difference in catalytic activity for CO₂ hydrogenation between **8** and **9** was further investigated. ¹H NMR results show a small composition difference between complexes **8** and **9** (**8a:8b** = 1.5:1, **9a:9b** = 1.3:1), which is not likely to cause such great difference in catalytic activity.

Scheme 2.6 shows the UV-Vis absorption spectra of complex **6**, **8** and **9** as well as their parent ligands **L6**, **L8** and **L9**. The resemblance of the absorption curves among the three complexes suggests the similarity of their electronic properties.



Scheme 2.6 UV-Vis absorption spectra of complex **6**, **8**, **9** and ligands **L6**, **L8**, **L9** (50 mM) in CH_2Cl_2 (DCM)

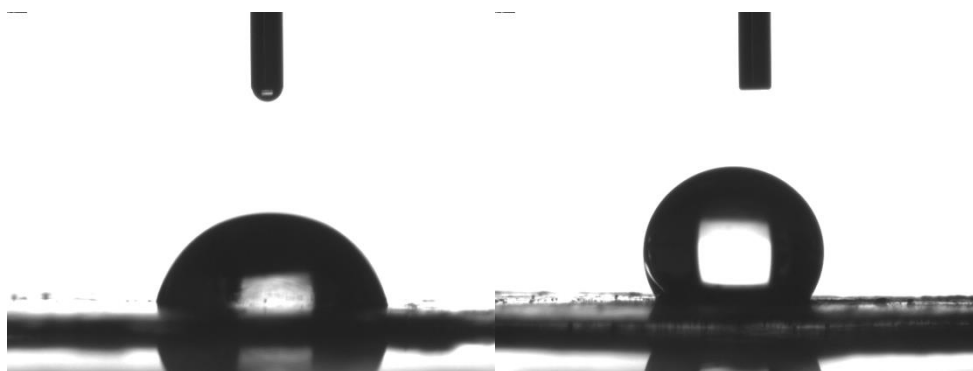


Scheme 2.7 HOMO (-1) and LUMO (+1) models of complex **6**, **8** and **9**.

The calculations were performed with the GAUSSIAN09 package.^[143] The Becke three parameters hybrid functional with the Lee-Yang-Parr correlation functional (B3LYP) was chosen for taking into account the exchange and correlation effects of electrons, and the 6-31+G(d) basis set was used for all the atoms.^[144, 145] The contours of frontier molecular orbitals are visualized with GaussView software.^[146] The calculation was performed by Dr./Prof. Xin Zhou.

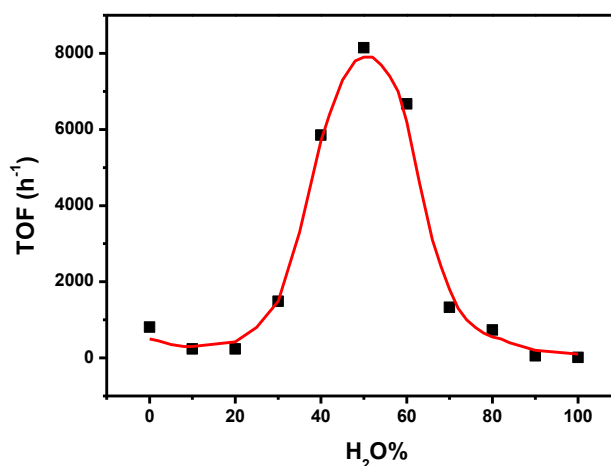
The DFT calculation (Scheme 2.7) results also show that the -OMe, -O(CH₂CH₂O)₂CH₃ and -O(CH₂)₁₇CH₃ substituents on the cyclometallated aryl ring of complex **6**, **8** and **9** are not much involved in the HOMO or LUMO of these molecules. In addition, the frontier orbitals of these complexes are similar in shape. These results indicate that the huge difference in CO₂ hydrogenation activity between **8** and **9** is not likely due to the electronic effect of the ligand.

Meanwhile, the hydrophilicity of complex **8** and **9** was tested by means of the contact angle measurement. The water contact angle for complex **8** is 80.97°, while the value for complex **9** is 123.4° (Scheme 2.8), showing that complex **8** is more hydrophilic than complex **9**. Thus a hydrophilic ligand is likely beneficial for this reaction under the given reaction conditions.



Scheme 2.8 Water contact angle measurement demonstration for **8** (left) and **9** (right).

During the initial reaction conditions screening, solvent composition was found to affect the reactivity to a great extent. As displayed in Scheme 2.9, using complex **8** as catalyst, the TOF for formate generation obtained in a mixture solution of MeOH/H₂O shows a similar trend, with TOF reaching the highest value (8140 h⁻¹, 60 °C) when the amount of methanol and water is equal. As discussed in section 2.2.2, this reaction is favorable in water and this result might be a compromise of the reactivity and the solubility of the catalyst.



Scheme 2.9 Hydrogenation of CO₂ with different MeOH/H₂O ratios.

Reaction conditions: complex **8** (0.2 μmol), 2.0 M KOH/MeOH/H₂O solution (10.0 mL), 5 MPa CO₂/H₂ (1:1), 60 °C, 1 h. Reactions were carried out in glass vials placed in a stainless steel autoclave.

Table 2.2 Hydrogenation of CO₂ in co-solvent: H₂O (1:1) solution

Entry	co-solvent	formate (mmol)	TON/TOF
1	MeOH	1.14	5720
2 ^a	DMF	3.50	1750
3	THF	0.02	100
4	DMSO	0	0
5	Ethylene glycol	0.61	3050
6 ^b	DMF	3.15	-
7 ^b	MeOH	0	0

General reaction conditions: complex **8** (0.2 μmol), co-solvent/H₂O (1:1) solution (10.0 mL), 1.0 M KOH, 5 MPa CO₂/H₂ (1:1), 40 °C, 1 h. TOF value is the rate for the initial 1 h; thus TON and TOF have the same values here. ^a: TON/TOF value was obtained with blank reaction result deducted (refer to ^b). ^b: Reaction carried out without catalyst - blank reaction.

In addition, this reaction was also conducted in mixtures of water and other

co-solvents (Table 2.2). Reactions in tetrahydrofuran (THF), dimethylformamide (DMF), dimethylsulfoxide (DMSO) and ethylene glycol (MW = 200) all show lower activities compared with MeOH.

Table 2.3 Hydrogenation of CO₂ in MeOH:H₂O (1:1) under various reaction conditions

Entry	$P(\text{CO}_2)/P(\text{H}_2)$ (MPa)	T (°C)	Initial TOF (h ⁻¹)
1	2.5/2.5	20	780
2	2.5/2.5	30	1960
3	2.5/2.5	40	5720
4	2.0/3.0	40	5640
5	3.0/2.0	40	5140

Reaction conditions: complex **8** (0.2 μmol), MeOH/H₂O (1:1) solution (10.0 mL), 1.0 M KOH, 1 h. TOF value is calculated using the first 1 h data.

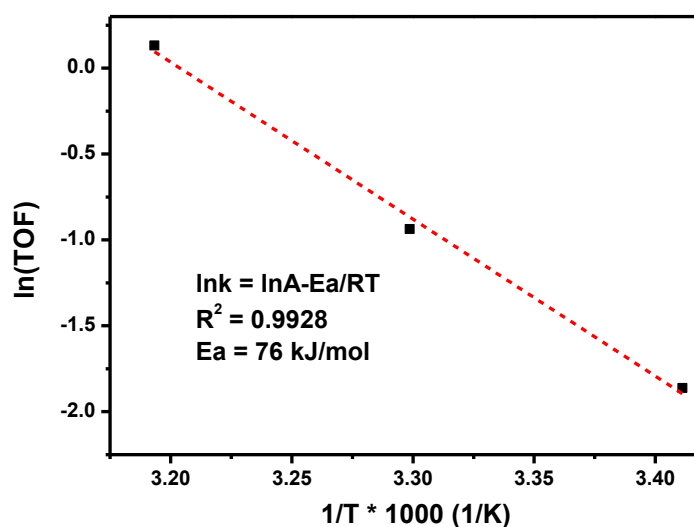


Figure 2.10 Arrhenius plot of formate producing rate for the hydrogenation of CO₂.

Reaction conditions: complex **8** (0.2 μmol), MeOH/H₂O (1:1) solution (10.0 mL), 1.0 M KOH, 5 MPa CO₂/H₂ (1:1), 20, 30, 40 °C, 1 h. Reactions were carried out in a stainless steel autoclave (300 mL) with a glass inner.

The catalytic hydrogenation of CO₂ to formate using complex **8** was investigated under various conditions. The rate for CO₂ hydrogenation increases with temperature rise (Table 2.3, entry 1-3). The temperature dependence of initial TOFs follows the Arrhenius equation (Scheme 2.10) and the estimated apparent activation energy (E_a) for CO₂ hydrogenation is 76 kJ•mol⁻¹, which is in the range of noble metal catalyzed CO₂ hydrogenation reactions.^[30, 49] Changes in the ratio of CO₂:H₂ from 1:1 to 2:3 and 3:2 result in a slight decrease in reactivity (Table 3, entries 3-5).

Table 2.4 Hydrogenation of CO₂ in MeOH:H₂O (1:1) solution

Entry	Solvent (mL)	T (°C)	Time (h)	TON	Initial TOF (h ⁻¹)	Final [formate] (M)
1	10	40	1		5720	
2	50	40	0.5	4910	9820 ^a	
3	50	40	14	59420		0.24
4 ^b	20	40	20	3503		0.70
5 ^c	40	80	1		57330	
6 ^{c,d}	40	80	12.5	102200		0.26

Reaction conditions: complex **8** (0.2 μmol), 1.0 M KOH/MeOH/H₂O (1:1) solution, 5.0 MPa CO₂/H₂ (1:1). TOF value is calculated using the first 1 h data. ^a: TOF value is calculated using the 0.5 h data. ^b: 4.0 μmol of complex **8**, 2.0 M KOH, 20.0 mL reaction solution. ^c: 2.0 M KOH. ^d: 0.1 μmol of complex **8**. Entries 1-4: Reactions were carried out in a stainless steel autoclave (300 mL) with a glass inner. Entries 5, 6: Reactions were carried out in a stainless steel autoclave (300 mL) without glass inner and negligible amount of formate was detected without catalyst.

When the reaction solution was expanded to 50 mL, a higher initial TOF of 9820 h⁻¹ was obtained at 40 °C and the turnover number reached 59420 after 14 hours (Table 2.4, entry 2, 3). Using 4.0 μmol of complex **8** at 40 °C, the final con-

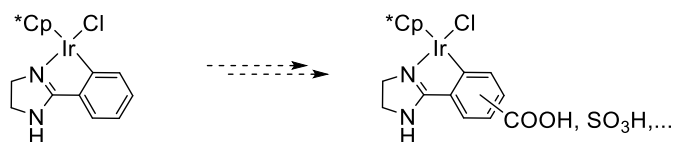
centration of formate reached 0.7 M (Table 2.4, entry 4). When the temperature was increased to 80 °C, the initial TOF increased to 57330 h⁻¹ (entry 5), and a TON of 102200 was obtained after 12.5 h (Table 2.4, entry 6). These results are comparable with the highest reactivity reported under similar mild conditions.^[67]

2.3 Summary

In summary, the cyclometallated Ir-N[^]C complexes show good performance for CO₂ hydrogenation to formate, extending the ligand type that could be used for the hydrogenation of CO₂ to FA/formate.

During the catalyst screening and reaction conditions optimization, it was found that the hydrogenation of CO₂ with the phenylimidazoline-type cyclometallated Ir-N[^]C complexes shows faster rates in a MeOH/H₂O (around 1:1) mixture solution than in pure solvent, and the catalyst bearing more hydrophilic ligand (complex **8**) is remarkably effective for this reaction compared with catalyst containing hydrophobic ligand (complex **9**). Using 0.2 μmol of complex **8**, a TOF of 9820 h⁻¹ was obtained at 40 °C under a total pressure of 5.0 MPa, and the TON could reach 102200 when temperature increased to 80 °C.

However, the attempt to synthesize more water-soluble cyclometallated Ir-N[^]C complexes (Scheme 2.11) failed; thus the organic solvent-free hydrogenation of CO₂ under mild conditions couldn't be fully achieved with this type of catalyst.



Scheme 2.11 Idea of synthesizing more water-soluble cyclometallated Ir-N[^]C complex

These complexes are of great significance not only for they can convert CO₂ into formate, but also because they provides a potential way for hydrogen storage

considering their excellent performance towards dehydrogenation of FA to give hydrogen under mild conditions.

2.4 Experimental Section

2.4.1 General information

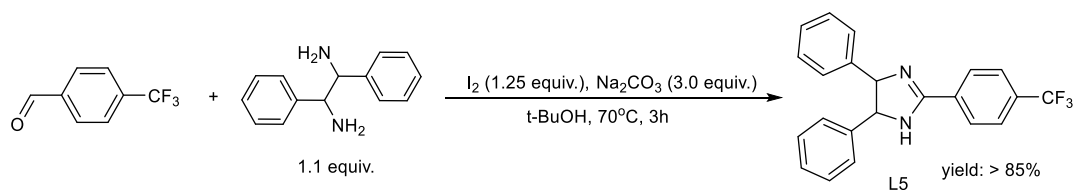
Instruments: NMR spectra were recorded on a Bruker Avance-400 spectrometer. The concentration of formate was measured by SHINEHA CIC-100 ion chromatograph with Shodex IC SI-52 4E column using Na₂CO₃ solution (3.6 mM) as the eluent. HRMS data were obtained from a Finnigan MAT 95 system. UV-Vis absorption spectra were recorded with SHIMADZU UV-2550. Contact angle measurement was performed by the Energy Research Resources Division of Dalian National Laboratory for Clean Energy. X-ray diffraction analysis was performed by the State Key Laboratory of Organometallic Chemistry (Shanghai).

Chemicals: Dry dichloromethane (DCM), hexane, methanol, tetrahydrofuran, and dimethylformamide were purchased from J&K. [Cp*IrCl₂]₂ was purchased from Strem Chemicals Inc. KOH was purchased from Acros. All other commercial compounds were purchased from Sigma-Aldrich Co. or Alfa Aesar and used without further purification. Solvent for CO₂ hydrogenation reaction was degassed and stored under argon before reaction.

2.4.2 Synthesis and characterization of ligands and complexes

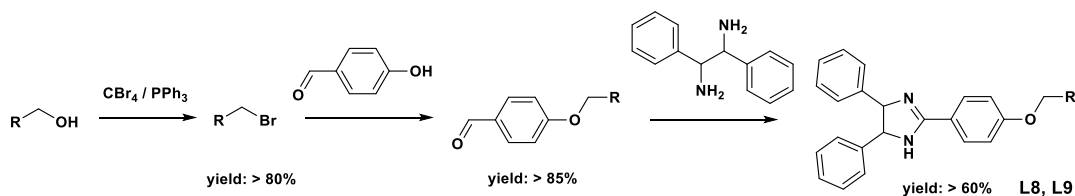
The preparation and characterization of ligands **L1-L4**, **L6**, **L10** and complexes **1-4**, **6** and **10** can be found in previous work.^[116] Details about ligand **L7** and complex **7** can be found in Jennifer Smith's thesis from the Xiao group and the characterization of **7** is quoted in this section for comparison.

Ligand **L5** was prepared according to literature procedures.^[147]

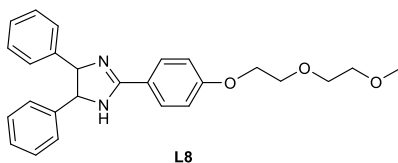


L5: white solid; ^1H NMR (400 MHz, CDCl_3) δ (ppm) = 8.05 (d, $J = 7.9$ Hz, 2H), 7.71 (d, $J = 7.9$ Hz, 2H), 7.33 (m, 10H), 5.50 (s, 1H), 4.94 (s, 2H); $^{13}\text{C}\{^1\text{H}\}$ NMR (100 MHz, CDCl_3) δ (ppm) = 161.99, 143.18, 133.60, 132.92 (q, $J_{\text{C-F}} = 32.4$ Hz), 128.95, 127.95, 127.86, 126.73, 125.72 (q, $J_{\text{C-F}} = 4.0$ Hz), 123.95 (q, $J_{\text{C-F}} = 270.7$ Hz), 29.85; $^{19}\text{F}\{^{13}\text{C}\}$ NMR (376 MHz, CDCl_3) δ (ppm) = -62.84; m/z (ESI^+) 367.1 $[\text{M}+\text{H}]^+$.

Ligands **L8** and **L9** were prepared according to literature procedures.^[147-149]

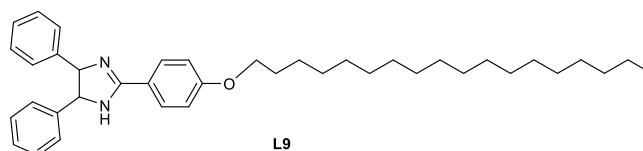


L8: white solid; ^1H NMR (400 MHz, CDCl_3) δ (ppm) = 7.87 (d, $J = 12.0$ Hz, 2H), 7.30 (m, 10H), 6.97 (d, $J = 12.0$ Hz, 2H), 4.87 (s, 2H), 4.20 (t, $J = 4.0$ Hz, 2H), 3.89 (t, $J = 4.0$ Hz, 2H), 3.75-3.73 (m, 2H), 3.61-3.58 (m, 2H), 3.40 (s, 3H); $^{13}\text{C}\{^1\text{H}\}$ NMR (100 MHz, CDCl_3) δ (ppm) = 162.83, 161.19, 143.62, 129.10, 128.79, 127.59, 126.72, 122.61, 114.64, 72.05, 70.93, 69.76, 67.66, 59.20, one resonance was not observed; m/z (ESI^+) 417.2 $[\text{M}+\text{H}]^+$.

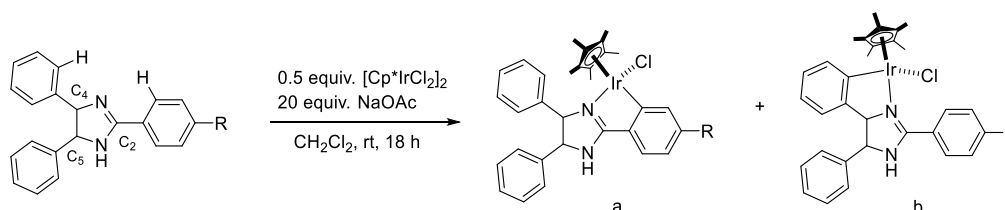


L9: white solid; ^1H NMR (400 MHz, CDCl_3) δ (ppm) 7.88 (d, $J = 8$, 2H), 7.37-7.26 (m, 10H), 6.95 (d, $J = 8.0$ Hz, 2H), 5.40 (b, 1H), 4.88 (s, 2H), 4.01 (t, $J = 4.0$ Hz, 2H), 1.81 (m, 2H), 1.48 (m, 2H), 1.27 (overlap, 28H), 0.89 (t, $J = 4$ Hz,

3H); $^{13}\text{C}\{^1\text{H}\}$ NMR (100 MHz, CDCl_3) δ (ppm) 162.85, 161.54, 143.77, 131.09, 129.04, 128.77, 127.55, 126.73, 122.35, 114.50, 68.29, 32.02, 29.80, 29.76, 29.70, 29.68, 29.49, 29.46, 29.28, some resonance were not observed due to overlap, 26.11, 22.79, 14.22; m/z (ESI $^+$) 567.4 $[\text{M}+\text{H}]^+$.



Complex **5**, **8** and **9** were prepared using the method of Davies et al.^[150] and experimental details can be found in previous publication.^[116] Iridium complexes **X** were synthesized from the corresponding ligands **LX**. Particularly, complexes **5**, **8** and **9** all consist of two inseparable regioisomers **5a/5b**, **8a/8b** and **9a/9b** resulting from the competing cyclometallation of the C₂ and C₄ phenyl rings in the NaOAc-mediated cyclometallation reaction.

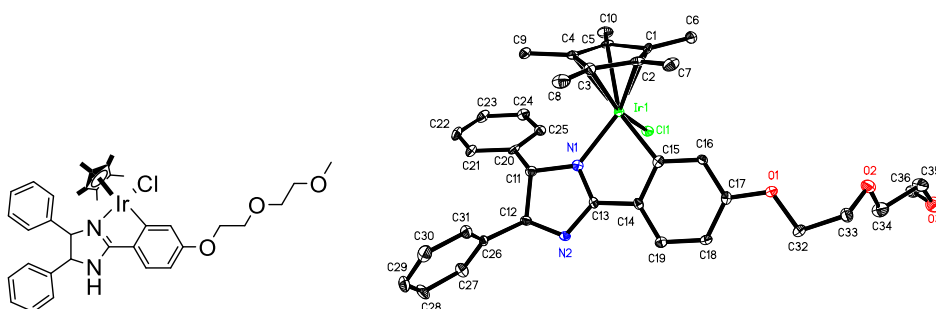


Complex 5 (R = CF_3): **5a:5b** = 1.5:1, yellow powder; 0.10 mmol scale, yield 59 mg, 86%; column: DCM/methanol=10:1 (several drops of ammonia); ^1H NMR (400 MHz, CDCl_3) δ (ppm) = 8.09 (s, 0.4H), 8.01 (s, 0.6H), 7.48–7.20 (m, overlapped, 10H), 7.21 (m, 1.4H), 7.11 (d, J = 7.9 Hz, 0.6H), 6.25 (s, 0.6H), 5.62 (s, 0.4H), 5.16 (d, J = 5.8 Hz, 0.4H), 4.96 (d, J = 11.5 Hz, 0.6H), 4.86 (d, J = 11.6 Hz, 0.6H), 4.76 (d, J = 5.8 Hz, 0.4H), 1.45 (s, 6H), 1.43 (s, 9H). $^{13}\text{C}\{^1\text{H}\}$ NMR (100 MHz, CDCl_3) δ (ppm) = 176.79, 175.79, 164.95, 164.71, 143.16, 141.62, 139.81, 139.07, 137.64, 132.50 (q, J = 4.0 Hz), 131.97 (q, J = 3.7 Hz), 129.14, 129.10, 128.91, 128.82, 128.75, 128.56, 128.41, 128.37, 127.84, 127.42, 127.31, 124.72, 124.68, 118.68 (q, J = 4.0 Hz), 118.48 (q, J = 4.0 Hz), 88.41, 87.80, 79.75, 79.62,

72.44, 72.08, 9.39, 9.14; $^{19}\text{F}\{^{13}\text{C}\}$ NMR (376 MHz, CDCl_3) δ (ppm) = -62.22; m/z (ESI^+) 693.2 $[\text{M}-\text{Cl}]^+$.

Complex 8 (R = $-\text{O}(\text{CH}_2\text{CH}_2\text{O})_2\text{CH}_3$): **8a:8b** = 1.5:1; yellow powder; 0.12 mmol scale, yield 88 mg, 90%; column: DCM/methanol=10:1 (several drops of ammonia); ^1H NMR (400 MHz, CDCl_3) δ (ppm) = 7.53-7.22 (m, overlapped, 15H), 6.62 (dd, J = 8.0, 4.0 Hz, 0.4H), 6.55 (dd, J = 8.0, 4.0 Hz, 0.6H), 5.63 (s, 0.6H), 5.32 (d, J = 12.0 Hz, 0.7H), 5.12 (d, J = 4.0 Hz, 0.4H), 4.98 (d, J = 12.0 Hz, 0.7H), 4.78 (d, J = 12.0 Hz, 0.7H), 4.68 (d, J = 4.0 Hz, 0.4H), 4.31-4.17 (m, 2H), 3.90 (q, J = 4.0 Hz, 2H), 3.76 (m, 2H), 3.61 (m, 2H), 3.42 (s, 3H), 1.45 (s, 15H); $^{13}\text{C}\{^1\text{H}\}$ NMR (100 MHz, CDCl_3) δ (ppm) = 176.76, 176.15, 167.54, 166.68, 161.62, 161.06, 143.90, 142.12, 140.16, 139.45, 129.04, 128.97, 128.83, 128.52, 128.40, 128.13, 127.67, 127.46, 127.39, 126.07, 126.02, 121.06, 120.83, 109.09, 108.66, 87.84, 87.26, 79.38, 77.30, 72.45, 72.07, 70.85, 70.00, 67.18, 67.11, 59.18, 9.50, 9.25; m/z (ESI^+) 743.3 $[\text{M}-\text{Cl}]^+$; Crystals suitable for XRD analysis were obtained from DCM/ Et_2O .

$\text{IrC}_{36}\text{H}_{42}\text{ClN}_2\text{O}_3$, $\text{CH}_2\text{Cl}_2/\text{Et}_2\text{O}$, $M = 778.36$, orange needle, 0.165 x 0.089 x 0.043 mm³ Triclinic, Space group $P-1$, $a = 8.8874(11)$ Å, $\alpha = 88.759(2)^\circ$, $b = 14.9235(19)$ Å, $\beta = 89.883(3)^\circ$, $c = 24.177(3)$ Å, $\gamma = 82.925(2)^\circ$, $V = 3181.4(7)$ Å³, $Z = 4$, $D_c = 1.625$ mg/m³, $T = 133(2)$ K 23350 reflections collected, 12476 independent reflections $R_{\text{int}} = 0.0556$, Goodness-of-fit on $F^2 = 0.959$, $RI = 0.0406$, $wR2 = 0.0652$, 0 restraints, 787 parameters, absorption coefficient = 4.319 mm⁻¹.



Complex 9 (R = -O(CH₂)₁₇CH₃): **9a:9b** = 1.3:1; yellow powder, 0.12 mmol scale, yield 107.2 mg, 92%; column: DCM/methanol=15:1 (several drops of ammonia); ¹H NMR (400 MHz, CDCl₃) δ (ppm) = 7.57-7.24 (m, overlapped, 11H), 6.58 (dd, *J* = 8.0, 4.0 Hz, 0.4H), 6.41 (dd, *J* = 8.0, 4.0 Hz, 0.5H), 5.83 (s, 0.4H), 5.35 (s, 0.4H), 5.12 (d, *J* = 8.0 Hz, 0.4H), 4.92 (d, *J* = 12.0 Hz, 0.5H), 4.68-4.63 (m, 0.8H), 4.13-3.87 (m, 2H), 1.85-1.75 (m, 2H), 1.48 (s, 15H), 1.27 (overlap, 30H), 0.89 (t, *J* = 4.0 Hz, 3H); ¹³C{¹H} NMR (100 MHz, CDCl₃) δ(ppm) = 176.81, 176.20, 167.38, 166.55, 162.06, 161.51, 143.96, 142.16, 140.22, 139.50, 129.03, 128.96, 128.82, 128.51, 128.38, 128.12, 127.65, 127.47, 127.40, 126.99, 126.08, 126.08, 114.51, 108.96, 108.48, 88.06, 87.80, 87.23, 79.91, 79.37, 77.30, 72.45, 72.03, 67.84, 67.76, 32.01, 29.79-29.45 (overlap), 26.25, 26.10, 22.77, 14.20, 9.71, 9.49, 9.25; *m/z* (ESI⁺) 893.5 [M-Cl]⁺.

Complex 7: yellow solid. ¹H NMR (400 MHz, CDCl₃) δ (ppm) = 7.51 (d, *J* = 6.9 Hz, 1H), 7.41-7.28 (m, 9H), 7.1 (m, 1H), 6.61 (s, 1H), 4.97 (d, *J* = 6.0 Hz, 0.35H), 4.92-4.84 (m, 1.3H), 4.71 (d, *J* = 6.0 Hz, 0.35H), 4.04 (s, 2H), 4.01 (s, 1H), 4.00 (s, 2H), 3.99 (s, 1H), 3.83 (s, 1H), 3.79 (s, 2H), 1.46 (s, 10H), 1.44 (s, 5H); ¹³C{¹H} NMR (100 MHz, CDCl₃) δ (ppm) = 176.7, 175.7, 161.4, 160.2, 156.7, 156.2, 151.5, 151.4, 144.1, 142.4, 140.4, 139.7, 136.0, 135.8, 128.9, 128.7, 128.3, 128.2, 128.1, 128.0, 127.5, 127.3, 120.1, 118.9, 113.9, 113.4, 87.6, 87.1, 78.5, 78.0, 72.3, 72.1, 61.2, 61.1, 60.4, 55.8, 9.5, 9.2; HRMS (ESI) found [M+H]⁺ 750.2206.

2.2.3 General procedure for CO₂ hydrogenation

A stock solution of a complex **1-10** was freshly made by dissolving a certain amount of the complex in dry DCM (0.4 mM). Under argon flow, the catalyst stock solution was added into a 100 or 300 mL autoclave and DCM volatilized to dry. KOH solid was then added into the autoclave followed by the degassed solvent.

The autoclave was tightened afterwards and purged three times with CO₂ before it was pressurized with CO₂ and then H₂ to get a certain pressure at room temperature. The reaction mixture was stirred at certain temperature for 0.5 - 20 h before it was cooled down with an ice-water bath. The determination of product amount was achieved with ¹H NMR or ion chromatograph:

(1) ¹H NMR method: The reaction mixture solution was dried under vacuum. 5 mL of 0.1 M sodium *p*-toluenesulfonate aqueous solution was added to dissolve the white solid. 0.1 mL of the mixture solution and 0.4 mL of D₂O were mixed together in a NMR tube and then submitted to get the ¹H NMR spectrum (e.g. Appendix, Scheme A.1).

(2) Ion chromatograph method: The reaction mixture was diluted and then submitted to the ion chromatograph to determine the product amount (after calibration).

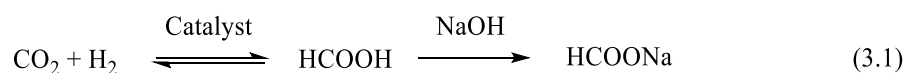
2.2.4 Contact angle measurement

Complex **8** and **9** powder was thoroughly dried under vacuum. Catalyst film (1 cm in diameter on mica sheet) for contact angle measurement was made using tablet machine. The film was blown with rubber suction bulb to obtain a flat surface proper for water contact measurement.

**Chapter 3 Hydrogenation of CO₂ to FA Catalyzed by Ir-*N,N'*
Diimine Catalysts**

3.1 Introduction

Catalytic hydrogenation of CO₂ to chemicals and fuels is an ideal way to reduce the atmospheric CO₂ concentration and fix CO₂ as a C1 resource, provided that hydrogen is produced from renewable resources.^[18, 151-154] Chapter 1 reviews homogeneous hydrogenation of CO₂ to FA/formate with molecular catalysts in a wide variety of organic solvents, ionic liquids, water and supercritical CO₂, usually in the presence of a base affording formate as the product (eqn. 3.1), which is the case we discussed in the last chapter.



In most of the currently reported catalyst systems, base is needed to enhance the hydrogenation of CO₂ to formate. Nevertheless, from the viewpoint of atom economy and eco-friendly process, the direct hydrogenation of CO₂ to FA in water without consuming stoichiometric amount of base is highly appreciated and of great significance. However, the development of novel catalysts for efficient hydrogenation of CO₂ in water without adding base remains challenging. Based on the reported half-sandwich iridium catalysts with bipyridine-derived ligands and the results obtained with the cyclometallated Ir-N[^]C complexes (last chapter), this chapter will focus on the design of [IrCp^{*}L] catalyst for the base-free aqueous hydrogenation of CO₂ to FA.

Several key challenges associated with this transformation were anticipated. First, the ideal catalyst should be active toward C=O double bond hydrogenation. Second, the catalyst should be soluble in aqueous solution. Third, CO₂-saturated water shows pH 4.0 at 20 °C,^[155] thus the catalyst must be stable under acidic conditions. Based on these considerations, this chapter mainly explores iridium complexes containing nonaromatic N,N'-diimine ligands.^[156-159] Although they

haven't been applied for CO₂ hydrogenation, these imidazoline analogues are potentially active towards this transformation in view of its good water solubility, coordination ability and electron-donating property.^[160, 161]

3.2 Hydrogenation of CO₂ to FA with Ir-*N,N'* Complex in Water

3.2.1 Ir-catalyzed CO₂ hydrogenation in water without base

The study started from identifying homogeneous iridium catalysts capable of hydrogenating CO₂ to FA in water without base. A series of *N,N'* ligands, **L11-L20**, were screened in combination with [IrCp*Cl₂]₂ for the hydrogenation of CO₂ and the results are listed in Table 3.1. FA was the only product detected by ¹H NMR (Appendix, Scheme B.1).

Through lowering the conjugacy level of the coordinating N atom and introducing hydrophilic group, i.e. the NH unit, the electron-donating ability and hydrophilicity both increase from **L11** to **L18**. Clearly, the TOF value increases dramatically from none (Table 3.1, entry 1, 2) to near 1000 h⁻¹ (Table 3.1, entries 7, 8). Noteworthy is that ligands **L14-L16**, which contain less electron-donating pyridine and are less water-soluble, show much lower activity than the analogues **L17-L18**. These results demonstrate that the half sandwich iridium catalysts with non-aromatic *N,N'*-diimine ligand are superior for CO₂ hydrogenation to FA compared with iridium complexes bearing aromatic pyridine-type ligands under the given reaction conditions. The two structure analogues **L17** and **L18** present similar high TOFs of 1000 h⁻¹ and 928 h⁻¹, respectively. Replacing the NH motif of **L17** with O, i.e. ligand **L19**, gives a lower TOF of 320 h⁻¹ for FA production (Table 3.1, entry 9). The *in situ* formed iridium catalyst with the tetrahydroxy-bipyrimidine ligand **L20** reported by Himeda and Fujita et al. gives a TOF of only 80 h⁻¹ under such reaction conditions (Table 3.1, entry 10).

Table 3.1 Ligands/catalysts screening for base-free aqueous CO₂ hydrogenation

$$\text{CO}_2 + \text{H}_2 \xrightleftharpoons[\text{H}_2\text{O}]{\text{Catalyst}} \text{HCO}_2\text{H}$$

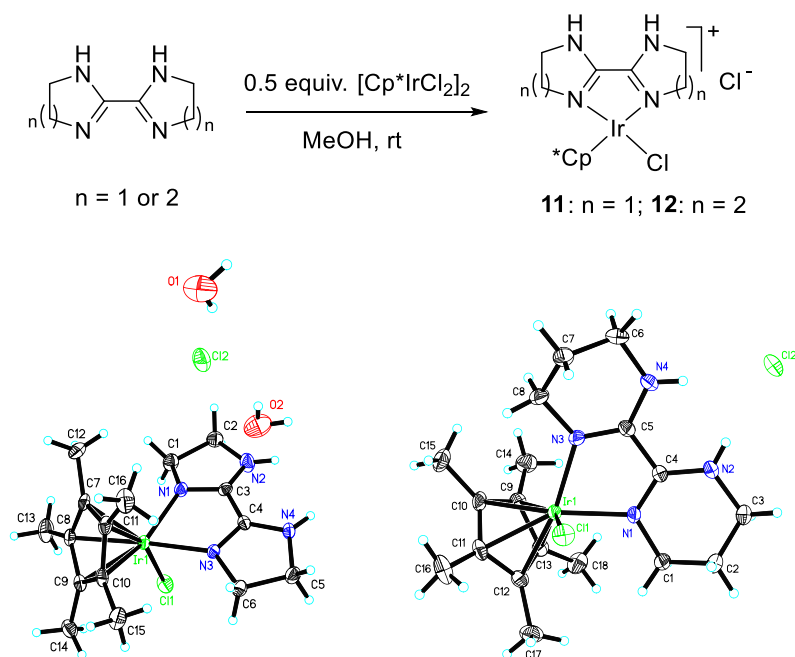
L11: 2,2'-bipyridine
 L12: 2,2'-bipyridine with a benzimidazole-like bridge
 L13: 2,2'-bipyridine with a benzimidazole-like bridge (different orientation)
 L14: 2,2'-bipyridine with a benzimidazole-like bridge (different orientation)
 L15: 2,2'-bipyridine with a 5-membered ring bridge
 L16: 2,2'-bipyridine with a 6-membered ring bridge
 L17: 2,2'-bipyridine with a 5-membered ring bridge (different orientation)
 L18: 2,2'-bipyridine with a 6-membered ring bridge (different orientation)
 L19: 2,2'-bipyridine with a 5-membered ring bridge (different orientation)
 L20: 2,2'-bipyridine with a 1,3,5-triazine-2,4,6-triol bridge
 complex 11: [IrCp*Cl]2+ with a 2,2'-bipyridine-like bridge and a chloride counterion
 complex 12: [IrCp*Cl]2+ with a 2,2'-bipyridine-like bridge and a chloride counterion

Entry	Cat.	HCO ₂ H (mmol) ^a	TOF (h ⁻¹)
1	[IrCp*Cl ₂] ₂ + L11	trace	/
2	[IrCp*Cl ₂] ₂ + L12	trace	/
3	[IrCp*Cl ₂] ₂ + L13	0.005	40
4	[IrCp*Cl ₂] ₂ + L14	0.003	24
5	[IrCp*Cl ₂] ₂ + L15	0.019	152
6	[IrCp*Cl ₂] ₂ + L16	0.008	64
7	[IrCp*Cl ₂] ₂ + L17	0.125	1000
8	[IrCp*Cl ₂] ₂ + L18	0.116	928
9	[IrCp*Cl ₂] ₂ + L19	0.040	320
10	[IrCp*Cl ₂] ₂ + L20	0.010	80
11	Complex 11 ^b	0.128	1024
12	Complex 12 ^c	0.119	952

General reaction conditions: [IrCp*Cl₂]₂ (0.125 μmol), Ir/L = 1/1.2, H₂O (10.0 mL), CO₂/H₂ = 1/1 (5.0 MPa), at 40 °C, 30 min; ^a: average values from two runs with an error less than 10%;

^b: Complex **11** as the catalyst (0.25 μmol); ^c: Complex **12** as the catalyst (0.25 μmol). No reac-

tion was detected without catalyst.



Scheme 3.1 Synthesis and X-Ray structures of complex **11** and **12**

L17 and **L18** can be viewed as conjugated N,N'-diimine ligands (non-aromatic ligands), essentially different from the aromatic bipyridine, bipyrimidine and biimidazole ligands, and have never been used for the hydrogenation of CO₂.^[162] Well-defined complex **11** and **12** were subsequently synthesized in high yields from [IrCp*Cl₂]₂ and ligand **L17** and **L18**, respectively (Scheme 3.1). These two complexes are air-stable and water-soluble, and their crystal structures were determined by X-ray diffraction. For both complexes in the solid state, the iridium atom bonds to the Cp* ligand, a chloride ligand and the two nitrogen atoms of the N,N'-ligand, forming a distorted octahedral coordination geometry with a chloride anion situated outside. The only difference is that complex **11** contains two water molecules, while complex **12** contains none.

With complexes **11** and **12** as the catalyst, TOFs of 1024 h⁻¹ and 952 h⁻¹ were achieved for the CO₂ hydrogenation. These are almost the same level as that of the

catalysts formed *in situ* (Table 3.1, entries 7 vs. 11, 8 vs. 12), indicating that both the prepared iridium complex and the *in situ* formed catalyst can transform into the active species rapidly under the given reaction conditions. Based on a series of exploration, complex **12** was used as the catalyst in the following studies due to its excellent stability.

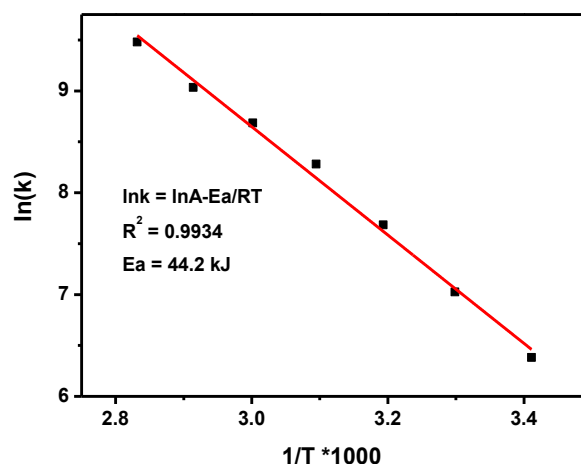
3.2.2 Reaction Mechanism Study

The complex **12** catalyzed hydrogenation of CO₂ was then investigated under varied reaction conditions to gain mechanistic insight. Firstly, the reaction rate increases with elevating of temperature, and a high TOF of 13104 h⁻¹ was obtained at 80 °C for FA production under 5.0 MPa of CO₂/H₂ (1/1) in water (Table 3.2). The apparent activation energy (E_a) is estimated to be 44 kJ•mol⁻¹ (Scheme 3.2), showing that this catalyst is intrinsically active for the hydrogenation of CO₂.

Table 3.2 Temperature effect on the CO₂ hydrogenation in water without base^a

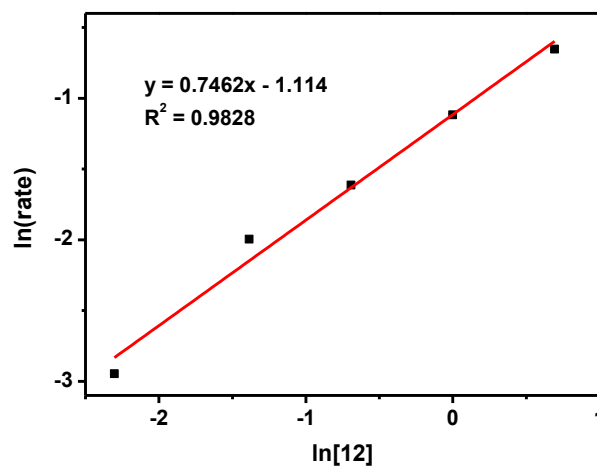
Entry	Temp. (°C)	HCOOH (mmol) ^b	Time (min)	TOF (h ⁻¹) ^c
1	20	0.0371	15	594
2	30	0.0715	15	1143
3	40	0.136	15	2176
4	50	0.165	10	3960
5	60	0.197	8	5910
6	70	0.210	6	8400
7	80	0.273	5	13104

^a: Reaction conditions: complex **12** as the catalyst (0.25 μmol), H₂O (50.0 mL), CO₂/H₂ = 1/1 (5.0 MPa). ^b: Averaged value from two runs with an error less than 10%; ^c: TOF calculated based on the indicated reaction time.

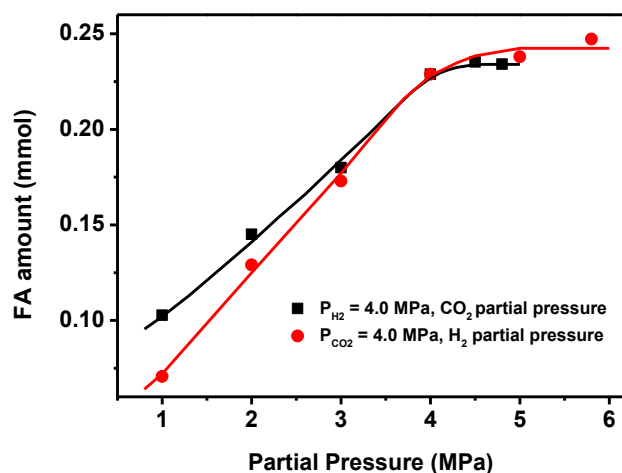


Scheme 3.2 Arrhenius plot of initial TOF values for hydrogenation of CO₂ using complex **12**

The effect of the catalyst concentration on the reaction rate was also investigated and the double logarithmic plot of the initial rate against the catalyst concentration shows linear dependence (Scheme 3.3), revealing approximately a pseudo-first order (0.75) in the concentration of catalyst precursor.



Scheme 3.3 Plot of Ln (rate) versus Ln([**12**]): complex **12** as the catalyst (0.1-5.0 μmol), H₂O (50.0 mL), 5.0 MPa of CO₂/H₂ (1/1), 40 °C, 15 min, conversion less than 10%.



Scheme 3.4 H_2 and CO_2 partial pressure-dependent initial reaction rate for the hydrogenation of CO_2 : complex **12** ($0.25 \mu\text{mol}$) in H_2O (50.0 mL) at 40°C . FA production was determined at 15 min after reaction started.

As shown in Scheme 3.4, the partial pressures of H_2 and CO_2 both affect the rate of CO_2 hydrogenation. When CO_2 pressure was maintained at 4.0 MPa , the H_2 pressure-dependent FA production increases with the increasing pressure of H_2 to approach a constant value (●). The CO_2 pressure-dependent FA production with H_2 pressure maintained at 4.0 MPa shows a similar trend and also exhibits saturation behavior (■). The hydrogenation activity with complex **12** linearly depends on P_{H_2} and P_{CO_2} at P_{H_2} and $P_{\text{CO}_2} < 4.0 \text{ MPa}$; thus it can be concluded that this reaction show first order dependence with respect to both substrates under the given conditions. These results appear to indicate that the turnover rate of the hydrogenation is determined by the step of CO_2 insertion into an iridium-hydride bond (*vide infra*).

A deuterium kinetic isotope effect (KIE) study was then conducted for the CO_2 hydrogenation. As shown in Table 3.3, when the solvent H_2O was replaced with D_2O , the reaction rate increased remarkably either using H_2 where the TOF increased from 280 h^{-1} in H_2O to 768 h^{-1} in D_2O (Table 3.3, entries 1 vs. 3) or using

D₂ with which the TOF increased from 272 h⁻¹ in H₂O to 548 h⁻¹ in D₂O (Table 3.3, entries 2 vs. 4). Inverse solvent isotope effect (SIE) of 0.36 and 0.48 was obtained from the reactions with H₂/D₂O and D₂/D₂O, respectively, which is also confirmed with ¹H NMR (Appendix, Scheme B.2), illustrating D₂O as solvent being more favorable for the CO₂ hydrogenation than H₂O. In addition, the results in Table 3.3 also indicate that in H₂O, the reaction rate decreased slightly by replacing H₂ with D₂ (Table 3.3, entries 1 vs. 2), and replacing H₂ with D₂ in D₂O also decreased the reaction rate (Table 3.3, entries 3 vs. 4).

Table 3.3 Kinetic isotope effect in aqueous hydrogenation of CO₂ with complex **12**^a

Entry	Gas (1/1)	Solvent	HCO ₂ H (mmol) ^b	TOF (h ⁻¹)	KIE ^c
1	CO ₂ /H ₂	H ₂ O	0.035	280	/
2	CO ₂ /D ₂	H ₂ O	0.034	272	1.03
3	CO ₂ /H ₂	D ₂ O	0.096	768	0.36
4	CO ₂ /D ₂	D ₂ O	0.073	584	0.48

^aGeneral reaction conditions: complex **12** (0.25 μmol), H₂O or D₂O (10.0 mL), CO₂/H₂ or CO₂/D₂ = 1/1 (2.0 MPa); at 40 °C, 30 min; ^b Average values from two runs with an error less than 10%. ^c KIE = TOF (entry 1)/TOF (entry n) (n = 2, 3, 4)

As mentioned in the last chapter, water effect in homogeneous hydrogenation of CO₂ has been widely noted and investigated. For instance, in organic solvents, small amount of added water can enhance the reaction rates presumably by stabilizing the transition state through an H-bonding interaction between the coordinated water molecule and the oxygen atom of the approaching CO₂ in its insertion to a metal-hydride bond.^[72] Moreover, in basic aqueous solution, a normal KIE was obtained with a proton-responsive iridium complex for CO₂ hydrogenation to formate,^[69] demonstrating the involvement of water in the rate-determining step to accelerate the heterolysis of H₂. In our case, the significant inverse KIE results

imply that water might play an additional role.^[163]

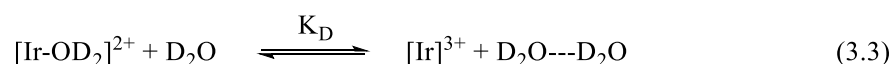
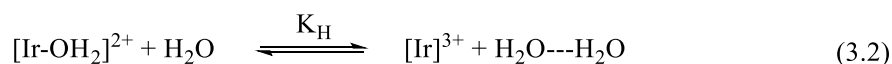
Table 3.4 Hydrogenation of CO₂ in water with additives^a

Entry	Cat. Precursor	Additive (eqv. to Ir)	HCO ₂ H (mmol) ^b	TOF (h ⁻¹) ^c
1	12	-	0.119	952
2	13	-	0.125	1000
3	12	NaCl (60)	0.089	712
4	12	NaCl (200)	0.074	592
5	12	NaCl (568)	0.043	344
6	12	NaCl (20000)	trace	/
7	12	NaI (2)	0.025	200
8	12	NaI (5)	0.010	80
9	12	NaI (100)	trace	/
10 ^d	13	PPh ₃ (5)	trace	/
11 ^d	13	-	0.128	1024

^a: General reaction conditions: Cat. (0.25 μmol), H₂O (10.0 mL), CO₂/H₂ = 1/1 (5.0 MPa), at 40 °C, 30 min; ^b: Measured on SHINEHA CIC-100 ion chromatograph with the Shodex column (IC SI-52 4E); ^c: Averaged rate for initial 30 min. ^d: Reaction solution: H₂O (9.5 mL) + MeOH (0.5 ml).

Inverse KIE (KIE<1) resulting from a SIE is a signature for pre-equilibrium aquo release from a metal center, which has been well documented in the literature.^[164, 165] It has been reported that many of the half-sandwich cyclopentadienyl [IrCp*(L)Cl] complexes hydrolyze in water to form [IrCp*(L)(H₂O)] complexes which are generally considered as the precursors of the active species.^[166, 167] In this context, the aquo iridium complex [Cp*Ir(**L18**)(H₂O)][BF₄]₂ (complex **13**) was synthesized and applied to the CO₂ hydrogenation, and a TOF of 1000 h⁻¹ for the production of FA was obtained, almost the same level as complex **12** (Table

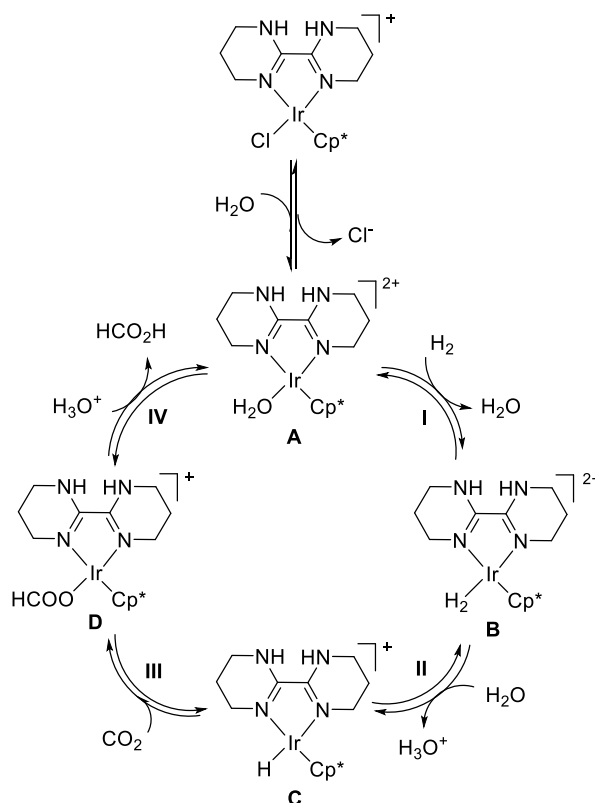
3.4, entries 1 vs. 2). Thus when used for the hydrogenation of CO₂ in water, complex **12** is proposed to hydrolyze first to form the aqua complex. Afterwards, an equilibrium process involving the dissociation of the coordinating water molecule from the iridium center occurs, which precedes the turnover-limiting step. Due to the easier dissociation of D₂O from the iridium center than H₂O or more favorable equilibrium of D₂O dissociation than H₂O (eqn. 3.2 & 3.3),^[165] the reaction rate in D₂O is expected to be faster, giving rise to the observed inverse KIE. Therefore, the aquo iridium species formed from complex **12** in water is considered to be an active species and water release from the iridium center could be an important process that affects the rate of this reaction.



It was also found that the addition of other coordinating ligands retarded this reaction, likely by diminishing the concentration of active species. For example, the FA production with complex **12** declines with the increasing amount of NaCl added in (Table 3.4, entries 3-6). With the addition of NaI, the rate drop was more significant (Table 3.4, entries 7-9). When PPh₃ was added to the hydrogenation reaction with complex **13** as the catalyst (Table 3.4, entry 10), no reaction was observed, probably because the strong coordination ability of PPh₃ leads to its difficult dissociation from iridium center, blocking the coordination of H₂.^[168] These results support indirectly the notion that water dissociation from the iridium center is a precondition for catalysis to occur.

The possible catalytic intermediates generated from complex **12** were monitored by ¹H NMR. When H₂ (1.5 Mpa, 25 °C) was filled to the H₂O/CD₃OD solution of **12**, a new peak at δ = -12.09 ppm (Appendix, Scheme B.4) appeared immediately, which can be assigned to the chemical shift of a [Ir-*H*]⁺ species.^[62, 67]

Switching to a H_2/CO_2 mixture (1.2 MPa), besides the peak of the $[\text{Ir-H}]^+$ species, another new peak at $\delta = 8.19$ ppm appeared, which is assigned to the chemical shift of $\text{H-CO}_2\text{H}$ (Appendix, Scheme B.5). In $\text{H}_2\text{O}/\text{D}_2\text{O}$ solution, although FA could be detected ($\delta = 8.30$ ppm, Appendix, Scheme B.6), the iridium hydride was not observed even for a long time under H_2/CO_2 pressure, possibly due to the instability of this iridium hydride in the more acidic water solution compared to the $\text{H}_2\text{O}/\text{CD}_3\text{OD}$ solution. It is important to note that during the *in-situ* ^1H NMR probing, the iridium complex (likely $[\mathbf{12}\text{-H}_2\text{O}]^{2+}$) remained as it was from the beginning. These observations indicate the aqua complex to be the catalyst resting state.



Scheme 3.5 Proposed mechanism for base-free aqueous CO_2 hydrogenation with complex **12**

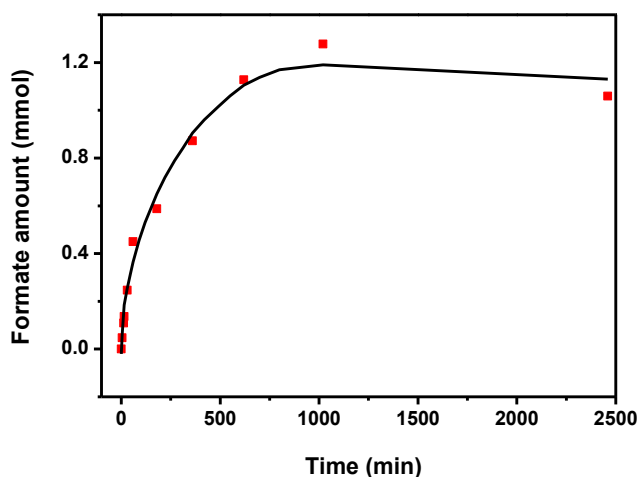
Based on these results, the catalytic cycle of the aqueous hydrogenation of CO_2 with complex **12** under acidic conditions is proposed in Scheme 3.5. Firstly, com-

plex **12** hydrolyzes rapidly in water, forming the aquo complex **A**. Then the catalytic cycle experiences the H₂-coordinated iridium species **B** (step I), the iridium hydride species **C** (step II) and the iridium formate species **D** (step III) in sequence, corresponding to the H₂ coordination step, H₂ splitting process and CO₂ insertion process, respectively. Each of these reactions is reversible, as will be presented in the next chapter. During the catalytic reaction, the iridium formate complex **D** is undetectable with ¹H NMR either in water or in H₂O/CD₃OD mixture (Appendix, Scheme B.5, B.6), suggesting the rapid exchange of the formate with a hydronium ion (H₃O⁺) to produce HCO₂H (step IV, $\delta = 8.30$ ppm in H₂O/D₂O, Appendix, Scheme B.6; $\delta = 8.19$ ppm in H₂O/CD₃OD, Appendix, Scheme B.5) and the regeneration of iridium aqua complex **A**.

The linear dependence of the reaction rate on the pressure of H₂ and CO₂ appears to suggest that the hydrogenation is turnover-limited by the step of CO₂ insertion under the conditions employed, which is also supported by the detection of a [Ir-H] species and the invisibility of the iridium formate species during ¹H NMR monitoring of the reaction.

3.2.3 Thermodynamics of the base-free aqueous hydrogenation of CO₂

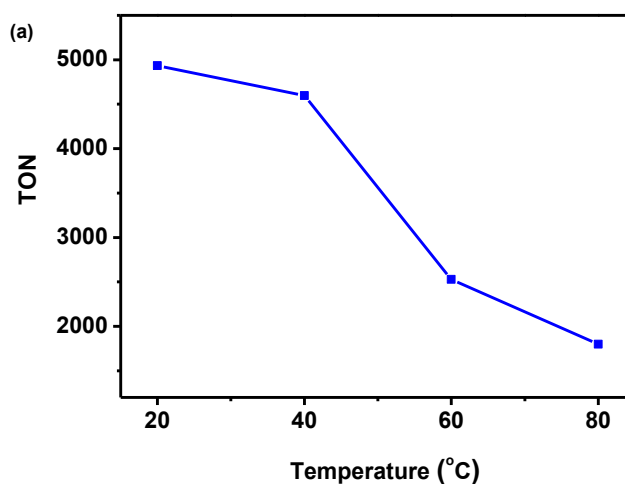
Apart from the kinetic study, the thermodynamics of the CO₂ hydrogenation to FA catalyzed by complex **12** was also investigated. Scheme 3.6 shows the time-dependent TONs at 40 °C under 5.0 MPa of CO₂/H₂. A TOF of 2174 h⁻¹ was achieved in the first fifteen minutes. The FA amount obtained after 17 h reached a constant value, implying that the equilibrium shown in eqn. 3.1 has been reached.

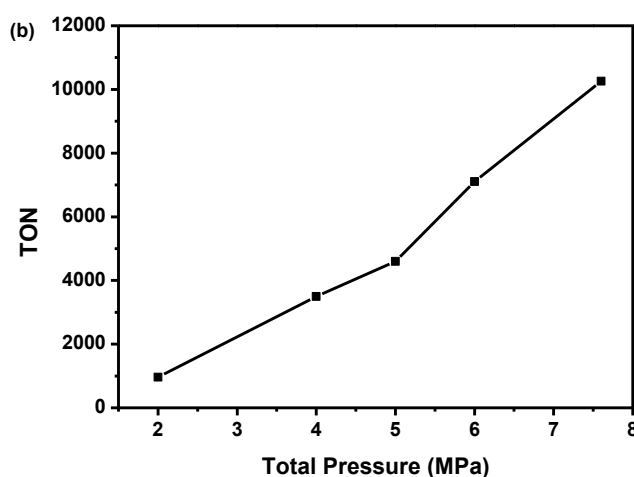


Scheme 3.6 Plot of FA amount versus the reaction time

Reaction conditions: complex **12** (0.25 μmol), H_2O (50.0 mL), 40 $^\circ\text{C}$, 5.0 MPa CO_2/H_2 (1/1).

Scheme 3.7a shows that the final TON increases with decreasing temperature, though the initial reaction rate increases with the increasing reaction temperature (Table 3.2). This agrees well with the reaction being exothermic. For long-time reaction, increasing the total pressure of H_2/CO_2 greatly increases the final TON (Scheme 3.7b), which shifts the reversible reaction forward (eqn. 3.1). Thus, naturally a high TON of 10258 was achieved at a low temperature of 40 $^\circ\text{C}$ and high pressure of 7.6 MPa of H_2/CO_2 (1:1).





Scheme 3.7 (a) TON of CO₂ hydrogenation at different temperatures; (b) TON of CO₂ hydrogenation under varied total gas pressure.

General conditions: complex **12** (0.25 μmol), H₂O (50.0 mL), 40 °C, CO₂/H₂ = 1/1, 8-90 h.

3.3 Hydrogenation of CO₂ to Formate with Ir-*N,N'* Complex

The hydrogenation of CO₂ to formate in the presence of base was also investigated with complex **12**. As shown in Table 3.5, the hydrogenation reaction proceeds faster. A TOF of 37488 h⁻¹ was obtained at 80 °C and 5.0 MPa of CO₂/H₂ (1:1) in 50 mL of 1 M NaHCO₃ aqueous solution (Table 3.5, entry 1), which is comparable with the best literature results under similar reaction conditions in water.^[66] A TON of 87200 was achieved when the reaction was carried out in 1 M of NaHCO₃ solution after 16 hours (Table 3.5, entry 2). When more soluble KHCO₃ was used as the base, a solution of 0.98 M potassium formate was yielded with a TON of 196800 in 24 h (Table 3.5, entry 3). As mentioned earlier, complex **11** is less stable than **12**. For the long-time hydrogenation of CO₂ in basic solution, complex **11** gave a TON of 53200 in 24 h, which is much less compared with complex **12** (Table 3.5, entry 4). Thus the following studies were performed with **12** as well.

Table 3.5 Results of the hydrogenation reaction in the presence of base^a

Entry	Base solution	Time	Formate (mmol)	TOF (h ⁻¹)	Final [Formate] (M)	TON
1	NaHCO ₃ (1M)	5 min	0.781	37488	-	-
2	NaHCO ₃ (1M)	16 h	21.8	-	0.44	87200
3	KHCO ₃ (2M)	24 h	49.2	-	0.98	196800
4 ^b	KHCO ₃ (2M)	24h	13.3	-	0.26	53200

^a: Complex **12** (0.25 μmol), base solution (50 mL), CO₂/H₂ = 1/1 (5.0 MPa), 80 °C; ^b: Complex **11** (0.25 μmol) was used as the catalyst.

Table 3.6 Temperature effect on the reaction in the presence of base^a

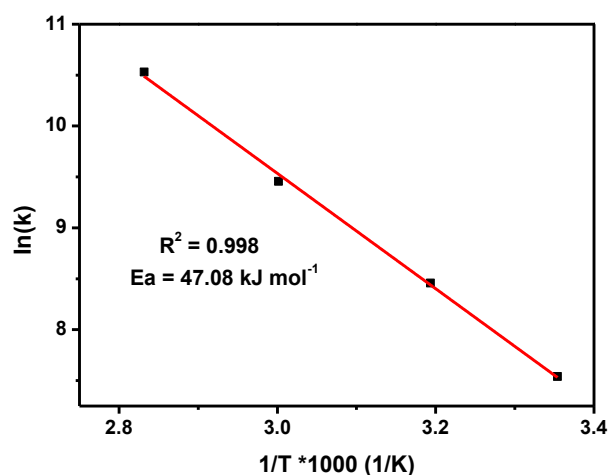
Entry	Temp. (°C)	HCOO ⁻ (mmol)	TOF (h ⁻¹)
1	25	0.471	1884
2	40	1.18	4720
3	60	3.20	12800
4	80 ^b	0.781	37488

^a: General conditions: complex **12** (0.25 μmol), NaHCO₃ (1M, 51 mL), CO₂/H₂ = 1/1 (5.0 MPa), 1h; ^b: reaction time is 5 min.

The apparent activation energy (E_a) of 47 kJ•mol⁻¹ was obtained from the temperature dependence of the initial reaction rate in aqueous NaHCO₃ solution (Table 3.6, Scheme 3.8), almost the same as that (44 kJ•mol⁻¹) obtained in water without base.

In the presence of base, KIE study was also performed. As shown in Table 3.7, when the hydrogenation of CO₂ was carried out in H₂O using NaHCO₃ as the base, a TOF of 2728 h⁻¹ and 2824 h⁻¹ was obtained with H₂ and D₂, respectively (Table 3.7, entries 1, 2). The KIE value of 0.97 indicates that H₂ heterolysis may not be the rate-determining step. When the reaction was carried out in D₂O (NaDCO₃ as base), the reaction rate decreased slightly, and a KIE of 1.12 and 1.24 was ob-

tained with H₂ and D₂ (Table 3.7, entries 3, 4). Compared with the KIE results in the absence of base, the KIE in the presence of base is not that significant. Worth noting is that a reverse KIE is not observed suggesting that water dissociation no longer affects the hydrogenation rate. The slightly higher KIE shown in entry 4 may indicate that CO₂ insertion into the Ir-H bond is rate limiting.



Scheme 3.8 Arrhenius plot of initial TOFs for CO₂ hydrogenation in the presence of base

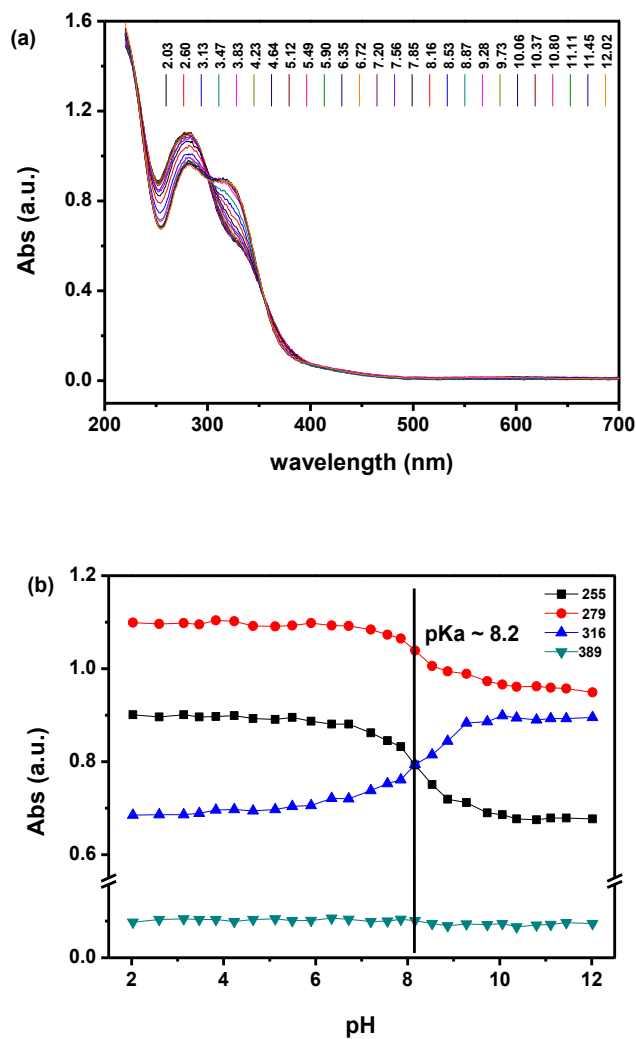
Table 3.7 KIE in the hydrogenation of CO₂ in the presence of base^a

Entry	Gas	Solution	HCOO ⁻ (mmol) ^b	TOF (h ⁻¹)	KIE
1	CO ₂ /H ₂	NaHCO ₃ /H ₂ O	0.341	2728	/
2	CO ₂ /D ₂	NaHCO ₃ /H ₂ O	0.353	2824	0.97
3	CO ₂ /H ₂	NaDCO ₃ /D ₂ O	0.304	2432	1.12
4	CO ₂ /D ₂	NaDCO ₃ /D ₂ O	0.275	2200	1.24

^a: Reaction conditions: complex **12** as the catalyst (0.25 μmol), NaHCO₃/H₂O or NaDCO₃/D₂O (1.0 M, 10.0 mL), CO₂/H₂ = 1/1 (2.0 MPa); 40 °C, 30 min. ^b: Average values from two runs with an error less than 10%.

The behavior of complex **12** in water under different pH conditions was studied using UV-Vis absorption spectroscopy. As shown in Scheme 3.9, the complex re-

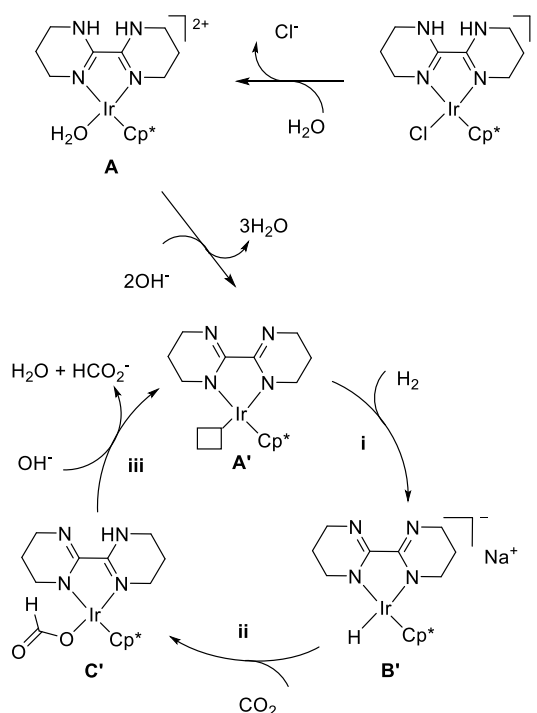
mains unchanged structurally below pH 6, and loses the NH proton on the ligand under basic conditions.^[68, 128, 169] The pKa value of complex **12** in water was estimated to be 8.2. ¹H NMR of complex **12** in H₂O/D₂O and CDCl₃ both manifest the disappearance of the NH proton after the addition of Na₂CO₃ and NaOtBu (Appendix, Scheme B.7, B.8).



Scheme 3.9 (a) The UV-Vis absorption spectra of complex **12** measured at pH values in the range from 2.0 to 12.0; (b) Absorbance changes at 255 nm, 279 nm, 316 nm and 389 nm as a function of pH change.

Based on these investigations and the *in situ* ¹H NMR results, the reaction mechanism of CO₂ hydrogenation to formate in the presence of base with com-

plex **12** is tentatively proposed in Scheme 3.10.



Scheme 3.10 Proposed mechanism for CO₂ hydrogenation in the presence of base

As mentioned above, complex **12** will lose the NH protons in basic solution. Deprotonation of the NH unit likely results in a ligand isomerization and the resulting electron-donating amide may expell the coordinating aquo ligand, forming the electro-neutral complex **A'** as shown in Scheme 3.10. This would explain why there is no SIE. When the hydrogenation of CO₂ was performed using complex **12** in NaOH/H₂O/D₂O solution which was bubbled with continuous flow of H₂/CO₂ (1:1) for 10 min, the intermediate iridium hydride (potentially **B'**) was detected at $\delta = -11.91$ ppm by ¹H NMR (Appendix, Scheme B.9). Additionally, a signal of 8.37 ppm was observed, which is ascribed to the free formate proton (*HCOO*⁻) dissociated from the Ir-formato complex **C'**. Since the formate proton signal of **C'** was not detected, CO₂ insertion is again proposed to be the RDS, which is in line with the KIE results, and the similarity in the E_a's obtained for the base-free and

base-promoted reactions. Nevertheless, further study still need to be done in the future to understand more about the reaction mechanism.

3.4 Summary

An efficient iridium complex has been developed for the direct hydrogenation of CO₂ to FA in water without base under mild conditions. A TOF over 13000 h⁻¹ was obtained at 80 °C and 5.0 MPa, which is the highest TOF reported to date under similar conditions.

The *in situ* ¹H NMR and kinetic isotopic effect study reveals that whilst the CO₂ insertion may be the rate-limiting step, the dissociation of the coordinated water molecule from the iridium complex affects considerably the turnover rate of the catalytic cycle. Thus, water appears to play a double role in this reaction, facilitating CO₂ insertion via hydrogen bonding, and limiting the catalytic turnover through coordination to the active catalytic center.

The successful application of the iridium N,N'-diimine complex for base-free CO₂ hydrogenation extends the ligand type and provides a strategy to develop new catalytic systems for CO₂ hydrogenation. Moreover, this iridium catalyst also shows satisfying reactivity for the hydrogenation of CO₂ in basic aqueous solution, making it more adaptable to various potential applications in the future.

3.5 Experimental Section

3.5.1 General information

Instruments: Details have been given in Chapter 2. Solution pH was measured on a ZDJ-400DH multi-function titrator which was calibrated before use. The X-Ray structures of complexes **11-13** were determined by State Key Laboratory of Organometallic Chemistry (Shanghai).

Chemicals: NaHCO₃, Na₂CO₃, KOH, and KHCO₃ were purchased from Tianjin Kemiou Chemical Reagent Co., Ltd. Sodium formate was purchased from Sinopharm Chemical Reagent Co. Ltd. [IrCp*Cl₂]₂, ligand **L11** and **L19** were purchased from J&K. 3-(Trimethylsilyl)-1-propane sulfonic acid sodium salt (DSS) was purchased from Aladdin. Deionized water used in this work was obtained from PURELAB Ultra water purification system. Other ligands were synthesized according to literature procedures.

3.5.2 Synthesis and characterization of ligands and complexes

L12^[170, 171]: white solid; ¹H NMR (400 MHz, d₆-DMSO): δ (ppm) = 13.53 (s, 2H), 7.64 (s, 4H), 7.27 (s, 4H); ¹³C {¹H} NMR (100 MHz, d₆-DMSO): δ (ppm) = 144.3, 123.5, 119.7, 112.4; *m/z* (ESI⁺) [M+H]⁺ calcd 235.0984, obsd 235.0973.

L13^[172]: white solid; ¹H NMR (400 MHz, CDCl₃): δ (ppm) = 11.34 (s, 1H), 8.64 (m, 1H), 8.48 (m, 1H), 7.87 (m, 2H), 7.40 (m, 2H), 7.28 (m, 2H); ¹³C {¹H} NMR (100 MHz, CDCl₃): δ (ppm) = 149.1, 148.5, 137.5, 124.7, 124.0, 122.8, 121.9, 120.2, 111.4; *m/z* (ESI⁺) [M+H]⁺ calcd 196.0875, obsd 196.0864.

L14^[173]: white solid; ¹H NMR (400 MHz, CDCl₃): δ (ppm) = 11.46 (s, 1H), 8.51 (d, *J* = 4.0 Hz, 1H), 8.21 (*J* = 8.0 Hz, 1H), 7.79 (m, 1H), 7.24 (m, 2H), 7.13 (s, 1H); ¹³C {¹H} NMR (100 MHz, CDCl₃): δ (ppm) = 148.7, 146.4, 137.4, 130.5, 123.3, 120.2, 117.7; *m/z* (ESI⁺) [M+H]⁺ calcd 146.0718, obsd 146.0711.

L15^[174]: white solid; ¹H NMR (400 MHz, CDCl₃): δ (ppm) = 8.56 (d, *J* = 4.5 Hz, 1H), 8.14 (d, *J* = 7.9 Hz, 1H), 7.76 (td, *J* = 7.8, 1.4 Hz, 1H), 7.34 (dd, *J* = 6.9, 5.3 Hz, 1H), 5.36 (br s, 1H), 3.84 (s, 4H); ¹³C {¹H} NMR (100 MHz, CDCl₃): δ (ppm) = 164.4, 148.6 (d, *J* = 20.0 Hz), 148.5, 136.7, 125.2, 122.4, 50.5; *m/z* (ESI⁺) [M+H]⁺ calcd 148.0875, obsd 148.0866.

L16^[175]: white solid; ¹H NMR (400 MHz, d₆-DMSO): δ (ppm) = 9.94 (s, 1H), 8.79 (d, *J* = 4.8 Hz, 1H), 8.17~8.10 (m, 2H), 7.77~7.74 (m, 1H), 3.52 (t, *J* = 5.6

Hz, 4H), 1.96 (m, 2H); ^{13}C { ^1H } NMR (100 MHz, d6-DMSO): δ (ppm) = 155.8, 150.2, 145.0, 138.9, 128.5, 122.6, 39.4, 18.3; m/z (ESI $^+$) [$\text{M}+\text{H}$] $^+$ calcd 162.1031, obsd 162.1025.

L17^[160, 161]: white solid; ^1H NMR (400 MHz, D $_2\text{O}$): δ (ppm) = 3.69 (s, 8H); ^{13}C { ^1H } NMR (100 MHz, D $_2\text{O}$): δ (ppm) = 159.44, 50.57 (br). HRMS: C $_6\text{H}_{10}\text{N}_4$, calcd 138.0905, obsd 138.0913.

L18^[160, 161]: white solid; ^1H NMR (400 MHz, D $_2\text{O}$): δ (ppm) = 3.18 (t, J = 6.0 Hz, 8H), 1.64-1.58 (m, 4H); ^{13}C { ^1H } NMR (100 MHz, D $_2\text{O}$): δ (ppm) = 152.3, 40.7, 19.4; HRMS: C $_8\text{H}_{14}\text{N}_4$, calcd 166.1218, obsd 166.1223.

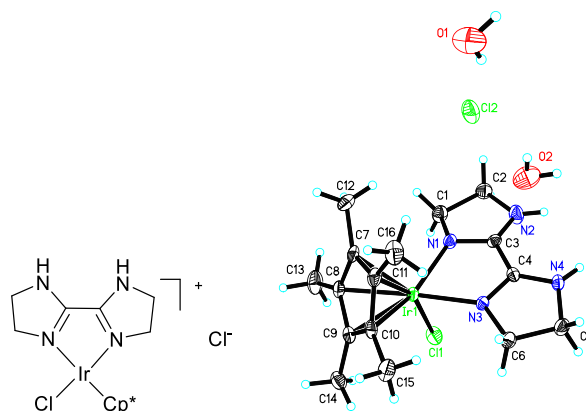
L20^[67]: white solid; ^1H NMR (400 MHz, d6-DMSO): δ (ppm) = 11.71 (b, 2H), 5.60 (s, 1H); ^{13}C { ^1H } NMR (100 MHz, d6-DMSO): δ (ppm) = 168.4, 153.8, 91.3; m/z (ESI $^+$) [$\text{M}+\text{H}$] $^+$ calcd 223.0467, obsd 223.0449.

Complex **11** [IrCp*(**L17**)Cl]Cl:

Under an argon atmosphere, dry methanol (30 mL) was added to the mixture of [IrCp*Cl $_2$] $_2$ (0.1 mmol) and **L17** (0.2 mmol) in a flask bottle which was stirred at room temperature. After approximately half an hour, the mixture became a yellow-green clear solution, and stirring was maintained overnight. Then, the methanol was removed under reduced pressure. Diethyl ether was added to the residue, which created a powder. After being filtered and washed with ether, a yellow powder was obtained. If the powder could not be formed after adding ether, column chromatography was used to purify the complex using CH $_2\text{Cl}_2$ /MeOH (50:1-20:1) as the eluent. Yield: 84%. Crystal of complex **11** that was suitable for X-ray diffraction was obtained from a mixture of CH $_2\text{Cl}_2$ and ether. ^1H NMR (400 MHz, D $_2\text{O}$): δ (ppm) = 3.88-3.99 (m, 8H), 1.67 (s, 15H); ^{13}C { ^1H } NMR (100 MHz, D $_2\text{O}$): δ (ppm) = 161.4, 87.8, 51.8, 46.7, 8.6; m/z (ESI $^+$) 501.1 [$\text{M}-\text{Cl}$] $^+$; elemental analysis for C $_{16}\text{H}_{25}\text{Cl}_2\text{IrN}_4\cdot\text{H}_2\text{O}$ calcd: C 34.66, H 4.91, N 10.10; found:

C 35.02, H 5.23, N 9.81.

$C_{16}H_{29}Cl_2IrN_4O_2$, CH_2Cl_2/Et_2O , $M = 572.53$, yellow crystals, $0.145 \times 0.111 \times 0.066 \text{ mm}^3$ Monoclinic, Space group $P 21/c$, $a = 7.6158 (8) \text{ \AA}$, $\alpha = 90^\circ$, $b = 11.7394(12) \text{ \AA}$, $\beta = 97.916(2)^\circ$, $c = 23.093(2) \text{ \AA}$, $\gamma = 90^\circ$, $V = 2044.9(4) \text{ \AA}^3$, $Z = 4$, $D_c = 1.860 \text{ mg/m}^3$, $T = 293 (2) \text{ K}$, 11740 reflections collected, 4020 independent reflections $R_{\text{int}} = 0.0340$, Goodness-of-fit on $F^2 = 1.121$, $RI = 0.0317$, $wR2 = 0.0681$, 6 restraints, 255 parameters, absorption coefficient = 6.807 mm^{-1} .

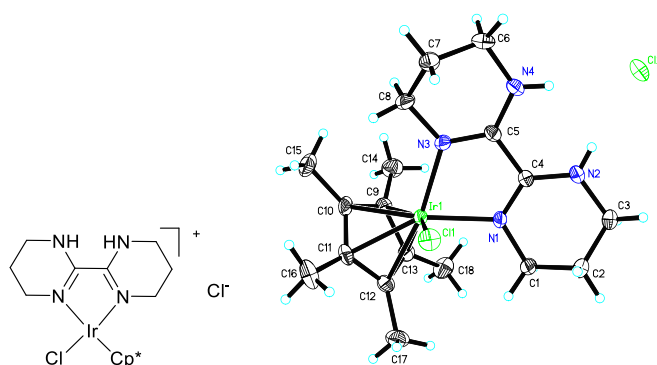


Complex **12** [IrCp*(**L18**)Cl]Cl:

Complex **12** was obtained using the similar procedure as for complex **11**: yellow solid; Yield: 85%. ^1H NMR (400 MHz, D_2O): δ (ppm) = 3.69 (t, $J = 5.6 \text{ Hz}$, 4H), 3.37 (t, $J = 5.6 \text{ Hz}$, 4H), 1.82-1.88 (m, 4H), 1.58 (s, 15H); $^{13}\text{C}\{^1\text{H}\}$ NMR (100 MHz, D_2O): δ (ppm) = 155.9, 87.4, 49.4, 37.9, 20.6, 8.3. m/z (ESI $^+$) 529.2 [M-Cl] $^+$; elemental analysis for $C_{18}H_{29}Cl_2IrN_4$ calcd: C 38.29, H 5.18, N 9.92; found: C 37.92, H 5.16, N 10.21.

$C_{18}H_{29}Cl_2IrN_4$, CH_2Cl_2/Et_2O , $M = 564.55$, yellow columnar crystals, $0.176 \times 0.143 \times 0.065 \text{ mm}^3$ Monoclinic, Space group $P 21/n$, $a = 11.1798 (7) \text{ \AA}$, $\alpha = 90^\circ$, $b = 10.9776(6) \text{ \AA}$, $\beta = 96.3380(10)^\circ$, $c = 16.8241(10) \text{ \AA}$, $\gamma = 90^\circ$, $V = 2052.2(2) \text{ \AA}^3$, $Z = 4$, $D_c = 1.827 \text{ mg/m}^3$, $T = 293 (2) \text{ K}$, 12184 reflections collected, 4046 independent reflections $R_{\text{int}} = 0.0314$, Goodness-of-fit on $F^2 = 1.049$, $RI = 0.0210$,

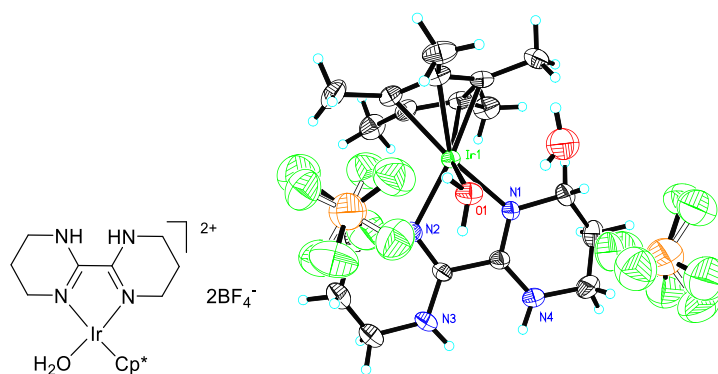
$wR2 = 0.0486$, 2 restraints, 239 parameters, absorption coefficient = 6.775 mm^{-1} .



Complex **13** ($[\text{IrCp}^*(\mathbf{L18})(\text{H}_2\text{O})][\text{BF}_4]_2$):

Complex **12** (0.1 mmol) and AgBF_4 (2 eqv.) were weighed and added to a round bottom flask along with H_2O (5.0 mL). The reaction was stirred vigorously at room temperature overnight. The reaction mixture was filtered and the solvent was removed in vacuo to give a bright yellow solid. Crystals suitable for X-ray diffraction analysis was obtained out of water. Yield, 65.0 mg, 95%; ^1H NMR (400 MHz, D_2O) δ (ppm) = 3.88 (t, $J = 5.2$ Hz, 4H), 3.48 (t, $J = 5.4$ Hz, 4H), 1.98 (m, 4H), 1.68 (s, 15H); ^{13}C $\{^1\text{H}\}$ NMR (100 MHz, D_2O) δ (ppm) = 157.6, 86.8, 49.2, 38.1, 20.2, 8.3; m/z (ESI^+) 247.1 $[\text{M}-2\text{BF}_4-\text{H}_2\text{O}]^{2+}$.

$\text{C}_{18}\text{H}_{33}\text{B}_2\text{F}_8\text{IrN}_4\text{O}_2$, $\text{CH}_2\text{Cl}_2/\text{Et}_2\text{O}$, $M = 703.30$, yellow bulk crystals, $0.33 \times 0.28 \times 0.25 \text{ mm}^3$ Triclinic, Space group $P-1$, $a = 8.6729$ (15) Å, $\alpha = 85.039(3)^\circ$, $b = 11.3034(19)$ Å, $\beta = 74.421(3)^\circ$, $c = 13.751(2)$ Å, $\gamma = 78.507(3)^\circ$, $V = 1271.8(4)$ Å³, $Z = 2$, $D_c = 1.837 \text{ mg/m}^3$, $T = 293 \text{ K}$, 13116 reflections collected, 7928 independent reflections $R_{\text{int}} = 0.0322$, Goodness-of-fit on $F^2 = 1.021$, $RI = 0.0486$, $wR2 = 0.1202$, 298 restraints, 397 parameters, absorption coefficient = 5.331 mm^{-1}



3.5.3 Procedure for catalytic hydrogenation of CO_2 in water

The *in situ* prepared catalysts were freshly formed from $[IrCp^*Cl_2]_2$ (1.0 equiv.) and ligands (2.4 equiv.) in degassed water with the help of ultrasonic wave. The catalyst stock solution was kept for the hydrogenation reaction within 10 h. Similarly, the stock solution of complex **11**, **12** and **13** were prepared using degassed water.

For the hydrogenation reaction without base, degassed water (9.0 mL) and the catalyst stock solution (1.0 mL) were added to a 300 mL glass-lined stainless steel autoclave reactor equipped with a stirring bar under argon protection. The autoclave was then sealed, purged three times with CO_2 carefully and finally pressurized to the required pressure. Then hydrogen was filled till the total pressure reached the desired value. The autoclave reactor was stirred in a water bath right away with temperature held at the desired value in advance. After the reaction, e.g. 30 min, the autoclave was put into an ice-water bath and gas was slowly released in a fume hood upon cooling. Afterwards, NaOH (1.0 M, 0.5 mL) was added to the reaction solution which was then diluted with water and submitted to SHINEHA CIC-100 ion chromatograph to determine the amount of formate generated.

For long-time reaction, the CO_2 hydrogenation reaction was performed directly

in the autoclave without glass lining to avoid the influence of solvent evaporation. The blank reaction was carried out without catalyst at 40 °C and 5.0 MPa of CO₂/H₂ (1/1) for 16 h, and only trace amount of FA was detected, which is negligible.

For the hydrogenation reaction in the presence of base, the procedure was exactly the same as described above, using basic aqueous solution (1 M NaHCO₃ or 2 M KHCO₃) instead of water.

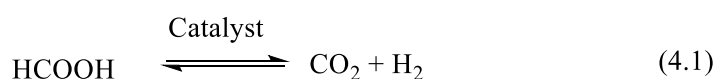
3.5.4 UV-Vis absorption measurement

The pH of the solutions was adjusted by mixing the stock solution of complex **12** (0.15 mM) in 0.02 M H₂SO₄ and 0.1 M NaOH. The UV/Vis spectra were recorded right after testing the pH value.

**Chapter 4 Formic Acid Dehydrogenation Catalyzed by Ir-*N,N'*
diimine Catalysts**

4.1 Introduction

Formic acid is a promising chemical hydrogen storage compound because it is a nontoxic liquid at ambient temperature and can be easily handled and transported.^[176-179] The dehydrogenation of FA (eqn. 4.1), as a companion reaction to CO₂ hydrogenation, is an indispensable step in a hydrogen storage system using FA as the hydrogen storage material. The hydrogenation of CO₂ to formate/FA under mild conditions has been discussed in Chapters 2 and 3; thus this chapter will focus on the dehydrogenation of FA using homogeneous catalysts.



The dehydrogenation of FA to generate hydrogen has been extensively studied in the past few years. Homogeneous catalysts based on ruthenium,^[32, 109, 110, 113, 122, 129, 180-182] rhodium,^[70, 124, 128] iridium,^[53, 66-68, 116, 120] iron^[114, 117, 118, 183, 184] and other complexes^[115, 138] have been widely investigated, and excellent results have been obtained. For example, in 2014, Pidko and coworkers reported a very high activity for FA dehydrogenation using a ruthenium PNP-pincer complex, which provides a TOF of 257000 h⁻¹ and TON of 706500 at 90 °C in DMF in the presence of an amine.^[32]

Meanwhile, the Xiao group has been developing transfer hydrogenation with cyclometallated [Cp*Ir(L)Cl] complexes using FA as the hydrogen source, and found that the Ir-hydride intermediates could be intercepted not only by the iminium cations, but also by protons to release H₂. In 2013, they reported a type of cyclometallated Ir-N[^]C complexes for the dehydrogenation of HCO₂H–NEt₃ mixtures to give H₂ and CO₂ under mild conditions with no CO formation, achieving high turnover frequencies up to 147000 h⁻¹ at 40 °C.^[116]

Most of the above mentioned catalytic systems for FA dehydrogenation require

bases (e.g. amine) or additives (e.g. LiBF_4) in organic solvents. Although several catalysts have been reported for FA dehydrogenation in the absence of bases or additives, these reactions were conducted in organic solvents. For practical application, the dehydrogenation of FA in water without bases or additives is highly preferable. At present, only a few catalytic systems have been reported to be active in water in the absence of bases or additives. For example, in 2009, Himeda used a pH-dependent iridium-bipyridine catalyst for FA dehydrogenation, achieving a TOF of 14000 h^{-1} at $90 \text{ }^\circ\text{C}$ without bases or additives in water.^[127] In 2014, Wang, Himeda and coworkers reported an iridium-biimidazole complex with a TOF of 34000 h^{-1} at $80 \text{ }^\circ\text{C}$, the highest TOF reported for FA dehydrogenation in water without bases or additives.^[128]

The FA dehydrogenation activity in water is much lower in the absence of bases or additives, and the available catalytic systems are limited to iridium complexes with aromatic bipyridine, bipyrimidine and biimidazole ligands. In Chapter 3, an iridium complex with a nonaromatic N,N' -diimine ligand was found to be highly effective for the base-free hydrogenation of CO_2 in water. Since FA dehydrogenation is the reverse reaction of CO_2 hydrogenation, the Ir- N,N' diimine complex was subsequently studied for the dehydrogenation of FA, which is described in this chapter.

4.2 FA Dehydrogenation with Ir- N,N' Diimine Complex in Water

4.2.1 FA dehydrogenation reaction

As expected, gas evolution was achieved for the dehydrogenation of FA with complex **11** and **12**, and the results are listed in Table 4.1. The evolved gas mixture is composed of H_2 and CO_2 (1:1) without detectable levels of CO (Appendix Scheme C.1), suggesting that the reaction undergoes dehydrogenation instead of

dehydration.

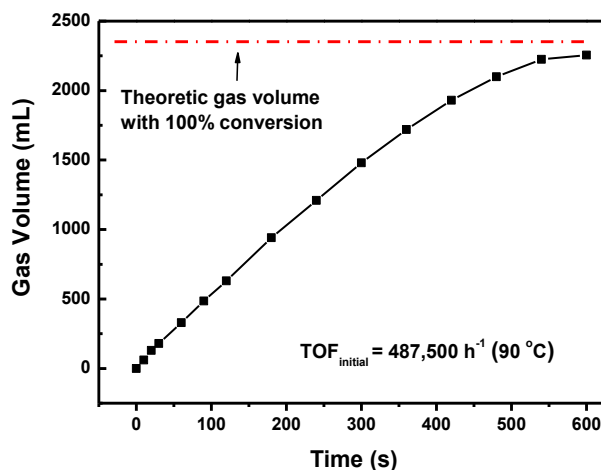
Table 4.1 Dehydrogenation of FA in water using complexes **11** and **12**

Entry	catalyst	T (°C)	TOF _{initial} (h ⁻¹)	Time (min)	H ₂ (mL)	TON	Con. (%)
1 ^a	11	60	50,000	20	240	10000	>99
2 ^a	12	60	30,000	20	175	7291	73
3 ^b	11	90	487,500	10	1128	47000	94
4 ^b	12	90	375,000	10	1040	43333	87

General conditions: No reaction occurred in the absence of catalysts. Each reaction was repeated at least twice with an error less than 5%. The volume of H₂ evolved was measured at the specified time. TON was estimated based on the H₂ amount in the same time interval. Con. refers to conversion of FA. ^a1.0 μmol of complex, 10.0 mL of H₂O, 10.0 mmol of FA, TOF was calculated based on the conversion in the first 2 min. ^b1.0 μmol of complex, 10.0 mL of H₂O, 50.0 mmol of FA, TOF was calculated based on the conversion in the first 20 s.

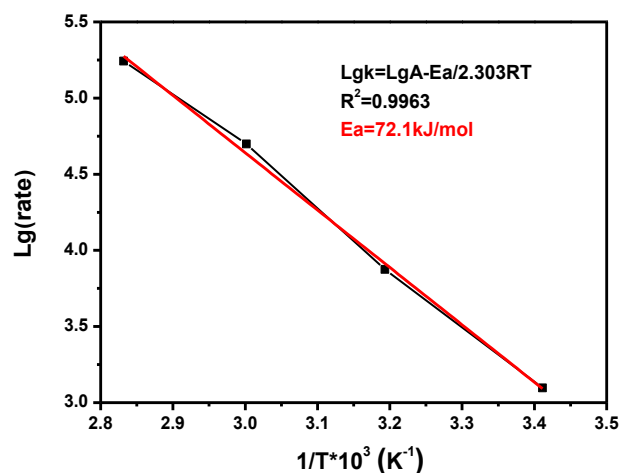
Using complex **11**, 10.0 mmol of FA can be completely dehydrogenated within 20 min at 60 °C, giving an initial TOF of 50000 h⁻¹ (Table 4.1, entry 1). Under the same conditions, the reaction with complex **12** provides a lower TOF of 30000 h⁻¹ (Table 4.1, entry 2). When the temperature is increased to 90 °C, a TOF as high as 487500 h⁻¹ can be achieved using complex **11** (Table 4.1, entry 3). The time course of gas evolution using complex **11** at 90 °C shows that over 300 mL of gas was evolved in the first minute and the FA conversion reached 95% after 10 min (Scheme 4.1). Complex **12** also shows a good TOF of 375000 h⁻¹ at 90 °C (Table

4.1, entry 4). Other N,N' ligands were also screened for this transformation; however, they all showed lower reactivity (Appendix, Table C.1).



Scheme 4.1 Time course of gas evolution using complex **11** at 90 °C

4.2.2 Reaction mechanism study

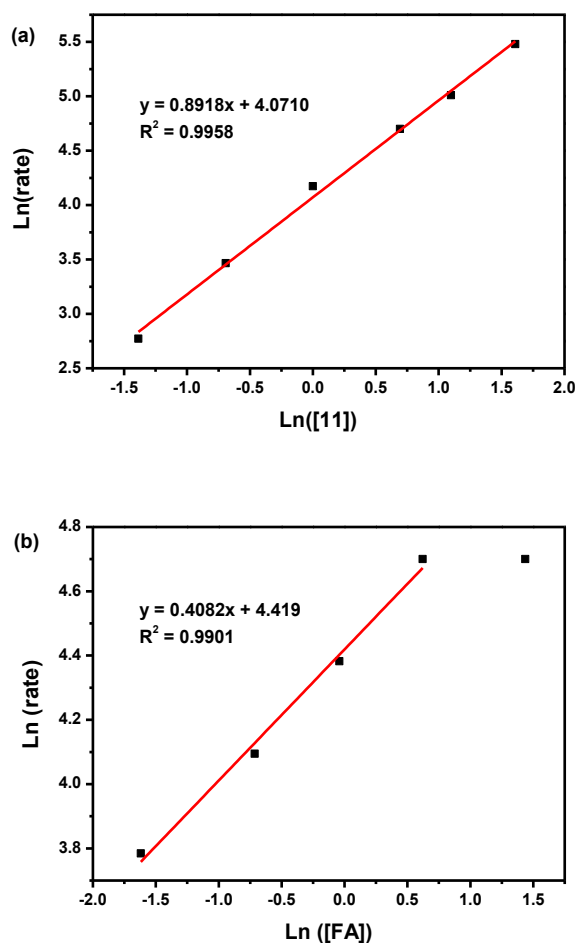


Scheme 4.2 Arrhenius fit of initial TOF values for dehydrogenation of FA.

Reaction conditions: complex **11** (1.0 μmol), FA (1.0 M, 10.0 mL), 20 °C, 40 °C, 60 °C, 80 °C.

The dependence of dehydrogenation rate on temperature, catalyst concentration, FA concentration and pH value was then investigated using complex **11**. The reaction rate increases with temperature, with the temperature dependence of the ini-

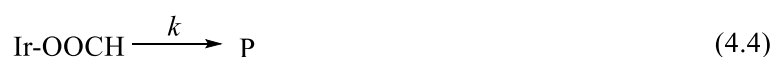
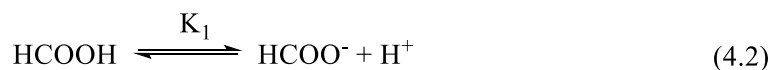
tial rates following the Arrhenius equation (Scheme 4.2). The estimated apparent activation energy (E_a) for FA dehydrogenation is 72.1 kJ mol^{-1} , which is in the typical range of noble-metal catalyzed dehydrogenation of FA.^{66, 110, 125, 128}



Scheme 4.3 (a) Plot of Ln (rate of H_2 evolution) versus Ln ([**11**): complex **11** ($0.25 \mu\text{mol}$ to $5.0 \mu\text{mol}$), FA (1.0 M , 10.0 mL), $60 \text{ }^\circ\text{C}$; (b) Plot of Ln (rate of H_2 evolution) versus Ln ([FA]): complex **11** ($1.0 \mu\text{mol}$), FA (0.2 M to 5.0 M , 10.0 mL), $60 \text{ }^\circ\text{C}$.

The rate dependence on concentrations of complex **11** and FA was examined. The double logarithmic plots of the initial rate against the concentration of complex **11** and FA both show linear dependence (Scheme 4.3). These results show that this reaction proceeds with an order of 0.89 with respect to complex **11** and indicate that complex **11** is converted into a monomeric active species rapidly. The

reaction order with respect to FA was estimated to be 0.41 (approximate 0.5), which implies that only one HCO_2^- coordinates to the iridium center in the transition state and that an equilibrium is probably involved between $[\text{Ir}]+\text{HCO}_2^-$ and $[\text{Ir}]-\text{HCO}_2^-$, the latter of which undergoes the dehydrogenation (see below).



If we assume that the dehydrogenation can be simplified by the equations 4.2-4.4, with equation 4.4, i.e. decarboxylation to generate the iridium hydride, being the turnover limiting step, a rate expression for the dehydrogenation can be derived as follows. k is the rate constant of the product (P) formation step; K_1 is the equilibrium constant of eqn. 4.2; K_2 is the equilibrium constant of eqn. 4.3. $[\text{Ir}]$ is the concentration of the iridium aqua complex. Applying steady-state approximation to $[\text{Ir-OOCH}]$ and $[\text{HCOO}^-]$, we have:

$$\text{Rate} = d[\text{H}_2]/dt = k[\text{Ir-OOCH}] = kK_2[\text{HCOO}^-][\text{Ir}] \quad (4.5)$$

$$\text{since } [\text{HCOO}^-][\text{H}^+] = [\text{HCOO}^-]^2 = K_1[\text{HCOOH}],$$

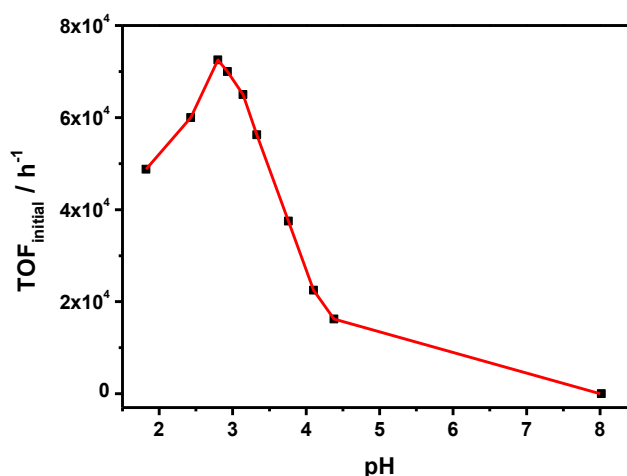
the reaction rate from eqn. 4.5 can be described as 4.6,

$$d[\text{H}_2]/dt = kK_2K_1^{0.5}[\text{Ir}][\text{HCOOH}]^{0.5} = k'[\text{Ir}][\text{HCOOH}]^{0.5} \quad (4.6)$$

Equation 4.6 agrees with the observations made above. In turn, this supports the assumption that the dehydrogenation is likely to be rate-limited by the step of decarboxylation.

Scheme 4.4 shows the TOF values obtained in the FA- HCO_2Na mixture solution at various pH values. The highest TOF value (72500 h^{-1}) was obtained at pH 2.8. The UV-Vis absorption spectra results at pH 2 to 13 (Appendix, Scheme C.2) show that the pKa1 of complex **11** due to deprotonation is around 9.0. Because the protonation status of **11** remains the same at $\text{pH} < 7.3$, the pH dependence of de-

hydrogenation may not be due to the deprotonation status of the ligand. The increase in TOF with decreasing pH from 8.0 to 2.8 indicates the importance of the hydronium ion (H_3O^+) concentration for this reaction. Meanwhile, the decrease in TOF with decreasing pH from 2.8 to 1.9 is consistent with the involvement of HCO_2^- species (eqn. 4.3) in this reaction, the concentration of which decreases at low pH. It is also consistent with the result obtained for neat FA (anhydrous) dehydrogenation under the same conditions, where no reaction was detected, because nearly neither H_3O^+ ions nor HCO_2^- exists in anhydrous FA.

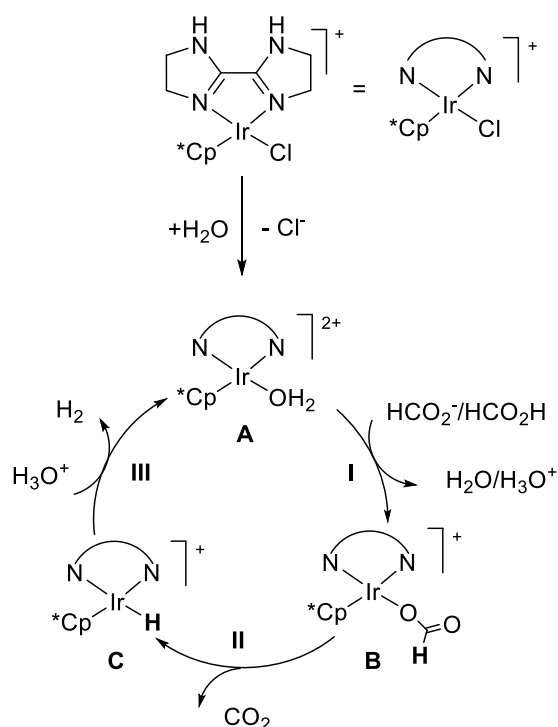


Scheme 4.4 pH dependence of the initial TOF

Reaction conditions: complex **11** (1.0 μmol), 60 °C, FA/ HCO_2Na (1.0 M, 10.0 mL).

Based on the results discussed above and the NMR studies (see Appendix C), a possible reaction mechanism was proposed (Scheme 4.5). The catalytic cycle likely starts from the water coordinated iridium complex **A**, which is derived from complex **11** in aqueous FA solution. Subsequent coordination of HCO_2^- to complex **A** forms the formate complex **B** (step I). After the release of CO_2 upon decarboxylation, the iridium hydride complex **C** is formed (step II), which was detected by NMR ($\delta = -12.20$ ppm, Appendix, Scheme C.3) in basic solutions. Next, the hydride **C** reacts with a hydronium ion (H_3O^+) to produce H_2 (step III), which

is accompanied by the regeneration of aqua iridium complex **A**.



Scheme 4.5 Catalytic cycle of FA dehydrogenation

To further understand this process, a kinetic isotope effect study was performed using complex **11**. As shown in Table 4.2, when the substrate HCO_2H was replaced with deuterated DCO_2H , the reaction rate decreased considerably. The KIE is 2.3 when DCO_2H replaces HCO_2H (Table 4.2, entry 2), but 1.7 when HCO_2D replaces HCO_2H (Table 4.2, entry 3). A KIE of 4.0 was obtained with DCO_2D in D_2O (Table 4.2, entry 4). The lower KIE values (Table 4.2, entries 2, 3) may be due to H-D scrambling at iridium. These results indicate again that the cleavage of the formate H-CO₂- bond is most likely involved in the rate-determining step under the given reaction conditions. In addition, Ir-H was not observed in acidic solution by 1H NMR (Appendix, Scheme C.4). Thus the generation of $[Ir]-H$ (step II), not the hydrogen elimination (step III), is proposed to be the rate-determining step.

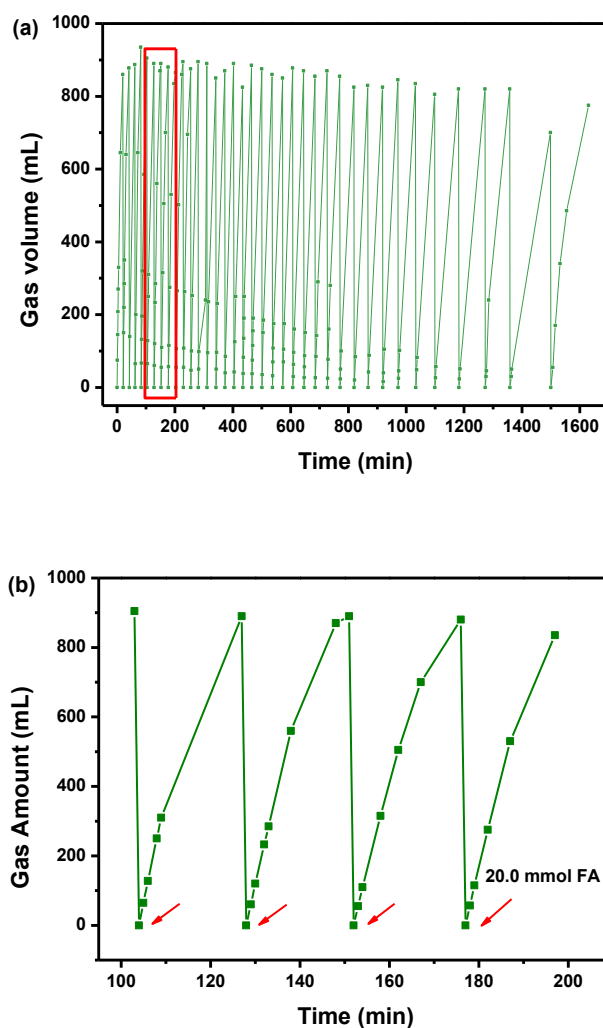
Table 4.2 KIE in the dehydrogenation of FA using complex **11^a**

Entry	Substrate	Solvent	TOF (h ⁻¹) ^b	KIE ^c
1	HCO ₂ H	H ₂ O	50000	/
2	DCO ₂ H	H ₂ O	21,880	2.3
3	HCO ₂ D	D ₂ O	29,375	1.7
4	DCO ₂ D	D ₂ O	12500	4.0

^a: Reaction conditions: complex **11** (1.0 μmol), FA solution (1.0 M, 10.0 mL), 60 °C; ^b: TOF was calculated in the first 2 min; ^c: KIE = TOF(entry 1)/TOF(entry n) (n = 2, 3, 4).

4.2.3 Catalytic stability test

The stability of our catalyst was also investigated. For the catalyst recycling test (Scheme 4.6), 20.0 mmol of FA was consumed in each cycle when using 2.0 μmol of complex **11** at 60 °C. This catalyst functioned continuously for 37 cycles with only slightly declining activity. When using the *in situ* generated iridium catalyst with ligand **L18** (Ir:L = 1:5) for FA dehydrogenation at 80 °C and charging FA at certain time intervals, a total TON of 2400000 was achieved in approximately 14 hours.



Scheme 4.6 Recycles of the dehydrogenation of FA.

Reaction conditions: complex **11** (2.0 μmol), FA (2.0 M, 10.0 mL), 60 $^{\circ}\text{C}$. FA (20.0 mmol) was added into the reaction at the beginning of each cycle. Part of (a) is enlarged as shown in (b).

The FA dehydrogenation can also take place smoothly in a closed system under pressurized conditions. In a 300 mL autoclave, the total pressure reached 4.4 MPa after 6 hours when using 1.0 μmol of *in situ* formed complex **12** to dehydrogenate FA (5.0 M, 50.0 mL) at 60 $^{\circ}\text{C}$ (less than 0.3% of FA left behind), indicating that high pressure of H_2 can be supplied using this catalyst.

4.3 Summary

In summary, the water-soluble iridium complexes such as **11** and **12** with nonaromatic N,N'-diimine ligands show extremely high FA dehydrogenation activity in water. Without the addition of any bases or additives, a TOF of up to 487500 h^{-1} with complex **11** and a TON of 2400000 with the *in situ* prepared catalyst from $[\text{IrCp}^*\text{Cl}_2]_2$ and **L18** were obtained. The high activity and good stability of these catalysts make hydrogen generation from FA more feasible for potential applications.

4.4 Experimental Section

4.4.1 General information

Instruments: Details have been given in Chapters 2 and 3. GC analysis results were obtained with Techcomp GC7890 II equipped with a TCD and a FID.

Chemicals: Formic acid (98%) and $[\text{IrCp}^*\text{Cl}_2]_2$ were purchased from J&K. Sodium formate was purchased from Sinopharm Chemical Reagent Co. Ltd.

4.4.2 Procedure for catalytic dehydrogenation of FA

An aqueous catalyst stock solution was prepared freshly before use and the reactions were carried out without protection.

First, 10.0 mL of the FA aqueous solution and a stir bar were placed in a Schlenk tube equipped with a side branch and rubber septa. Afterwards, the tube was preheated at given temperature (e.g. $60 \text{ }^\circ\text{C}$) in a water bath until the required temperature was attained. Then, freshly prepared aqueous catalyst stock solution was injected into the reaction through the septa, and the timing started immediately. The side branch was connected to the gas collection apparatus (standard water displacement apparatus, using a graduated cylinder to determine volume).

The volume of gas generated was recorded.

For the reaction carried out in neat FA, FA was dehydrated using anhydrous Na_2SO_4 for 3 h before use. 10.0 mL of dehydrated FA and stir bar were placed in a Schlenk tube, and preheated at 60 °C for 10 min. Then complex **11** (1.0 μmol) was added in and the tube was sealed immediately. No observable gas evolution was detected within 20 min. Next, 5.0 mL of water was injected into the reaction, and gas evolution occurred gradually. Thus the FA dehydrogenation using complex **11** requires H_3O^+ and HCO_2^- .

For the long-time reaction, a stir bar, water (7.0 mL) and FA (2.2001 g, 98%) were placed in a Schlenk tube equipped with a side branch and rubber septa. After the tube was preheated at 80 °C in water bath, the stock solution of *in situ* generated iridium catalyst (1.0 mL, 0.05 μmol of $[\text{IrCp}^*\text{Cl}_2]_2$ and 0.5 μmol of **L18**) was injected into the reaction through the septa, and the timing was started. The side branch was connected to the gas collection apparatus. At the reaction times of 80 min, 200 min, 270 min and 400 min, 2.7503 g, 1.9310g, 2.3395 g and 2.1102 g of FA were added, respectively. After 14 hours of reaction, no gas was observable, and the residue of FA was determined to be 0.111 mmol by ion chromatograph. Thus the amount of the reacted FA was as follows:

$$\begin{aligned} n_{FA} &= \frac{2.2001 + 2.7498 + 1.9310 + 2.3385 + 2.1102}{46.03} \times 1000 \times 98\% - 0.111 \\ &= 241.10 \text{ mmol} \end{aligned}$$

Thus,

$$TON = \frac{241.10 \times 1000}{0.1} = 2,411,000 \approx 2,400,000.$$

4.4.3 Calculation of TON and TOF

TON was calculated according to eqn. 4.2. No blank reaction was observed with-

out catalyst. The solvent and water vapor was neglected.

$$\text{TON} = \frac{V_{total}}{2 * V_{m,20^{\circ}C} \cdot n_{cat}} \quad (4.2)$$

Calculation of $V_{m,H_2,20^{\circ}C}$ was carried out using van der Waals eqn. 4.3.

$$V_{m,H_2,20^{\circ}C} = \frac{RT}{p} + b - \frac{a}{RT} = 24.16 \text{ L} \cdot \text{mol}^{-1} \approx 24 \text{ L} \cdot \text{mol}^{-1} \quad (4.3)$$

R: $8.3145 \text{ m}^3\text{Pa mol}^{-1} \text{ K}^{-1}$

T: 298.15 K

p: 101325 Pa

b: $26.7 \cdot 10^{-6} \text{ m}^3 \text{ mol}^{-1}$

a: $2.49 \cdot 10^{-10} \text{ Pa m}^3 \text{ mol}^{-2}$

Calculation of $V_{m,CO_2,20^{\circ}C}$ was carried out using van der Waals eqn. 4.4.

$$V_{m,H_2,20^{\circ}C} = \frac{RT}{p} + b - \frac{a}{RT} = 24.10 \text{ L} \cdot \text{mol}^{-1} \approx 24 \text{ L} \cdot \text{mol}^{-1} \quad (4.4)$$

R: $8.3145 \text{ m}^3\text{Pa mol}^{-1} \text{ K}^{-1}$

T: 298.15 K

p: 101325

a: $36.5 \cdot 10^{-10} \text{ Pa m}^3\text{mol}^{-2}$

b: $42.7 \cdot 10^{-6} \text{ m}^3\text{mol}^{-1}$

The TOF calculation is time related (h^{-1}) based on the TON calculation. For example, at 90°C , using 0.002 mol % (1.0 μmol) complex **11** in 5.0 M aqueous solution of FA, 130 mL gas was released in the first 20 s, thus,

$$\text{TOF} = \frac{\frac{130}{2 * 24}}{0.001} \times \frac{3600}{20} = 487,500 \text{ h}^{-1}$$

4.4 Gas composition analysis

A GC with a TCD and a FID detector equipped with a methaniser confirmed the products of FA decomposition were H_2 and CO_2 with no detectable level of CO. The molar ratio of H_2 and CO_2 was measured to be approximate 1:1 after calibra-

tion (twice, experimental error less than 4%). Since we used the water replacement method to quantify the amount of H₂, the gas composition after water absorption was also tested. The amounts of H₂ and CO₂ were approximately equal because most of our reactions finished within 20 minutes, a short time insufficient for considerable amounts of CO₂ to be absorbed by tap water especially when considering the TOF measurement (within the initial 2 min).

**Chapter 5 Iodide-Promoted Dehydrogenation of FA on a
Rhodium Complex**

5.1 Introduction

As discussed previously, hydrogen generation from FA has attracted much attention in recent years. This chemistry could provide a technology for hydrogen supply for e.g. small mobile or stationary applications. Accordingly studies into catalytic dehydrogenation of FA have been carried out by a number of research groups, with some reporting excellent TOFs. In the arena of homogeneous catalysis, the highest TOF of 487500 h^{-1} was obtained using the Ir-N,N' diimine complex which was discussed in Chapter 4.^[185] However most of the reported catalysts consist of relatively complicated or expensive bidentate/tridentate ligands along with the metal center, although they can be highly active in the dehydrogenation. Considering the practicality of the FA dehydrogenation in real life, developing efficient catalyst systems without using complicated or delicate ligands would be preferable for FA dehydrogenation.

Halide ions, one of the most common and simplest additives and ancillary ligands for transition metal complex catalysts, have frequently been found to exert some unusual influence on catalytic reactions.^[186, 187] In particular, the significant promoting effect of the iodide anion in hydrogenation and transfer hydrogenation reactions has been recognized.^[187-190] Although the mechanistic details of the iodide effect on these reactions remain unclear, its softness, trans effect and size may play a role. Xiao's group has reported the precatalyst $[\text{RhCp}^*\text{Cl}_2]_2$ to catalyze the transfer hydrogenation of N-heterocycles with the FT azeotrope in the presence of halide ions and particularly iodide.^[188] The hydrogen is derived from the decomposition of FA, showing that the $[\text{RhCp}^*\text{Cl}_2]_2\text{-X}^-$ combination is capable of FA dehydrogenation. Therefore in this chapter, the dehydrogenation of $\text{HCO}_2\text{H}/\text{NEt}_3$ with $[\text{RhCp}^*\text{Cl}_2]_2$ was investigated, including especially the effect of I.

5.2 [RhCp*Cl₂]₂ Catalyzed FA Dehydrogenation

5.2.1 FA dehydrogenation in the presence of additives

The [RhCp*Cl₂]₂ catalyzed FA dehydrogenation was examined in the absence or presence of halide anions at 60 °C in the FT azeotrope, where the F/T molar ratio is 2.5. The amount of evolved gas was determined by water displacement method, and GC confirmed the products to be H₂ and CO₂ (1:1 ratio) with negligible level of CO (Appendix, Scheme D.1). As shown in Table 5.1 and Scheme 5.1, both the TOF and TON are increased on the addition of potassium halides, with KI enabling the fastest reaction. In its presence the initial TOF increased most significantly to 4375 h⁻¹ from 625 h⁻¹ in its absence. Comparing the TOF values obtained with KI, NaI and LiI, it can be concluded that this activity enhancement arises from the halide anions rather than the alkali cations. In addition, the presence of I⁻ makes this catalyst more productive, increasing the TON from 151 to 706 (at 40% FA conversion, Table 5.1, entries 1, 5) after 30 min.

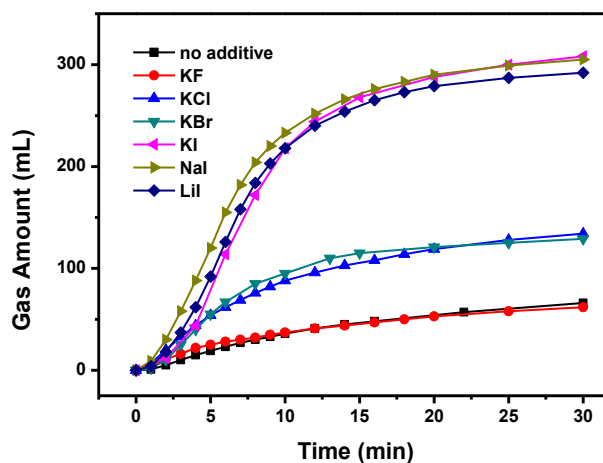
Table 5.1 Dehydrogenation of FA in the presence of different alkali halide salts^a

Entry	Additive	Gas amount (mL) ^b	TON (30 min) ^b	Con.	TOF _{max} (h ⁻¹) ^c
1	-	66	151	9 %	625
2	KF	62	142	8 %	875
3	KCl	134	307	17 %	1625
4	KBr	129	296	17 %	2009
5	KI	308	706	40 %	4375
6	NaI	305	699	40 %	4375
7	LiI	292	669	38 %	4250

^a: General reaction conditions: 5.0 μmol of [RhCp*Cl₂]₂, 1.0 mmol of alkali halide, 1.5 mL of FT azeotrope, at 60 °C. Approximately 16 mmol of FA is included in 1.5 mL FT azeotrope. ^b:

The amount of gas and TON were recorded and calculated after 30 min reaction. ^c: TOF_{max}

was calculated based on the volume of evolved gas from 3 to 6 min after the reaction had started to rule out the influence of temperature fluctuation due to the injection of FT solution and to avoid the initial induction period (See Figure 5.1). Each reaction was repeated at least twice with an error less than 5%. No reaction was observed without catalyst.



Scheme 5.1 Time course of gas evolution during the dehydrogenation of FA.

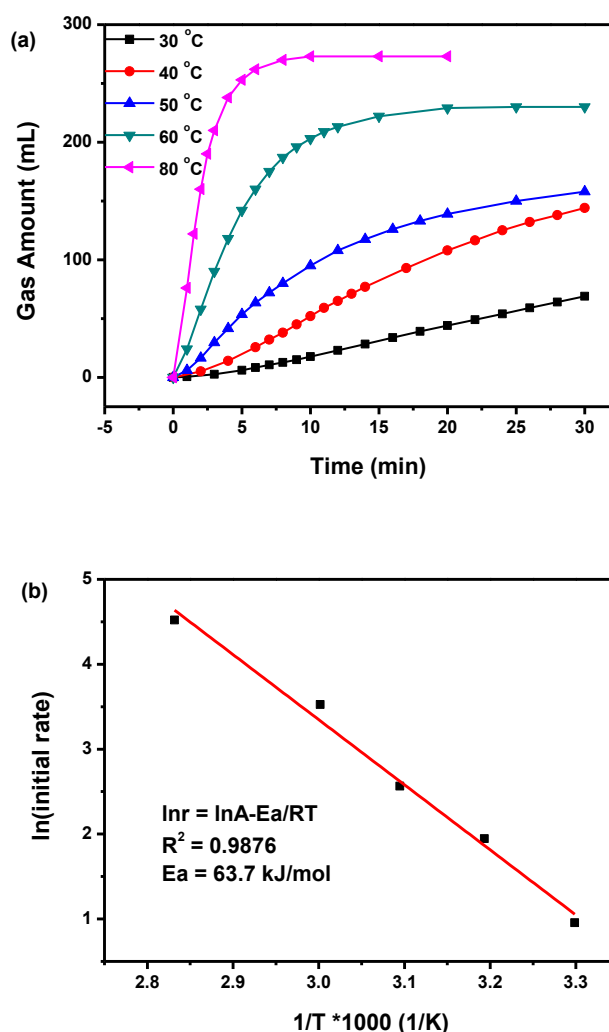
Reaction conditions: 5.0 μmol of $[\text{RhCp}^*\text{Cl}_2]_2$, 1.0 mmol of inorganic salts (6 mol%), 1.5 mL of FT azeotropic solution, at 60 $^\circ\text{C}$.

Other rhodium complexes as well as those based on iridium and ruthenium were also investigated as catalyst precursors in combination with I $^-$ for FA dehydrogenation (Appendix, Table D.1). All the complexes tested showed very low activity, except for $[\text{Ru}(\text{p-cymene})\text{Cl}_2]_2$, which gave a moderate TOF of 1500 h^{-1} . This value is 6 times higher than that of the reaction without I $^-$ (Appendix, Table D.1, entries 2-3), indicating that the promoting effect of I $^-$ is not limited to $[\text{RhCp}^*\text{Cl}_2]_2$.

5.2.2 Kinetics of FA dehydrogenation

To gain an understanding of the dehydrogenation reaction, the rate dependence on temperature, catalyst concentration, KI amount and FA/triethylamine (TEA) ratio were investigated. The reaction rate increases with temperature, and the tempera-

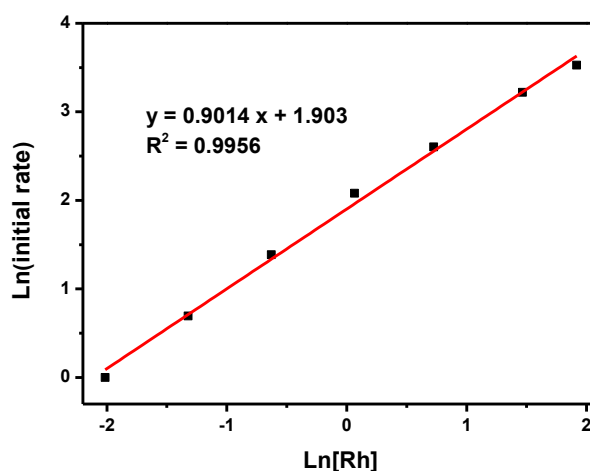
ture dependence of the initial rates follows the Arrhenius equation (Scheme 5.2). The apparent activation energy (E_a) for the FA dehydrogenation is estimated to be ca 64 kJ mol^{-1} , which is near the typical range of noble metal catalyzed hydrogen generation from FA in aqueous solution.^[125, 128, 185]



Scheme 5.2 (a) Time course of gas evolution during the dehydrogenation of FA at 30 °C to 80 °C; (b) Arrhenius plot of initial rate for FA dehydrogenation.

Reaction conditions: 5.0 μmol of $[\text{RhCp}^*\text{Cl}_2]_2$ and 1.0 mmol of KI in 1.5 mL of FT azeotrope at temperatures from 30 °C to 80 °C; The initial rate refers to the fastest rate obtained right after the short induction period. Thus the E_a value derived here is only an estimation of activation energy because $\log r$ is used instead of $\log k$.

The rate dependence on catalyst concentration [Rh] was explored using 0.1 ~ 5.0 μmol of $[\text{RhCp}^*\text{Cl}_2]_2$ in combination with 500 μmol of KI in 1.5 mL of FT azeotrope at 60 $^\circ\text{C}$ (Appendix, Scheme D.2). The double logarithmic plot of the initial rate against the catalyst concentration shows a linear dependence on the [Rh] (Scheme 5.3). As can be seen, the reaction proceeds with an order of 0.90 with respect to the catalyst concentration [Rh], which is close to 1.0. This is consistent with a mononuclear rhodium species being involved in the catalytic cycle (also see below), and no other polymeric compounds are likely to be the active catalyst. Beyond the [Rh] concentration of 1.07 mM, the initial TOF declines gradually (Appendix, Scheme D.2b). This may result from catalyst aggregation at a higher concentration (*vide infra*).

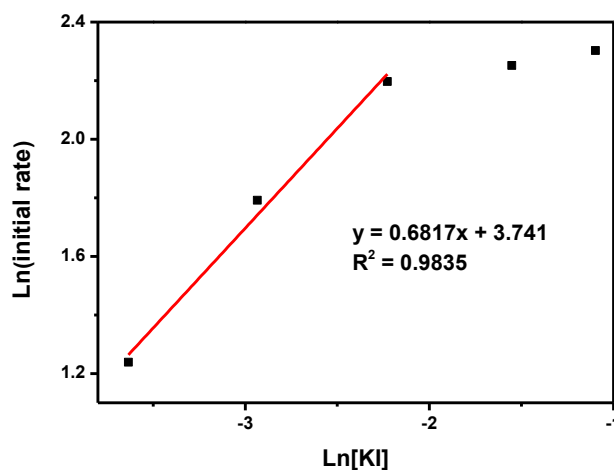


Scheme 5.3 Plot of $\ln(\text{initial rate of H}_2 \text{ evolution})$ versus $\ln[\text{Rh}]$ ([Rh] means rhodium monomer concentration).

Conditions: 0.1 ~ 5.0 μmol of $[\text{RhCp}^*\text{Cl}_2]_2$, 500 μmol of KI, 1.5 mL of FT azeotrope, at 60 $^\circ\text{C}$.

The rate dependence on the concentration of KI was investigated using 0.8 μmol of $[\text{RhCp}^*\text{Cl}_2]_2$ with 40 ~ 500 μmol of KI in 1.5 mL of FT azeotrope (Appendix, Scheme D.3). The reaction rate shows a fraction order of 0.68 on iodide concentration, up to $[\text{KI}] \approx 0.1 \text{ M}$ ($n\text{KI} = 160 \mu\text{mol}$) (Scheme 5.4). This result in-

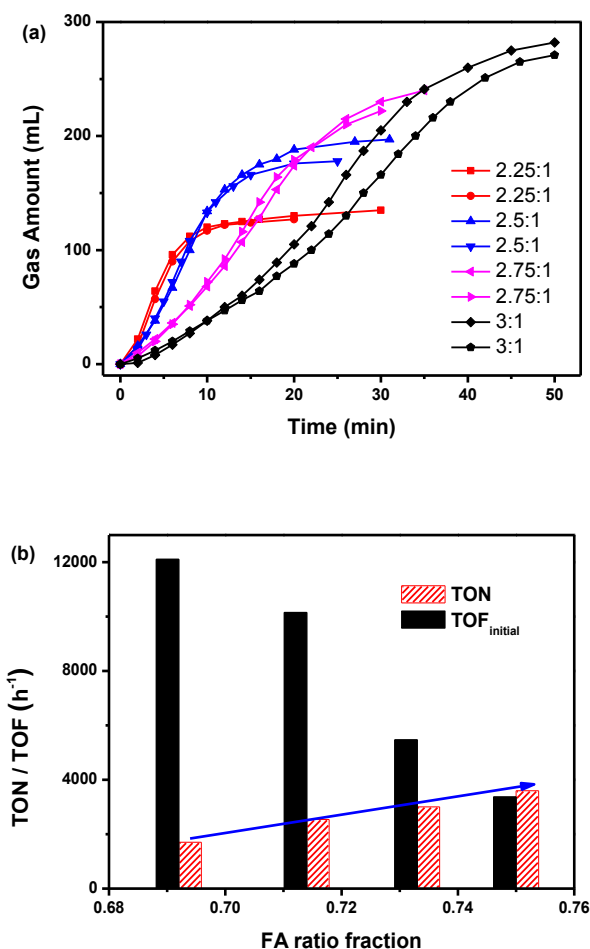
indicates that the iodide ion is likely to be involved in the rate-determining step (RDS) and equilibria prior to it.



Scheme 5.4 Plot of Ln(initial rate of H₂ evolution) versus ln[KI].

Conditions: 0.8 μmol of [RhCp*Cl₂]₂, 40 ~ 500 μmol of KI, 1.5 mL of FT azeotrope, at 60 °C.

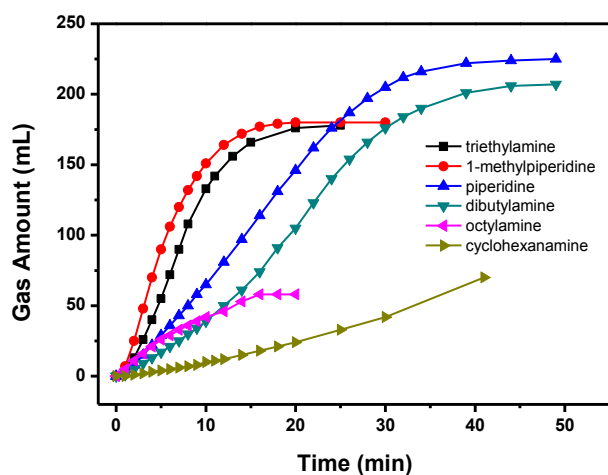
With different FA/TEA ratios, the time course of gas evolution was recorded as shown in Scheme 5.5a. The FT mixture solutions were prepared with the molar ratio of FA/TEA in the range of 2.25:1 to 3:1. Scheme 5.5b shows the variation of the initial TOF and TON with the FA molar fraction in the starting solution. As can be seen, the final TONs increase approximately linearly with increasing FA amount (arrow line). In contrast, the initial TOFs show a reverse dependence on the FA molar fraction, with more FA giving rise to lower TOFs. Since [HCOO⁻] is reversely proportional to [HCOOH] in the FA/TEA mixture, the reverse dependence suggests that the dehydrogenation rate depends on [HCOO⁻]. In line with this, no gas bubble was observed in neat FA and no Rh-H species was detected in neat FA either (Appendix, Scheme D.4). These observations appear to indicate that the dehydrogenation is rate-limited by the step of hydride formation, where coordination of the formate is necessary.



Scheme 5.5 (a) Time course of gas evolution during the dehydrogenation of FA in FT solution with different F/T ratio: 0.8 μmol of $[\text{RhCp}^*\text{Cl}_2]_2$, 320.0 μmol of KI, 1.5 mL of FT solution with the mole ratio of FA/TEA in the range from 2.25:1 to 3:1, at 60 °C. Each reaction was repeated twice. The blue -▲- line represents FA dehydrogenation conducted in FT azeotropic solution and the blue -▼- line represents reaction conducted in physically mixed FT solution (2.5:1). **(b)** TON and TOF values observed in FT solutions with different FA/TEA ratios. TON was measured using the final gas amount as shown in (a), from 20 to 50 min. The TOF was calculated based on the volume of evolved gas from 3 to 6 min after the reaction had started to rule out the influence of temperature fluctuation due to the injection of FT solution and to avoid the initial induction period.

In addition to TEA, other amines were also tested for the reaction as shown in Scheme 5.6 (the pK_a value of the amines are listed in Appendix, Table D.2). Tertiary amines show superior reactivity compared with primary and secondary

amines. This may result from the latter two types of amines being better hydrogen bond donors, reducing the concentration of free iodide ions needed for higher dehydrogenation rates (*vide supra*).

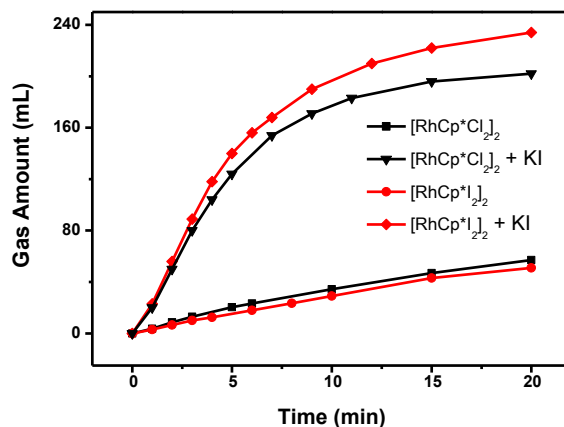


Scheme 5.6 FA dehydrogenation using various amines: 0.8 μmol of $[\text{RhCp}^*\text{Cl}_2]_2$, 320 μmol of KI, 1.5 mL of FA/amine (2.5:1) solution, at 60 $^\circ\text{C}$.

5.2.3 The structure of active catalysts

Effort was then made to investigate the role of I⁻ in this reaction. Firstly, a contrast experiment was conducted using $[\text{RhCp}^*\text{Cl}_2]_2$ and $[\text{RhCp}^*\text{I}_2]_2$ as catalyst precursors. As shown in Scheme 5.7, without KI, the FA dehydrogenation rates for both rhodium complexes are low and essentially identical. When KI is added, both reactions are accelerated considerably and to a similar extent. These findings rule out the possibility of the iodide effect arising from the iodide-ligated rhodium dimer $[\text{RhCp}^*\text{I}_2]_2$, and suggest that the same active catalyst is generated in the presence of I⁻ regardless of which rhodium precursor is used. The necessity for a large excess of coordinating I⁻ also indicates that the active catalyst is less likely to be other forms of dimeric $\text{Cp}^*\text{Rh(III)-I}$ species. It is noted that replacing KI with the same amount of KCl has only an insignificant effect on the

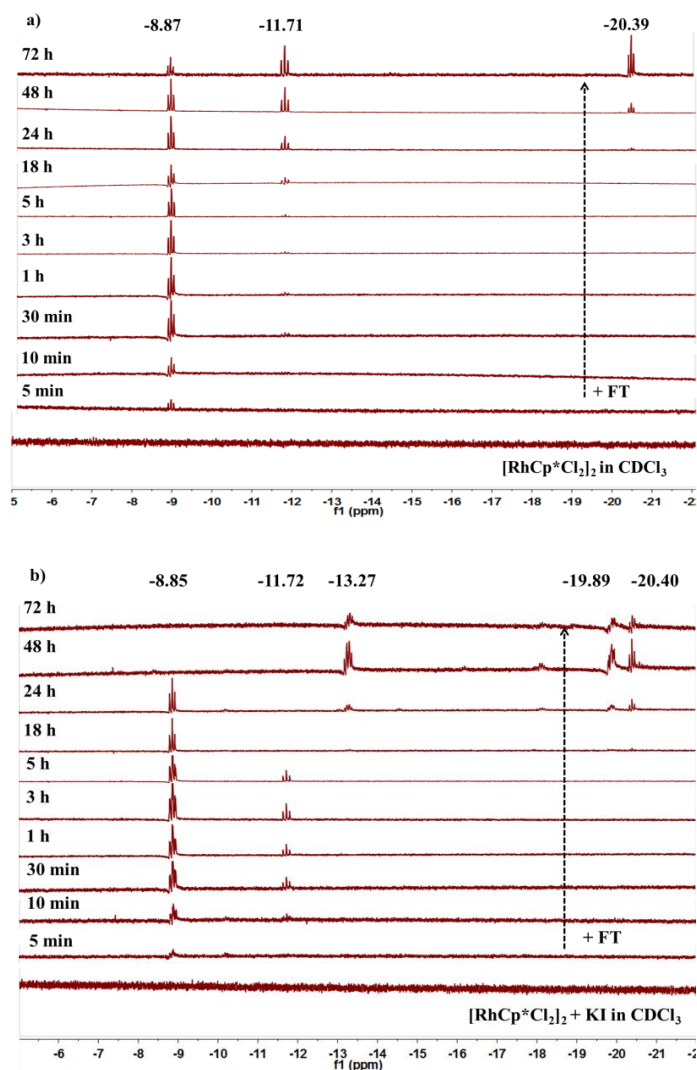
dehydrogenation catalyzed by $[\text{Cp}^*\text{RhI}_2]_2$ (Appendix, Scheme D.5).



Scheme 5.7 FA dehydrogenation using $[\text{RhCp}^*\text{Cl}_2]_2$ and $[\text{RhCp}^*\text{I}_2]_2$: 5.0 μmol of $[\text{RhCp}^*\text{X}_2]_2$, 1 mmol of KI when added, 1.5 mL of FT azeotrope, 60 $^\circ\text{C}$.^[191]

The FA dehydrogenation with $[\text{RhCp}^*\text{Cl}_2]_2$ at room temperature in the absence or presence of I⁻ was monitored by ^1H NMR spectroscopy over a period of 72 h (Appendix, Scheme D.6; for details see the experimental section). Comparing Scheme D.6a and D.6b (Appendix) shows that the FA (indicated by the formate proton signal) was consumed to a greater extent after 72 h in the presence of I⁻ (54 % vs. 18 % FA conversion), which is consistent with the results from Figure 5.1. The hydride part (-5 ~ -22 ppm) of Scheme D.6 is enlarged and shown as Scheme 5.8 here. Without KI (Scheme 5.8a), a Rh-H hydride triplet at -8.87 ppm along with a new chemical shift at 1.90 ppm (Cp* proton, Appendix, Scheme D.6e) appeared instantly (less than 5 min) upon mixing the rhodium precursor with FT azeotrope in CDCl_3 , indicating quick formation of a binuclear rhodium species with a bridging hydride.^[192] Other rhodium species bearing bridging hydride ligands started to appear later (-11.71 and -20.39 ppm). In the presence of KI (Scheme 5.8b), the NMR spectra show that similar rhodium species are formed quickly in addition to a new peak at -8.85 ppm, which overlaps with a slightly

smaller peak centred at -8.87 ppm (Appendix, Scheme D.6g). The latter presumably arises from the same species as the one in the absence of the iodide. However, the peak at -11.72 ppm disappeared after 5 h while the one at -8.85 ppm disappeared after 24 h, accompanied with the appearance of new, unknown rhodium species with bridging hydride.

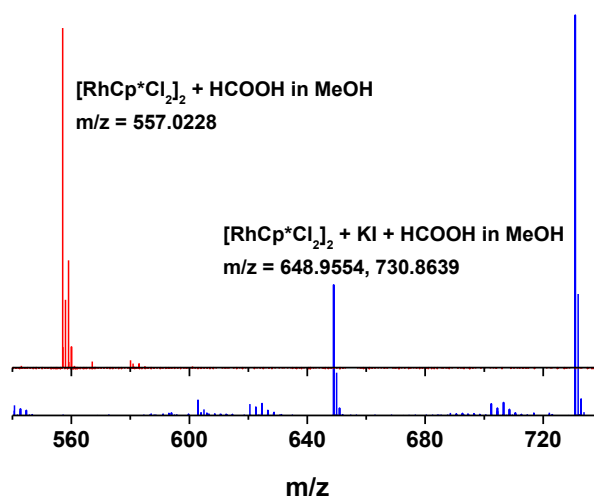


Scheme 5.8 ^1H NMR spectra of $[\text{RhCp}^*\text{Cl}_2]_2$ reacting with FT azeotrope in CDCl_3 (hydride part): (a) without KI; (b) in the presence of KI (250 μmol).

General conditions: 5.0 μmol of $[\text{RhCp}^*\text{Cl}_2]_2$, 0.1 mL of FT azeotrope, room temperature. Timing started after the injection of FT solution.

It is also worth noting that there is no visible doublet hydride resonance during

the catalytic reaction, again indicating that the dehydrogenation is likely to be turnover-limited by the step of hydride formation. Since gas evolution was observed over the entire period of 72 h in both cases, the disappearance of the triplets mentioned is consistent with the corresponding binuclear rhodium species being not active catalyst.

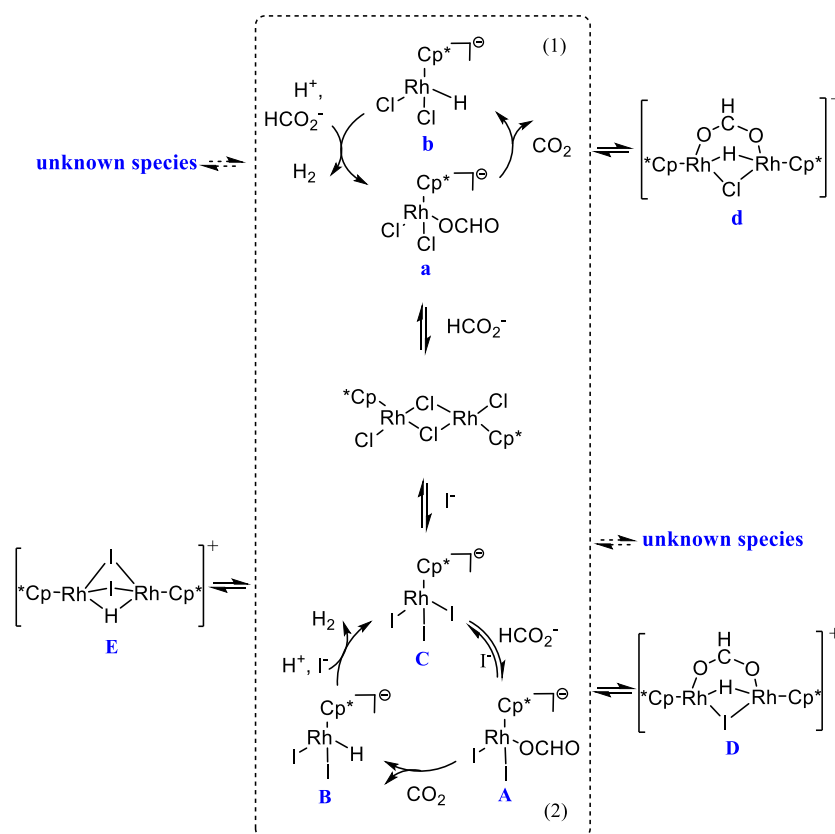


Scheme 5.9 Mass spectrometry of $[\text{RhCp}^*\text{Cl}_2]_2$ reacting with FT azeotrope in methanol. Conditions: 1.6 μmol of $[\text{RhCp}^*\text{Cl}_2]_2$, 0.2 mL of FT azeotrope, 1.0 mL of methanol, room temperature. Upper: without KI; lower: 120 μmol of KI.

Mass spectrometry was then employed in an attempt to identify these rhodium species. Scheme 5.9 shows the mass fragment of $[\text{RhCp}^*\text{Cl}_2]_2$ reacting with the FT azeotrope in methanol within 5 min after the reaction had started (see Appendix, Scheme D.7 for full spectrogram). In the absence of KI, the mass peak at m/z 557.0228 can be ascribed to $[\text{Rh}_2\text{Cp}^*_2\text{Cl}(\text{H})(\text{OCHO})]^+$ (**d**, Scheme 5.10, *vide infra*), a rhodium dimer complex containing a bridging hydride and a bridging formate ligand (^1H NMR: 7.39 ppm).^[193, 194] When KI was added, the newly generated mass peak at m/z 648.9554 supports the formation of $[\text{Rh}_2\text{Cp}^*_2\text{I}(\text{H})(\text{OCHO})]^+$ (**D**, Scheme 5.10),^[195] an analogue of **d**, while the one at

m/z 730.8639 may correspond to $[\text{Rh}_2\text{Cp}^*_2(\text{H})\text{I}_2]^+$ (**E**, Scheme 5.10).^[196] Each of these species is expected to display a triplet hydride signal in their ^1H NMR spectra and thus appears to correspond well to those revealed in Scheme 5.8.

5.2.4 Proposed reaction mechanism



Scheme 5.10 Plausible reaction mechanism for the dehydrogenation of FA using $[\text{RhCp}^*\text{Cl}_2]_2$ in the absence (1) or presence (2) of I^- .

Taken together, a plausible reaction mechanism is tentatively suggested for the $[\text{RhCp}^*\text{Cl}_2]_2$ catalysed dehydrogenation of FA (Scheme 5.10). With or without KI, the dimeric $[\text{RhCp}^*\text{Cl}_2]_2$ firstly dissociates under the reaction conditions, turning into the catalytically active monomeric rhodium species **a** in the absence of I^- and **C** in its presence.^[197] The latter is in fast equilibrium with the formate **A**, the iodo analogue of **a**. Subsequently, the rhodium hydrides **b** and **B** are formed from **a** and **A** via decarboxylation, protonation of which releases H_2 and regenerates the

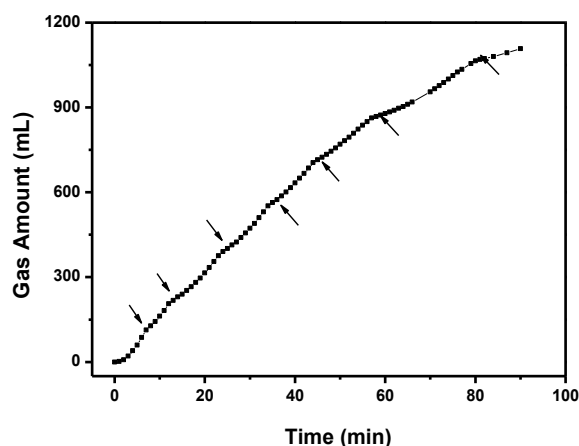
active catalysts.

During the catalytic turnover, the spectator dimeric species **d**, **D** and **E** containing bridging hydride are formed upon dimerization of the monomers in the catalytic cycle. As the reaction progresses, other unknown rhodium species are formed as shown by the ^1H NMR in Scheme 5.8. These species are not considered as reactive species. However, they may be in fast equilibrium with the catalytically active monomers; otherwise the catalyst would deactivate quickly.^[193] As indicated above, the overall dehydrogenation is likely to be controlled by the step of hydride formation in turnover.^[198, 199] Thus, the promoting effect of iodide can be ascribed to decarboxylation from **A** being easier than from **a**, which in turn may be due to the iodide being a better ligand to the Rh(III) than the chloride.^[200] Since the decarboxylation could proceed via a transition state involving dissociation of the formate to form an ion pair,^[117, 121, 199, 201, 202] a better coordinating iodide anion would be expected to stabilise better the transition state that contains a positively charged Rh(III). However, excess iodide will shift the equilibrium between **C** and **A** to favour **C**, thereby giving rise to the saturation kinetics seen above (Scheme 5.4).

5.2.5 Catalytic stability test

The stability of this catalyst system for FA dehydrogenation was also investigated. During a single FA decomposition reaction using 5.0 μmol of $[\text{RhCp}^*\text{Cl}_2]_2$ and 1.0 mmol of KI in 1.5 mL of FT azeotrope at 60 $^\circ\text{C}$, the catalyst is observed to lose activity eventually (at con. < 50%, Scheme 5.1), and gas evolution could not be fully recovered with the addition of either formic acid or FT azeotrope (Appendix, Scheme D.8). This could be caused by the irreversible formation of some deactivated rhodium hydride species as a result of the consumption of FA (Appendix, Scheme D.9). Nevertheless, the addition of KI prolongs the life time

(TON) of the catalytic system; in its absence, the catalyst is of low activity right from the beginning (Scheme 5.7). One way to keep this reaction going is to add an additional amount of FA into the system at certain time intervals. This is shown in Scheme 5.11, where more than 1000 mL of H₂ were released upon seven consecutive additions of FA, although the dehydrogenation rate became slower progressively. Thus the TON was enhanced from 706 (Table 5.1) to over 2540.



Scheme 5.11 Longer time reaction with intermittent addition of FA.

Conditions: 5.0 μmol of $[\text{RhCp}^*\text{Cl}_2]_2$, 1.0 mmol of KI, 1.5 mL of FT azeotrope, 60 °C. The amount of FA added was roughly based on the amount of evolved gas, 0.12 mL, 0.12 mL, 0.12 mL, 0.12 mL, 0.12 mL, 0.15 mL, 0.15 mL.

5.3 Summary

In this chapter, the FA dehydrogenation catalysed by a simple, commercially readily available rhodium catalyst, $[\text{RhCp}^*\text{Cl}_2]_2$, is studied and the catalytic activity is found to be enhanced by the addition of halide ions. The catalytic activity increases with the atomic number of halide ions, and with I the activity is increased 7 folds. Not only does the iodide ion increase the reaction rate, it also prolongs the catalyst lifetime. Kinetic studies and NMR monitoring suggest the active catalyst to be mononuclear in equilibrium with binuclear hydrides outside

of the catalytic cycle. The catalytic turnover appears to be controlled by the rate of hydride formation, which is facilitated by iodide anions coordinated to the Rh(III) center.

5.4 Experimental Section

5.4.1 General information

Instruments: Details have been given in Chapter 2, 3 and 4.

Chemicals: $[\text{RhCp}^*\text{Cl}_2]_2$, formic acid, triethylamine (TEA), 1-methylpiperidine, piperidine, dibutylamine, octylamine, and cyclohexylamine were purchased from Aldrich. A second bottle of $[\text{RhCp}^*\text{Cl}_2]_2$ was purchased from Energy Chemical. KF, KCl, KBr, KI, NaI, and LiI were purchased from Fisher. $[\text{RuCl}_2(\text{p-cymene})]_2$ was purchased from Alfa Aesar. $\text{RhCl}_3 \cdot x\text{H}_2\text{O}$ and $[\text{Rh}(\text{OAc})_2]_2$ were purchased from Shanxi Kaida Chemical Engineering Co. Ltd. $[\text{IrCp}^*\text{Cl}_2]_2$, $[\text{Rh}(\text{nbd})_2]\text{BF}_4$, $[\text{Rh}(\text{cod})_2]\text{BF}_4$, and $[\text{Rh}(\text{cod})\text{Cl}]_2$ were purchased from J&K. FT azeotrope was distilled and stocked under argon.

5.4.2 Synthesis and characterization of ligands and complexes

$[\text{RhCp}^*\text{I}_2]_2$ was prepared by referring to the literature.^[203] A suspension of $[\text{RhCp}^*\text{Cl}_2]_2$ (0.1 mmol, 61.8 mg) and NaI (1.0 mmol, 149.9 mg) in acetone (30 mL) was refluxed under argon overnight and the solvent was then evaporated. The residual was dissolved in dichloromethane (DCM) and filtered. Dark violet crystals were obtained after recrystallization from DCM/petroleum ether. ^1H NMR (400 MHz, CDCl_3) δ (ppm) = 1.99 (s, 30H).

5.4.3 *In situ* ^1H NMR analysis

The identification of intermediate **d** is based on a reported rhodium dimer com-

plex:^[192] ¹H NMR (400 MHz, CDCl₃): δ (ppm) = -8.87 (t, $J_{\text{RhH}} = 26.8$ Hz, Rh-**H**-Rh), 1.90 (s, C₅Me₅), 7.39 (t, $J_{\text{HH}} = 3.2$ Hz, **HCO**₂). MS (ESI, m/z): 557.0 ([M]⁺).

D is identified as a structure analogue of **d**: ¹H NMR (400 MHz, CDCl₃): δ (ppm) = -8.85 (t, $J_{\text{RhH}} = 30.4$ Hz, Rh-**H**-Rh), 1.89 (s, C₅Me₅), 7.07 (t, $J_{\text{HH}} = 3.2$ Hz, **HCO**₂). MS (ESI, m/z): 648.9 ([M]⁺).

The structure of **E** is speculated based on the following data: ¹H NMR (400 MHz, CDCl₃): δ (ppm) = -11.72 (t, $J_{\text{RhH}} = 32.8$ Hz, Rh-**H**-Rh), 1.96 (s, C₅Me₅). MS (ESI, m/z): 730.9 ([M]⁺).

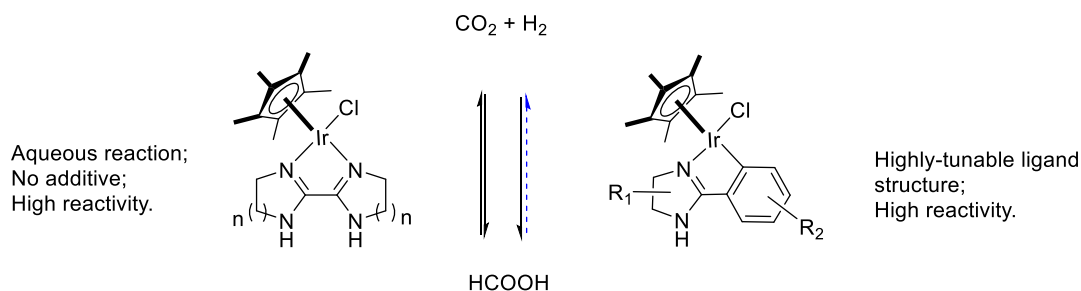
During the *in-situ* ¹H NMR test, various rhodium hydrides were observed with the prolonged reaction time or addition of more FA. It is difficult to assign these hydrido proton peaks, because they may be one (several) of or a mixture of all those unknown intermediates (various bridging H mode) which were formed due to the lack of H⁺ gradually. Meanwhile it explains the importance of maintaining the FT ratio during the long time reaction.



Chapter 6 Conclusions and Perspectives

6.1 Conclusions

This thesis describes efforts made to tackle the challenges in homogeneous hydrogenation of CO_2 to formate/formic acid and formic acid dehydrogenation. From the previous chapters, we can see that problems were identified in this area and new solutions were discovered out of our research. Scheme 6.1 gives a summary of the research covered in this thesis.



Scheme 6.1 Summary of the research of the thesis

- (1) Cyclometallated Ir-N^C complexes and Ir-N,N' diimine complexes have been developed and found to be effective for the hydrogenation of CO_2 to FA/formate and for FA dehydrogenation. These results not only extend the ligand scope for this transformation, which previously was concentrated on the phosphine ligands, pincer ligands and aromatic N,N' ligands, but also provide potential catalysts for hydrogen storage via CO_2 cycling.
- (2) From the view point of atom economy and green chemistry, this thesis has accomplished the base-free aqueous hydrogenation of CO_2 to FA and FA dehydrogenation under mild conditions.
- (3) Chapter 2 and Chapter 4 described the detailed mechanism study on CO_2 hydrogenation and FA dehydrogenation, which to some extent reveals the role of solvent (H_2O)/additive (I) playing in the reactions.

6.2 Deficiencies

Apart from the achievements summed up above, there are several non-negligible deficiencies in this thesis and much more work need to be done considering the following points:

- (1) Chapter 2 should have studied more ligands and more details of the mechanism for a better understanding of the ligand structure influence on the catalytic activity.
- (2) Water has been found to play an important role in the hydrogenation of CO₂ reaction described in Chapters 2 and 3; however it hasn't been explained clearly.
- (3) The water-soluble cyclometallated Ir-N[^]C complex hasn't been obtained in this thesis, which is expected to be effective towards the hydrogenation of CO₂ and FA dehydrogenation in water.

6.3 Perspectives

From the viewpoint of catalyst design, both the cyclometallated Ir-N[^]C complexes and the Ir-N,N' diimine complexes are worth further studying in terms of electronic property and hydrophilicity, e.g. *via* changing the substituents on the ligand ring or synthesizing the acyclic ligands.

Besides FA, methanol as another product of CO₂ hydrogenation is also of important industrial value. FA is usually the intermediate product for homogeneous hydrogenation of CO₂ to methanol. Thus with these highly efficient iridium catalysts, methanol could be possibly produced *via* catalyst integration. Similarly, other chemicals like formamide may also be obtained through this strategy.

These two types of iridium complexes may find themselves useful for other hydrogenation/dehydrogenation reactions, such as the reduction of esters or C=N

bonds etc., through the Ir-H hydride generated *in situ*. Functionalized with chiral groups, these complexes may even be effective for asymmetric hydrogenation.

Notes and References

- [1] Pearson, P. N.; Palmer, M. R.; Atmospheric carbon dioxide concentrations over the past 60 million years[J]. *Nature*, **2000**, *406*: 695-699.
- [2] He, L.-N.; Wang, J.-Q.; Wang, J.-L.; Carbon dioxide chemistry: Examples and challenges in chemical utilization of carbon dioxide[J]. *Pure. Appl. Chem.*, **2009**, *81*(11): 2069–2080.
- [3] Mikkelsen, M.; Jørgensen, M.; Krebs, F. C.; The teraton challenge. A review of fixation and transformation of carbon dioxide[J]. *Energy Environ. Sci.*, **2010**, *3*(1): 43-81.
- [4] Sakakura, T.; Choi, J.-C.; Yasuda, H.; Transformation of carbon dioxide[J]. *Chem. Rev.*, **2007**, *107*: 2365-2387.
- [5] Aresta, M.; Dibenedetto, A.; Utilisation of CO₂ as a chemical feedstock: opportunities and challenges[J]. *Dalton Trans.*, **2007**, (28): 2975-2992.
- [6] Chen, X.; Shen, S.; Guo, L.; Mao, S. S.; Semiconductor-based photocatalytic hydrogen generation[J]. *Chem. Rev.*, **2010**, *110*: 6503-6570.
- [7] Shi, Z.; Wen, X.; Guan, Z.; Cao, D.; Luo, W.; Zou, Z.; Recent progress in photoelectrochemical water splitting for solar hydrogen production[J]. *Annals of Physics*, **2015**, *358*: 236-247.
- [8] Zou, X.; Zhang, Y.; Noble metal-free hydrogen evolution catalysts for water splitting[J]. *Chem. Soc. Rev.*, **2015**, *44*(15): 5148-5180.
- [9] From wikipedia: https://en.wikipedia.org/wiki/Carbon_capture_and_storage
- [10] Das Neves Gomes, C.; Jacquet, O.; Villiers, C.; Thuéry, P.; Ephritikhine, M.; Cantat, T.; A diagonal approach to chemical recycling of carbon dioxide: organocatalytic transformation for the reductive functionalization of CO₂[J]. *Angew. Chem. Int. Ed.*, **2012**, *51*(1): 187-190.
- [11] Aresta, M.; Carbon dioxide as chemical feedstock[M]. Copyright © 2010 Wiley-VCH Verlag GmbH & Co. KGaA.
- [12] Huang, K.; Sun, C.-L.; Shi, Z.-J.; Transition-metal-catalyzed C-C bond formation through the fixation of carbon dioxide[J]. *Chem. Soc. Rev.*, **2011**, *40*(5): 2435-2452.
- [13] Darensbourg, D. J.; Making plastics from carbon dioxide: Salen metal complexes as catalysts for the production of polycarbonates from epoxides and CO₂[J]. *Chem. Rev.*, **2007**, *107*: 2388-2410.
- [14] Sakakura, T.; Kohno, K.; The synthesis of organic carbonates from carbon dioxide[J].

-
- Chem. Commun.*, **2009**, (11): 1312-1330.
- [15] Benson, E. E.; Kubiak, C. P.; Sathrum, A. J.; Smieja, J. M.; Electrocatalytic and homogeneous approaches to conversion of CO₂ to liquid fuels[J]. *Chem. Soc. Rev.*, **2009**, 38(1): 89-99.
- [16] Wang, W.; Wang, S.; Ma, X.; Gong, J.; Recent advances in catalytic hydrogenation of carbon dioxide[J]. *Chem. Soc. Rev.*, **2011**, 40(7): 3703-3727.
- [17] Wang, W.-H.; Himeda, Y.; Muckerman, J. T.; Manbeck, G. F.; Fujita, E.; CO₂ hydrogenation to formate and methanol as an alternative to photo- and electrochemical CO₂ reduction[J]. *Chem. Rev.*, **2015**, 115 (23): 12936–12973.
- [18] Jessop, P. G.; Ikariya, T.; Noyori, R.; Homogeneous hydrogenation of carbon dioxide[J]. *Chem. Rev.*, **1995**, 95(2): 259-271.
- [19] Gattrell, M.; Gupta, N.; Co, A.; A review of the aqueous electrochemical reduction of CO₂ to hydrocarbons at copper[J]. *J. Electroanal. Chem.*, **2006**, 594(1): 1-19.
- [20] Rosen, B. A.; Salehi-Khojin, A.; Thorson, M. R.; Zhu, W.; Whipple, D. T.; Kenis, P. J. A.; Masel, R. I.; Ionic liquid-mediated selective conversion of CO₂ to CO at low overpotentials[J]. *Science*, **2011**, 334: 643-644.
- [21] Costentin, C.; Drouet, S.; Robert, M.; Savéant, J.-M.; A local proton source enhances CO₂ electroreduction to CO by a molecular Fe catalyst[J]. *Science*, **2012**, 338: 90-94.
- [22] Chen, Y.; Li, C. W.; Kanan, M. W.; Aqueous CO₂ reduction at very low overpotential on oxide-derived Au nanoparticles[J]. *J. Am. Chem. Soc.*, **2012**, 134(49): 19969-19972.
- [23] Balaraman, E.; Gunanathan, C.; Zhang, J.; et al. Efficient hydrogenation of organic carbonates, carbamates and formates indicates alternative routes to methanol based on CO₂ and CO[J]. *Nat. Chem.*, **2011**, 3(8): 609-614.
- [24] Tominaga, K.-I.; Sasaki, Y.; Kawai, M.; Watanabe, T.; Saito, M.; Ruthenium complex catalysed hydrogenation of carbon dioxide to carbon monoxide, methanol and methane[J]. *J. Chem. Soc., Chem. Commun.*, **1993**: 629-631.
- [25] Wesselbaum, S.; Vom Stein, T.; Klankermayer, J.; Leitner, W.; Hydrogenation of carbon dioxide to methanol by using a homogeneous ruthenium-phosphine catalyst[J]. *Angew. Chem. Int. Ed. Engl.*, **2012**, 51(30): 7499-7502.
- [26] Farlow, M. W.; Adkins, H.; The hydrogenation of carbon dioxide and a correction of the reported synthesis of urethans[J]. *J. Am. Chem. Soc.*, **1935**, 57(11): 2222-2223.
- [27] Inoue, Y.; Izumida, H.; Sasaki, Y.; Hashimoto, H.; Catalytic fixation of carbon dioxide to formic acid by transition-metal complexes under mild conditions[J]. *Chem. Lett.*, **1976**,

5(8): 863-864.

- [28] Tai, C.-C.; Pitts, J.; Linehan, J. C.; Main, A. D.; Munshi, P.; Jessop, P. G.; In situ formation of ruthenium catalysts for the homogeneous hydrogenation of carbon dioxide[J]. *Inorg. Chem.*, **2002**, *41*(6): 1606-1614.
- [29] Ohnishi, Y.-Y.; Matsunaga, T.; Nakao, Y.; Sato, H.; Sakaki, S.; Ruthenium(II)-catalyzed hydrogenation of carbon dioxide to formic acid. Theoretical study of real catalyst, ligand effects, and solvation effects[J]. *J. Am. Chem. Soc.*, **2005**, *127*: 4021-4032.
- [30] Wang, W.-H.; Hull, J. F.; Muckerman, J. T.; Fujita, E.; Himeda, Y.; Second-coordination-sphere and electronic effects enhance iridium(III)-catalyzed homogeneous hydrogenation of carbon dioxide in water near ambient temperature and pressure[J]. *Energy Environ. Sci.*, **2012**, *5*(7): 7923-7926.
- [31] Jeletic, M. S.; Mock, M. T.; Appel, A. M.; Linehan, J. C.; A cobalt-based catalyst for the hydrogenation of CO₂ under ambient conditions[J]. *J. Am. Chem. Soc.*, **2013**, *135*(31): 11533-11536.
- [32] Filonenko, G. A.; Van Putten, R.; Schulpen, E. N.; Hensen, E. J. M.; Pidko, E. A.; Highly efficient reversible hydrogenation of carbon dioxide to formates using a ruthenium PNP-pincer catalyst[J]. *ChemCatChem.*, **2014**, *6*(6): 1526-1530.
- [33] Ezhova, N. N.; Kolesnichenko, N. V.; Bulygin, A. V.; Slivinskii, E. V.; Han, S.; Hydrogenation of CO₂ to formic acid in the presence of the Wilkinson complex[J]. *Russ. Chem. Bull., Int. Ed.*, **2002**, *51*(12): 2165-2169.
- [34] Graf, E.; Leitner, W.; Direct formation of formic acid from carbon dioxide and dihydrogen using the $[\{\text{Rh}(\text{cod})\text{Cl}\}_2]\text{-Ph}_2\text{P}(\text{CH}_2)_4\text{PPh}_2$ catalyst system[J]. *J. Chem. Soc., Chem. Commun.*, **1992**: 623-624.
- [35] Federsel, C.; Boddien, A.; Jackstell, R.; Jennerjahn, R.; Dyson, P. J.; Scopelliti, R.; Laurency, G.; Beller, M.; A well-defined iron catalyst for the reduction of bicarbonates and carbon dioxide to formates, alkyl formates, and formamides[J]. *Angew. Chem. Int. Ed. Engl.*, **2010**, *49*(50): 9777-9780.
- [36] Federsel, C.; Ziebart, C.; Jackstell, R.; Baumann, W.; Beller, M.; Catalytic hydrogenation of carbon dioxide and bicarbonates with a well-defined cobalt dihydrogen complex[J]. *Chem. Eur. J.*, **2012**, *18*(1): 72-75.
- [37] Hsu, S.-F.; Rommel, S.; Eversfield, P.; Muller, K.; Klemm, E.; Thiel, W. R.; Plietker, B.; A rechargeable hydrogen battery based on Ru catalysis[J]. *Angew. Chem. Int. Ed. Engl.*, **2014**, *53*(27): 7074-7078.

-
- [38] Huff, C. A.; Sanford, M. S.; Catalytic CO₂ hydrogenation to formate by a ruthenium pincer complex[J]. *ACS Catal.*, **2013**, 3(10): 2412-2416.
- [39] Lau, C. P.; Chen, Y. Z.; Hydrogenation of carbon dioxide to formic acid using a 6,6'-dichloro-2,2'-bipyridine complex of ruthenium, cis-[Ru(6,6'-Cl₂bpy)₂(H₂O)₂](CF₃SO₃)₂[J]. *J. Mol. Catal. A: Chem.*, **1995**, 101: 33-36.
- [40] Jessop, P. G.; Ikariya, T.; Noyori, R.; Homogeneous hydrogenation of supercritical carbon-dioxide[J]. *Nature*, **1994**, 368: 231-233.
- [41] Munshi, P.; Main, A. D.; Linehan, J. C.; Tai, C.-C.; Jessop, P. G.; Hydrogenation of carbon dioxide catalyzed by ruthenium trimethylphosphine complexes: the accelerating effect of certain alcohols and amines[J]. *J. Am. Chem. Soc.*, **2002**, 124(9): 7963-7971.
- [42] Jessop, P. G.; Hsiao, Y.; Ikariya, T.; Noyori, R.; Homogeneous catalysis in supercritical fluids: hydrogenation of supercritical carbon dioxide to formic acid, alkyl formates, and formamides[J]. *J. Am. Chem. Soc.*, **1996**, 118 (2): 344-355.
- [43] Wesselbaum, S.; Hintermair, U.; Leitner, W.; Continuous-flow hydrogenation of carbon dioxide to pure formic acid using an integrated scCO₂ process with immobilized catalyst and base[J]. *Angew. Chem. Int. Ed.*, **2012**, 51(34): 8585-8588.
- [44] Gassner, F.; Leitner, W.; Hydrogenation of carbon dioxide to formic acid using water-soluble rhodium catalysts[J]. *J. Chem. Soc., Chem. Commun.*, **1993**, 19: 1465-1466.
- [45] Jo ó F.; Laurency, G.; N ádasdibc, L.; Elekb, J.; Homogeneous hydrogenation of aqueous hydrogen carbonate to formate under exceedingly mild conditions-a novel possibility of carbon dioxide activation[J]. *Chem. Commun.*, **1999**: 971-972.
- [46] Elek. J.; N ádasdi, L.; Papp, G.; Laurency, G., Jo ó F.; Homogeneous hydrogenation of carbon dioxide and bicarbonate in aqueous solution catalyzed by water-soluble ruthenium(II) phosphine complexes[J]. *Applied Catalysis A: General*, **2003**, 255(1): 59-67.
- [47] J ószai, I.; Jo ó F.; Hydrogenation of aqueous mixtures of calcium carbonate and carbon dioxide using a water-soluble rhodium(I)-tertiary phosphine complex catalyst[J]. *J. Mol. Catal. A: Chem.*, **2004**, 224(1-2): 87-91.
- [48] Kath ó Á.; Opre, Z.; Laurency, G.; Jo ó F.; Water-soluble analogs of [RuCl₃(NO)(PPh₃)₂] and their catalytic activity in the hydrogenation of carbon dioxide and bicarbonate in aqueous solution[J]. *J. Mol. Catal. A: Chem.*, **2003**, 204-205: 143-148.
- [49] Laurency, G.; Joo, F.; N ádasdi, L.; Formation and characterization of water-soluble

-
- hydrido-ruthenium(II) complexes of 1,3,5-triaza-7-phosphaadamantane and their catalytic activity in hydrogenation of CO₂ and HCO₃⁻ in aqueous solution[J]. *Inorg. Chem.*, **2000**, *39*: 5083-5088.
- [50] Horváth, H.; Laurenczy, G.; Kathó, A.; Water-soluble (η^6 -arene)ruthenium(II)-phosphine complexes and their catalytic activity in the hydrogenation of bicarbonate in aqueous solution[J]. *J. Organomet. Chem.*, **2004**, *689*(6): 1036-1045.
- [51] Laurenczy, G.; Jedner, S.; Alessio, E.; Dyson, P. J.; In situ NMR characterisation of an intermediate in the catalytic hydrogenation of CO₂ and HCO₃⁻ in aqueous solution [J]. *Inorg. Chem. Commun.*, **2007**, *10*(5): 558-562.
- [52] Tanaka, R.; Yamashita, M.; Nozaki, K.; Catalytic hydrogenation of carbon dioxide using Ir(III)-pincer complexes[J]. *J. Am. Chem. Soc.*, **2009**, *131*: 14168–14169.
- [53] Tanaka, R.; Yamashita, M.; Chung, L. W.; Morokuma, K.; Nozaki, K.; Mechanistic studies on the reversible hydrogenation of carbon dioxide catalyzed by an Ir-PNP Complex[J]. *Organometallics*, **2011**, *30*(24): 6742-6750.
- [54] Van der Boom, M. E.; Milstein, D.; Cyclometalated phosphine-based pincer complexes: mechanistic insight in catalysis, coordination, and bond activation[J]. *Chem. Rev.*, **2003**, *103*: 1759-1792.
- [55] Liu, F.; Pak, E. B.; Singh, B.; Jensen, C. M.; Goldman, A. S.; Dehydrogenation of n-alkanes catalyzed by iridium “pincer” complexes: regioselective formation of α -olefins[J]. *J. Am. Chem. Soc.*, **1999**, *121*: 4086-4087.
- [56] Haenel, M. W.; Oevers, S.; Angermund, K.; Kaska, W. C.; Fan, H.-J.; Hall, M. B.; Thermally stable homogeneous catalysts for alkane dehydrogenation[J]. *Angew. Chem. Int. Ed.*, **2001**, *40*(19): 3596-3600.
- [57] Schmeier, T. J.; Dobereiner, G. E.; Crabtree, R. H.; Hazari, N.; Secondary coordination sphere interactions facilitate the insertion step in an iridium(III) CO₂ reduction catalyst[J]. *J. Am. Chem. Soc.*, **2011**, *133*(24): 9274-9277.
- [58] Langer, R.; Diskin-Posner, Y.; Leitus, G.; Shimon, L. J.; Ben-David, Y.; Milstein, D.; Low-pressure hydrogenation of carbon dioxide catalyzed by an iron pincer complex exhibiting noble metal activity[J]. *Angew. Chem. Int. Ed.*, **2011**, *50*(42): 9948-9952.
- [59] Azua, A.; Sanz, S.; Peris, E.; Water-soluble Ir^{III} N-heterocyclic carbene based catalysts for the reduction of CO₂ to formate by transfer hydrogenation and the deuteration of aryl amines in water[J]. *Chem. Eur. J.*, **2011**, *17*(14): 3963-3967.
- [60] Sanz, S.; Benítez, M.; Peris, E.; A new approach to the reduction of carbon dioxide: CO₂

-
- reduction to formate by transfer hydrogenation in *i*PrOH[J]. *Organometallics*, **2010**, 29(1): 275-277.
- [61] Sanz, S.; Azua, A.; Peris, E.; '(η^6 -arene)Ru(bis-NHC)' complexes for the reduction of CO₂ to formate with hydrogen and by transfer hydrogenation with *i*PrOH[J]. *Dalton Trans.*, **2010**, 39(27): 6339-6343.
- [62] Himeda, Y.; Onozawa-Komatsuzaki, N.; Sugihara, H.; Kasuga, K.; Simultaneous tuning of activity and water solubility of complex catalysts by acid-base equilibrium of ligands for conversion of CO₂[J]. *Organometallics*, **2007**, 26: 702-712.
- [63] Himeda, Y.; Miyazawa, S.; Hirose, T.; Interconversion between formic acid and H₂/CO₂ using rhodium and ruthenium catalysts for CO₂ fixation and H₂ storage[J]. *ChemSusChem*, **2011**, 4(4): 487-493.
- [64] Himeda, Y.; Onozawa-Komatsuzaki, N.; Sugihara, H.; Arakawa, H.; Kasuga, K.; Transfer hydrogenation of a variety of ketones catalyzed by rhodium complexes in aqueous solution and their application to asymmetric reduction using chiral Schiff base ligands[J]. *J. Mol. Catal. A: Chem.*, **2003**, 195(1-2): 95-100.
- [65] Himeda, Y.; Onozawa-Komatsuzaki, N.; Sugihara, H.; Kasuga, K.; Highly efficient conversion of carbon dioxide catalyzed by half-sandwich complexes with pyridinol ligand: The electronic effect of oxyanion[J]. *J. Photochem. Photobiol., A: Chem.*, **2006**, 182(3): 306-309.
- [66] Maenaka, Y.; Suenobu, T.; Fukuzumi, S.; Catalytic interconversion between hydrogen and formic acid at ambient temperature and pressure[J]. *Energy Environ. Sci.*, **2012**, 5(6): 7360-7367.
- [67] Hull, J. F.; Himeda, Y.; Wang, W. -H.; Hashiguchi, B.; Periana, R.; Szalda, D. J.; Muckerman, J. T.; Fujita, E.; Reversible hydrogen storage using CO₂ and a proton-switchable iridium catalyst in aqueous media under mild temperatures and pressures[J]. *Nat. Chem.*, **2012**, 4(5): 383-388.
- [68] Suna, Y.; Ertem, M. Z.; Wang, W.-H.; Kambayashi, H.; Manaka, Y.; Muckerman, J. T.; Fujita, E.; Himeda, Y.; Positional effects of hydroxy groups on catalytic activity of proton-responsive half-sandwich Cp*Iridium(III) complexes[J]. *Organometallics*, **2014**, 33(22): 6519-6530.
- [69] Wang, W.-H.; Muckerman, J. T.; Fujita, E.; Himeda, Y.; Mechanistic insight through factors controlling effective hydrogenation of CO₂ catalyzed by bioinspired proton-responsive iridium(III) complexes[J]. *ACS Catal.*, **2013**, 3(5): 856-860.

-
- [70] Himeda, Y.; Onozawa-Komatsuzaki, N.; Sugihara, H.; Arakawa, H.; Kasuga, K.; Half-sandwich complexes with 4,7-dihydroxy-1,10-phenanthroline: Water-soluble, highly efficient catalysts for hydrogenation of bicarbonate attributable to the generation of an oxyanion on the catalyst ligand[J]. *Organometallics*, **2004**, *23*: 1480-1483.
- [71] Himeda, y.; Onozawa-Komatsuzaki, N.; Sugihara, H.; Kasuga, K.; Recyclable catalyst for conversion of carbon dioxide into formate attributable to an oxyanion on the catalyst ligand[J]. *J. Am. Chem. Soc.*, **2005**, *127*(38): 13118–13119.
- [72] Tsai, J.-C.; Nicholas, K. M.; Rhodium-catalyzed hydrogenation of carbon dioxide to formic acid[J]. *J. Am. Chem. Soc.*, **1992**, *114*(13): 5117-5124.
- [73] Hayashi, H.; Ogo, S.; Fukuzumi, S.; Aqueous hydrogenation of carbon dioxide catalysed by water-soluble ruthenium aqua complexes under acidic conditions[J]. *Chem. Commun.*, **2004**, (23): 2714-2715.
- [74] Ogo, S.; Kabe, R.; Hayashi, H.; Harada, R.; Fukuzumi, S.; Mechanistic investigation of CO₂ hydrogenation by Ru(II) and Ir(III) aqua complexes under acidic conditions: two catalytic systems differing in the nature of the rate determining step[J]. *Dalton Trans.*, **2006**, (39): 4657-4663.
- [75] Moret, S.; Dyson, P. J.; Laurenczy, G.; Direct synthesis of formic acid from carbon dioxide by hydrogenation in acidic media[J]. *Nat. Commun.*, **2014**, *5*: 1-13.
- [76] Bren, K. L.; Multidisciplinary approaches to solar hydrogen[J]. *Interface Focus*, **2015**, *5*(3): 20140091.
- [77] Abe, R.; Recent progress on photocatalytic and photoelectrochemical water splitting under visible light irradiation[J]. *J. Photochem. Photobiol., C: Photochem. Rev.*, **2010**, *11*(4): 179-209.
- [78] Chen, X.; Li, C.; Gratzel, M.; Kostecki, R.; Mao, S. S.; Nanomaterials for renewable energy production and storage[J]. *Chem. Soc. Rev.*, **2012**, *41*(23): 7909-7937.
- [79] Ma, Y.; Wang, X.; Li, C.; Charge separation promoted by phase junctions in photocatalysts[J]. *Chin. J. Catal.*, **2015**, *36*(9): 1519-1527.
- [80] Gloaguen, F.; Rauchfuss, T. B.; Small molecule mimics of hydrogenases: hydrides and redox[J]. *Chem. Soc. Rev.*, **2009**, *38*(1): 100-108.
- [81] Losse, S.; Vos, J. G.; Rau, S.; Catalytic hydrogen production at cobalt centres[J]. *Coord. Chem. Rev.*, **2010**, *254*(21-22): 2492-2504.
- [82] Thoi, V. S.; Sun, Y.; Long, J. R.; Chang, C. J.; Complexes of earth-abundant metals for catalytic electrochemical hydrogen generation under aqueous conditions[J]. *Chem. Soc.*

Rev., **2013**, 42(6): 2388-2400.

- [83] Clough, A. J.; Yoo, J. W.; Mecklenburg, M. H.; Marinescu, S. C.; Two-dimensional metal-organic surfaces for efficient hydrogen evolution from water[J]. *J. Am. Chem. Soc.*, **2015**, 137(1): 118-121.
- [84] Darkrim, F. L.; Malbrunot, P.; Tartaglia, G. P.; Review of hydrogen storage by adsorption in carbon[J]. *International Journal of Hydrogen Energy*, **2002**, 27: 193-202.
- [85] Dong, J.; Wang, X.; Xu, H.; Zhao, Q.; Li, J.; Hydrogen storage in several microporous zeolites[J]. *Int. J. Hydrogen Energy*, **2007**, 32(18): 4998-5004.
- [86] Murray, L. J.; Dinca, M.; Long, J. R.; Hydrogen storage in metal-organic frameworks[J]. *Chem. Soc. Rev.*, **2009**, 38(5): 1294-1314.
- [87] Meregalli, V.; Parrinello, M.; Review of theoretical calculations of hydrogen storage in carbon-based materials[J]. *Appl. Phys. A: Mater. Sci. & Process.*, **2001**, 72(2): 143-146.
- [88] Sculley, J.; Yuan, D.; Zhou, H.-C.; The current status of hydrogen storage in metal-organic frameworks-updated[J]. *Energy Environ. Sci.*, **2011**, 4(8): 2721-2735.
- [89] Sakintuna, B.; Lamaridarkrim, F.; Hirscher, M.; Metal hydride materials for solid hydrogen storage: A review[J]. *Int. J. Hydrogen Energy*, **2007**, 32(9): 1121-1140.
- [90] Graetz, J.; New approaches to hydrogen storage[J]. *Chem. Soc. Rev.*, **2009**, 38(1): 73-82.
- [91] Grochala, W.; Edwads, P. P.; Thermal decomposition of the non-interstitial hydrides for the storage and production of hydrogen[J]. *Chem. Rev.*, **2004**, 104: 1283-1315.
- [92] Felderhoff, M.; Weidenthaler, C.; Von Helmolt, R.; Eberle, U.; Hydrogen storage: the remaining scientific and technological challenges[J]. *Phys. Chem. Chem. Phys.*, **2007**, 9(21): 2643-2653.
- [93] Van Den Berg, A. W. C.; Areán, C. O.; Materials for hydrogen storage: current research trends and perspectives[J]. *Chem. Commun.*, **2008**, (6): 668-681.
- [94] Zhu, Q.-L.; Xu, Q.; Liquid organic and inorganic chemical hydrides for high-capacity hydrogen storage[J]. *Energy Environ. Sci.*, **2015**, 8(2): 478-512.
- [95] Williams, R.; Crandall, R. S.; Bloom, A.; Use of carbon dioxide in energy storage[J]. *Appl. Phys. Lett.*, **1978**, 33(5): 381.
- [96] Bi, Q.-Y.; Lin, J.-D.; Liu, Y.-M.; Du, X.-L.; Wnag, J.-Q.; He, H.-Y.; Cao, Y.; An aqueous rechargeable formate-based hydrogen battery driven by heterogeneous Pd catalysis[J]. *Angew. Chem. Int. Ed. Engl.*, **2014**, 53(49): 13583-13587.
- [97] Grasemann, M.; Laurenczy, G.; Formic acid as a hydrogen source—recent developments and future trends[J]. *Energy Environ. Sci.*, **2012**, 5(8): 8171-8181.

-
- [98] Loges, B.; Boddien, A.; Gärtner, F.; Junge, H.; Beller, M.; Catalytic generation of hydrogen from formic acid and its derivatives: Useful hydrogen storage materials[J]. *Top. Catal.*, **2010**, *53*(13-14): 902-914.
- [99] Fukuzumi, S.; Bioinspired energy conversion systems for hydrogen production and storage[J]. *Eur. J. Inorg. Chem.*, **2008**, (9): 1351-1362.
- [100] Joó, F.; Breakthroughs in hydrogen storage-Formic acid as a sustainable storage material for hydrogen[J]. *ChemSusChem*, **2008**, *1*(10): 805-808.
- [101] Enthaler, S.; Von Langermann, J.; Schmidt, T.; Carbon dioxide and formic acid—the couple for environmental-friendly hydrogen storage?[J]. *Energy Environ. Sci.*, **2010**, *3*(9): 1207-1217.
- [102] Johnson, T. C.; Morris, D. J.; Wills, M.; Hydrogen generation from formic acid and alcohols using homogeneous catalysts[J]. *Chem. Soc. Rev.*, **2010**, *39*(1): 81-88.
- [103] Tedsree, K.; Li, T.; Jones, S.; Chan, C. W. A.; Yu, K. M. K.; Bagot, P. A. J.; Marquis, E. A.; Smith, G. D. W.; Tsang, S. C. E.; Hydrogen production from formic acid decomposition at room temperature using a Ag-Pd core-shell nanocatalyst[J]. *Nature Nanotech.*, **2011**, *6*(5): 302-307.
- [104] Zhu, Q.-L.; Tsumori, N.; Xu, Q.; Sodium hydroxide-assisted growth of uniform Pd nanoparticles on nanoporous carbon MSC-30 for efficient and complete dehydrogenation of formic acid under ambient conditions[J]. *Chem. Sci.*, **2014**, *5*(1): 195-199.
- [105] Noyori, R.; Hashiguchi, S.; Asymmetric transfer hydrogenation catalyzed by chiral ruthenium complexes[J]. *Acc. Chem. Res.*, **1997**, *30*: 97-102.
- [106] Ikariya, T.; Blacker, A. J.; Asymmetric transfer hydrogenation of ketones with bifunctional transition metal-based molecular catalysts[J]. *Acc. Chem. Res.*, **2007**, *40*: 1300-1308.
- [107] Wei, Y.; Wu, X.; Wang, C.; Xiao, J.; Transfer hydrogenation in aqueous media[J]. *Catal. Today*, **2015**, *247*: 104-116.
- [108] Coffey, R. S.; The decomposition of formic acid catalysed by soluble metal complexes[J]. *Chem. Commun.*, **1967**: 923-924.
- [109] Loges, B.; Boddien, A.; Junge, H.; Beller, M.; Controlled generation of hydrogen from formic acid amine adducts at room temperature and application in H₂/O₂ fuel cells[J]. *Angew. Chem. Int. Ed. Engl.*, **2008**, *47*(21): 3962-3965.
- [110] Boddien, A.; Loges, B.; Junge, H.; Beller, M.; Hydrogen generation at ambient conditions: application in fuel cells[J]. *ChemSusChem*, **2008**, *1*(8-9): 751-758.

-
- [111] Sponholz, P.; Mellmann, D.; Junge, H.; Beller, M.; Towards a practical setup for hydrogen production from formic acid[J]. *ChemSusChem*, **2013**, 6(7): 1172-1176.
- [112] Majewski, A.; Morris, d.; Kendall, K.; Wills, M.; Continuous-flow method for the generation of hydrogen from formic acid[J]. *ChemSusChem*, **2010**, 3(4): 431-434.
- [113] Morris, D. J.; Clarkson, G. J.; Wills, M.; Insights into hydrogen generation from formic acid using ruthenium complexes[J]. *Organometallics*, **2009**, 28(14): 4133-4140.
- [114] Zell, T.; Butschke, B.; Ben-David, Y.; Milstein, D.; Efficient hydrogen liberation from formic acid catalyzed by a well-defined iron pincer complex under mild conditions[J]. *Chem. Eur. J.*, **2013**, 19: 8068-8072.
- [115] Myers, T. W.; Berben, L. A.; Aluminium–ligand cooperation promotes selective dehydrogenation of formic acid to H₂ and CO₂[J]. *Chem. Sci.*, **2014**, 5(7): 2771-2777.
- [116] Barnard, J. H.; Wang, C.; Berry, N. G.; Xiao, J.; Long-range metal–ligand bifunctional catalysis: Cyclometallated iridium catalysts for the mild and rapid dehydrogenation of formic acid[J]. *Chem. Sci.*, **2013**, 4(3): 1234-1244.
- [117] Bielinski, E. A.; Lagaditis, P. O.; Zhang, Y.; Mercado, B. Q.; Wurtele, C.; Bernskoetter, W. H.; Hazari, N.; Schneider, S.; Lewis acid-assisted formic acid dehydrogenation using a pincer-supported iron catalyst[J]. *J. Am. Chem. Soc.*, **2014**, 136(29): 10234-10237.
- [118] Boddien, A.; Mellmann, D.; Gartner, F.; Jackstell, R.; Junge, H.; Dyson, P. J.; Laurency, G.; Ludwig, R.; Beller, M.; Efficient dehydrogenation of formic acid using an iron catalyst[J]. *Science*, **2011**, 333(6050): 1733-1736.
- [119] Mellmann, D.; Barsch, E.; Bauer, M.; Grabow, K.; Boddien, A.; Kammer, A.; Sponholz, P.; Bentrup, U.; Jackstell, R.; Junge, H.; Laurency, G.; Ludwig, R.; Beller, M.; Base-free non-noble-metal-catalyzed hydrogen generation from formic acid: scope and mechanistic insights[J]. *Chem. Eur. J.*, **2014**, 20(42): 13589-13602.
- [120] Oldenhof, S.; De Bruin, B.; Lutz, M.; Siegler, M. A.; Patureau, F. W.; Van Der Vlugt, J. I.; Reek, J. N. H.; Base-free production of H₂ by dehydrogenation of formic acid using an iridium-bisMETAMORPhos complex[J]. *Chem. Eur. J.*, **2013**, 19(35): 11507-11511.
- [121] Oldenhof, S.; De Bruin, B.; Lutz, M.; Siegler, M. A.; Patureau, F. W.; Van Der Vlugt, J. I.; Reek, J. N. H.; Base-free production of H₂ by dehydrogenation of formic acid using an iridium-bisMETAMORPhos complex[J]. *Chem. Eur. J.*, **2013**, 19(35): 11507-11511.
- [122] Fellay, C.; Dyson, P. J.; Laurency, G.; A viable hydrogen-storage system based on selective formic acid decomposition with a ruthenium catalyst[J]. *Angew. Chem. Int. Ed. Engl.*, **2008**, 47(21): 3966-3968.

-
- [123] Fellay, C.; Yan, N.; Dyson, P. J.; Laurency, G.; Selective formic acid decomposition for high-pressure hydrogen generation: A mechanistic study[J]. *Chem. Eur. J.*, **2009**, *15*(15): 3752-3760.
- [124] Fukuzumi, S.; Kobayashi, T.; Suenobu, T.; Efficient catalytic decomposition of formic acid for the selective generation of H₂ and H/D exchange with a water-soluble rhodium complex in aqueous solution[J]. *ChemSusChem*, **2008**, *1*(10): 827-834.
- [125] Fukuzumi, S.; Kobayashi, T.; Suenobu, T.; Unusually large tunneling effect on highly efficient generation of hydrogen and hydrogen isotopes in pH-selective decomposition of formic acid catalyzed by a heterodinuclear iridium–ruthenium complex in water[J]. *J. Am. Chem. Soc.*, **2010**, *132*: 1496–1497.
- [126] Wang, W.-H.; Xu, S.; Manaka, Y.; Suna, Y.; Kambayashi, H.; Muckerman, J. T.; Fujita, E.; Himeda, Y.; Formic acid dehydrogenation with bioinspired iridium complexes: A kinetic isotope effect study and mechanistic insight[J]. *ChemSusChem*, **2014**, *7*(7): 1976-1983.
- [127] Himeda, Y.; Highly efficient hydrogen evolution by decomposition of formic acid using an iridium catalyst with 4,4'-dihydroxy-2,2'-bipyridine[J]. *Green Chem.*, **2009**, *11*(12): 2018-2022.
- [128] Manaka, Y.; Wang, W.-H.; Suna, Y.; Kambayashi, H.; Muckerman, J. T.; Fujita, E.; Himeda, Y.; Efficient H₂ generation from formic acid using azole complexes in water[J]. *Catal. Sci. Technol.*, **2014**, *4*(1): 34-37.
- [129] Boddien, A.; Gartner, F.; Federsel, C.; Sponholz, P.; Mellmann, D.; Jackstell, R.; Junge, H.; Beller, M.; CO₂-"neutral" hydrogen storage based on bicarbonates and formates[J]. *Angew. Chem. Int. Ed. Engl.*, **2011**, *50*(28): 6411-6414.
- [130] Boddien, A.; Federsel, C.; Sponholz, P.; Mellmann, D.; Jackstell, R.; Junge, H.; Laurency, G.; Beller, M.; Towards the development of a hydrogen battery[J]. *Energy Environ. Sci.*, **2012**, *5*(10): 8907-8911.
- [131] Wang, C., Pettman, A.; Basca, J.; Xiao, J.; A versatile catalyst for reductive amination by transfer hydrogenation[J]. *Angew. Chem. Int. Ed. Engl.*, **2010**, *49*(41): 7548-7552.
- [132] Wang, C., Pettman, A.; Basca, J.; Xiao, J.; A versatile catalyst for reductive amination by transfer hydrogenation[J]. *Angew. Chem. Int. Ed.*, **2010**, *49*(41): 7548-7552.
- [133] Tang, W.; Lau, C.; Wu, X.; Xiao, J.; Cyclometalated iridium complexes as highly active catalysts for the hydrogenation of imines[J]. *Synlett.*, **2013**, *25*(1): 81-84.
- [134] Talwar, D.; Salguero, N. P.; Robertson, C. M.; Xiao, J.; Primary amines by transfer

-
- hydrogenative reductive amination of ketones by using cyclometalated Ir^{III} catalysts[J]. *Chem. Eur. J.*, **2014**, 20(1): 245-252.
- [135] Li, Y.-N.; He, L.-N.; Liu, A.-H.; Lang, X.-D.; Yang, Z.-Z.; Yu, B.; Luan, C.-R.; In situ hydrogenation of captured CO₂ to formate with polyethyleneimine and Rh/monophosphine system[J]. *Green Chem.*, **2013**, 15(10): 2825-2829.
- [136] Liu, C.; Xie, J.-H.; Tian, G.-L.; Li, W.; Zhou, Q.-L.; Highly efficient hydrogenation of carbon dioxide to formate catalyzed by iridium(III) complexes of imine–diphosphine ligands[J]. *Chem. Sci.*, **2015**, 6(5): 2928-2931.
- [137] Ziebart, C.; Federsel, C.; Anbarasan, P.; Jackstell, R.; Baumann, W.; Spannenberg, A.; Beller, M.; Well-defined iron catalyst for improved hydrogenation of carbon dioxide and bicarbonate[J]. *J. Am. Chem. Soc.*, **2012**, 134(51): 20701-20704.
- [138] Enthaler, S.; Brück, A.; Kammer, A.; Junge, H.; Irran, E.; Güllak, S.; Exploring the reactivity of nickel pincer complexes in the decomposition of formic acid to CO₂/H₂ and the hydrogenation of NaHCO₃ to HCOONa[J]. *ChemCatChem*, **2015**, 7(1): 65-69.
- [139] Sortais, J.-B.; Ritleng, V.; Voelklin, A.; Holuigue, A.; Smail, H.; Barloy, L.; Sirlin, C.; Verzijl, G. K. M.; Boogers, J. A. F.; De Vries, A. H. M.; De Vries, J. G.; Pfeffer, M.; Cycloruthenated primary and secondary amines as efficient catalyst precursors for asymmetric transfer hydrogenation[J]. *Organic Letters*, **2005**, 7(7): 1247-1250.
- [140] Pannetier, N.; Sortais, J.-B.; Dieng, P. S.; Barloy, L.; Sirlin, C.; Pfeffer, M.; Kinetics and mechanism of ruthenacycle-catalyzed asymmetric hydrogen transfer[J]. *Organometallics*, **2008**, 27(22): 5852–5859.
- [141] Please refer to Jennifer Smith's thesis for complex **7**. The characterizations can be found in the experimental section.
- [142] Koinuma, H.; Yoshida, Y.; Hirai, H.; Preparation of chlorocarbonylbis(triphenylphosphine)rhodium from tris(triphenylphosphine)chlororhodium, carbon dioxide, and molecular hydrogen[J]. *Chem. Lett.*, **1975**, 4(12): 1223-1226.
- [143] Frisch, M. J.; Trucks, G. W.; Schlegel, H. B.; Scuseria, G. E.; Robb, M. A.; Cheeseman, J. R.; Scalmani, G.; Barone, V.; Mennucci, B.; Petersson, G. A.; Gaussian 09, revision C.01; Gaussian, Inc.: Wallingford, CT, **2009**.
- [144] Becke, A. D.; Density-functional thermochemistry. III. The role of exact exchange[J]. *J. Chem. Phys.*, **1993**, 98(7): 5648-5652.
- [145] Lee, C.; Yang, W.; Parr, R. G.; Development of the Colle-Salvetti correlation-energy

-
- formula into a functional of the electron density[J]. *Phys. Rev. B: Condens. Matter*, **1988**, 37(2): 785-789.
- [146] Dennington, R.; Keith, T.; Millam, J.; Eppinnett, K.; Hovell, W. L.; Gilliland, R. GaussView 3; Semichem Inc.: Shawnee Mission, KS, **2003**.
- [147] Ishihara, M.; Togo, H.; An efficient preparation of 2-imidazolines and imidazoles from aldehydes with molecular iodine and (diacetoxyiodo)benzene[J]. *Synlett.*, **2006**, (2): 227-230.
- [148] Gurudutt, K. N.; Srinivas, P.; Srinivas, S.; An elegant synthesis of [1-¹⁴C] hexadecyltrimethylammonium bromide [CTAB][J]. *J. Labelled Compd. Radiopharm.*, **1993**, 33(1): 33-38.
- [149] Szymańska, I.; Dolusic, E.; Dehaen, W.; Maes, W.; Ito, T.; Radecka, H.; Determination of interaction strength between corrole and phenol derivatives in aqueous media using atomic force microscopy[J]. *Supramol. Chem.*, **2009**, 21(7): 555-563.
- [150] Davies, D. L.; Al-Duaij, O.; Fawcett, J.; Giardiello, M.; Hilton, S. T.; Russell, D. R.; Room-temperature cyclometallation of amines, imines and oxazolines with [MCl₂Cp*]₂ (M = Rh, Ir) and [RuCl₂(p-cymene)]₂[J]. *Dalton Trans.*, **2003**: 4132-4138.
- [151] Leitner, W.; Carbon dioxide as a raw material: The synthesis of formic acid and its derivatives from CO₂[J]. *Angew. Chem. Int. Ed. Engl.*, **1995**, 34(20): 2207-2221.
- [152] Liu, X.-M.; Lu G. Q.; Yan, Z.-F.; Beltramini, J.; Recent advances in catalysts for methanol synthesis via hydrogenation of CO and CO₂[J]. *Ind. Eng. Chem. Res.*, **2003**, 42(25): 6518-6530.
- [153] Jessop, P. G.; Joó, F.; Tai, C.-C.; Recent advances in the homogeneous hydrogenation of carbon dioxide[J]. *Coord. Chem. Rev.*, **2004**, 248(21-24): 2425-2442.
- [154] Razali, N. A. M.; Lee, K. T.; Bhatia, S.; Mohamed, A. R.; Heterogeneous catalysts for production of chemicals using carbon dioxide as raw material: A review[J]. *Renew. Sust. Energ. Rev.*, **2012**, 16(7): 4951-4964.
- [155] Cotton, F. A.; Wilkinson, G.; Murillo, C. A.; Bochmann, M.; Advanced Inorganic Chemistry, Wiley-Interscience, New York, 6th edn, **1999**, 226-227.
- [156] Fujioka, H.; Murai, K.; Ohba, Y.; Hiramatsu, A.; Kita, Y.; A mild and efficient one-pot synthesis of 2-dihydroimidazoles from aldehydes[J]. *Tetrahedron Lett.*, **2005**, 46(13): 2197-2199.
- [157] Ishihara, M.; Togo, H.; Direct oxidative conversion of aldehydes and alcohols to 2-imidazolines and 2-oxazolines using molecular iodine[J]. *Tetrahedron*, **2007**, 63(6):

1474-1480.

- [158] Nasr-Esfahani, M.; Montazerzohori, M.; Mehrizi, S.; Efficient and one-pot catalytic synthesis of 2-imidazolines and bis-imidazolines with *p*-toluenesulfonic acid under solvent free conditions[J]. *J. Heterocyclic Chem.*, **2011**, 48(2): 249-254.
- [159] Geden, J. V.; Pancholi, A. K.; Shipman, M.; Palladium-catalyzed multicomponent synthesis of 2-aryl-2-imidazolines from aryl halides and diamines[J]. *J. Org. Chem.*, **2013**, 78(8): 4158-4164.
- [160] Wang, J. C.; Bauman, J. E.; Complexes of 2,2'-bi-2-imidazoline with transition metal ions[J]. *Inorg. Chem.*, **1965**, 4(11), 1613-1615.
- [161] Gogoi, P.; Konwar, D.; An efficient and one-pot synthesis of imidazolines and benzimidazoles via anaerobic oxidation of carbon–nitrogen bonds in water[J]. *Tetrahedron Lett.*, **2006**, 47: 79-82.
- [162] During the preparation of this thesis and our publication, Himeda and Onishi et al. reported an iridium complex with the diimidazoline ligand for the hydrogenation of CO₂ in the presence of Base: Xu, S.; Onishi, N.; Tsurusaki, A.; Manaka, Y.; Wang, W.-H.; Muckerman, J. T.; Fujita, E.; Himeda, Y.; Efficient Cp*Ir catalysts with imidazoline ligands for CO₂ hydrogenation[J]. *Eur. J. Inorg. Chem.*, **2015**, 34: 5591–5594.
- [163] The slightly larger solubility of H₂ in D₂O than that in H₂O is also possible to cause a reverse KIE, but the value should not be such distinct.
- [164] Flagg, S. C.; Giri, N.; Pektas, S.; Maroney, M. J.; Knapp, M. J.; Inverse solvent isotope effects demonstrate slow aquo release from hypoxia inducible factor-prolyl hydroxylase (PHD2)[J]. *Biochemistry*, **2012**, 51(33): 6654-6666.
- [165] Generally the dissociation process is kinetically fast. Hangasky, J.; Saban, E.; Knapp, M. J.; Inverse solvent isotope effects arising from substrate triggering in the factor inhibiting hypoxia inducible factor[J]. *Biochemistry*, **2013**, 52(9): 1594-1602.
- [166] Liu, Z.; Sadler, P. J.; Organoiridium complexes: Anticancer agents and catalysts[J]. *Acc. Chem. Res.*, **2014**, 47(4): 1174-1185.
- [167] Poth, T.; Paulus, H.; Elias, H.; Dücker-Benfer, C.; Van Eldik, R.; Kinetics and mechanism of water substitution at half-sandwich iridium(III) aqua cations Cp*Ir(A–B)(H₂O)^{2+/+} in aqueous solution (Cp* = η⁵-pentamethylcyclopentadienyl anion; A–B = bidentate N,N or N,O ligand)[J]. *Eur. J. Inorg. Chem.*, **2001**, 5: 1361–1369.
- [168] ¹H NMR results show that in the presence of PPh₃, the coordinating H₂O on complex **2** would be replaced. Appendix, Scheme B.3.

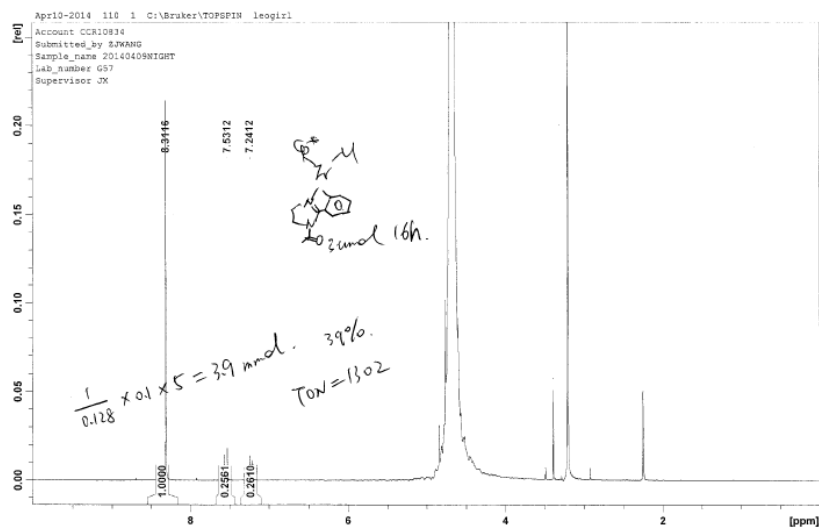
-
- [169] Okamura, M.; Yoshida, M.; Kuga, R.; Sakai, K.; Kondo, M.; Masaoka, S.; A mononuclear ruthenium complex showing multiple proton-coupled electron transfer toward multi-electron transfer reactions[J]. *Dalton Trans.*, **2012**, 41(42): 13081-13089.
- [170] Fieselmann, B. F.; Hendrickson, D. N.; Stucky, G. D.; Synthesis, electron paramagnetic resonance, and magnetic studies of binuclear bis(η^5 -cyclopentadienyl)titanium(III) compounds with bridging pyrazolate, biimidazolate, and bibenzimidazolate anions[J]. *Inorg. Chem.*, **1978**, 17 (8): 2078–2084.
- [171] Patel, M. N.; Dosi, P. A.; Bhatt, B. S.; Nucleic acid interaction and antibacterial behaviours of a ternary palladium(II) complexes[J]. *Spectrochim. Acta, Part A: Mol. Biomol. Spectrosc.*, **2012**, 86: 508-514.
- [172] Samanta, S.; Das, S.; Biswas, P.; Photocatalysis by 3,6-disubstituted-s-tetrazine: visible-light driven metal-free green synthesis of 2-substituted benzimidazole and benzothiazole[J]. *J. Org. Chem.*, 2013, 78: 11184–11193.
- [173] Stupka, G.; Gremaud, L.; Williams, A. F.; Control of redox potential by deprotonation of coordinated 1H-imidazole in complexes of 2-(1H-Imidazol-2-yl)pyridine[J]. *Helvetica Chimica Acta*, **2005**, 88(3): 487-495.
- [174] Fujioka, H.; Murai, K.; Ohba, Y.; Hiramatsu, A.; Kita, Y.; A mild and efficient one-pot synthesis of 2-dihydroimidazoles from aldehydes[J]. *Tetrahedron Lett.*, **2005**, 46(13): 2197-2199.
- [175] Shogo, T.; Hideo, T.; Direct oxidative conversion of aldehydes into 2-substituted 1,4,5,6-tetrahydropyrimidines using molecular iodine or 1,3-diiodo-5,5-dimethylhydantoin[J]. *Heterocycles*, **2010**, 82(1): 593-601.
- [176] Makowski, P.; Thomas, A.; Kuhn, P.; Goettmann, F.; Organic materials for hydrogen storage applications: from physisorption on organic solids to chemisorption in organic molecules[J]. *Energy Environ. Sci.*, **2009**, 2(5): 480-490.
- [177] Jiang, H.-L.; Singh, S. K.; Yan, J.-M.; Zhang, X.-B.; Xu, Q.; Liquid-phase chemical hydrogen storage: Catalytic hydrogen generation under ambient conditions[J]. *ChemSusChem*, **2010**, 3(5): 541-549.
- [178] Dalebrook, A. F.; Gan, W.; Grasemann, M.; Moret, S.; Laurency, G.; Hydrogen storage: Beyond conventional methods[J]. *Chem. Commun.*, **2013**, 49(78): 8735-8751.
- [179] Yadav, M.; Xu, Qiang.; Liquid-phase chemical hydrogen storage materials[J]. *Energy Environ. Sci.*, **2012**, 5(12): 9698-9725.
- [180] Mellone, I.; Peruzzini, M.; Rosi, L.; Mellmann, D.; Junge, H.; Beller, M.; Gonsalvi, L.;

-
- Formic acid dehydrogenation catalysed by ruthenium complexes bearing the tripodal ligands triphos and NP₃[J]. *Dalton Trans.*, **2013**, 42(7): 2495-2501.
- [181] Guerriero, A.; Bricout, H.; Sordakis, K.; Peruzzini, M.; Monflier, E.; Hapiot, F.; Laurency, G.; Gonsalvi, L.; Hydrogen production by selective dehydrogenation of HCOOH catalyzed by Ru-biaryl sulfonated phosphines in aqueous solution[J]. *ACS Catal.*, **2014**, 4(9): 3002-3012.
- [182] Rodríguez-Lugo, R. E.; Trincado, M.; Vogt, M.; Tewes, F.; Santiso-Quinones, G.; Grützmacher, H.; A homogeneous transition metal complex for clean hydrogen production from methanol-water mixtures[J]. *Nature Chemistry*, **2013**, 5(4): 342-347.
- [183] Boddien, A.; Loges, B.; Gärtner, F.; Torborg, C.; Fumino, K.; Junge, H.; Ludwig, R.; Beller, M.; Iron-catalyzed hydrogen production from formic acid[J]. *J. Am. Chem. Soc.*, **2010**, 132(26): 8924–8934.
- [184] Bertini, F.; Mellone, I.; Ienco, A.; Peruzzini, M.; Gonsalvi, L.; Iron(II) complexes of the linear *rac*-tetraphos-1 ligand as efficient homogeneous catalysts for sodium bicarbonate hydrogenation and formic acid dehydrogenation[J]. *ACS Catal.*, **2015**, 5(2): 1254-1265.
- [185] Wang, Z.; Lu, S.-M.; Li, J.; Wang, J.; Li, C.; Unprecedentedly high formic acid dehydrogenation activity on an iridium complex with an N,N'-diimine ligand in water[J]. *Chem. Eur. J.*, **2015**, 21(36): 12592-12595.
- [186] Keith, F.; Lautens, M.; Halide effects in transition metal catalysis[J]. *Angew. Chem. Int. Ed.*, **2002**, 41(1): 26-47.
- [187] Maitlis, P. M.; Haynes, A.; James, B. R.; Catellani, M.; Chiusoli, G. P.; Iodide effects in transition metal catalyzed reactions[J]. *Dalton Trans.*, **2004**, (21): 3409-3419.
- [188] Wu, J.; Wang, C.; Tang, W.; Pettman, A.; Xiao, J.; The remarkable effect of a simple ion: iodide-promoted transfer hydrogenation of heteroaromatics[J]. *Chem. Eur. J.*, **2012**, 18(31): 9525-9529.
- [189] Wu, J.; Tang, W.; Pettman, A.; Xiao, J.; Efficient and chemoselective reduction of pyridines to tetrahydropyridines and piperidines *via* rhodium-catalyzed transfer hydrogenation[J]. *Adv. Synth. Catal.*, **2013**, 355(1): 35-40.
- [190] Wei, Y.; Wu, J.; Xue, D.; Wang, C.; Liu, Z.; Zhang, Z.; Chen, G.; Xiao, J.; Highly efficient rhodium-catalyzed transfer hydrogenation of nitroarenes into amines and formamides[J]. *Synlett.*, **2014**, 25, 1295-1298.
- [191] The reactivity here is slightly lower compared with Scheme 5.1 because a different bottle of [RhCp*Cl₂]₂ was used.

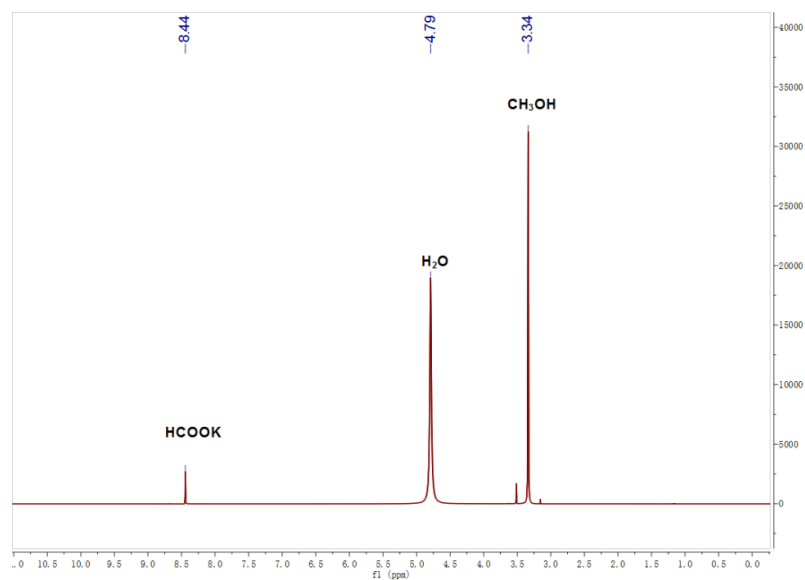
-
- [192] Fischer, C.; Kohrt, C.; Drexler, H.-J.; Baumann, W.; Heller, D.; Trinuclear rhodium hydride complexes[J]. *Dalton Trans.*, **2011**, 40(16): 4162-4166.
- [193] Blacker, A. J.; Duckett, S. B.; Grace, J.; Perutz, R. N.; Whitwood, A. C.; Reactivity, structures, and NMR spectroscopy of half-sandwich pentamethylcyclopentadienyl rhodium amido complexes relevant to transfer hydrogenation[J]. *Organometallics*, **2009**, 28: 1435-1446.
- [194] **d** is one of the most possible configurations based on $[\text{Rh}_2\text{Cp}^*_2\text{Cl}(\text{H})(\text{OCHO})]^+$.
- [195] **D** is one of the most possible configurations based on $[\text{Rh}_2\text{Cp}^*_2\text{IH}(\text{OCHO})]^+$.
- [196] **E** is one of the most possible configurations based on $[\text{Rh}_2\text{Cp}^*_2\text{HI}_2]^+$.
- [197] **C** is one of the most possible speculated configurations, but without direct support by experimental data.
- [198] The possibility of the protonation step being the RDS cannot be ruled out, however, as the equilibrium between the monomer and dimer could render the concentration of the monomeric Rh-H too low to be detected by the ^1H NMR.
- [199] In line with this view, we have recently shown that hydride formation is more energy costly than hydride transfer in a kinetic, NMR and DFT study of an iridium-catalyzed transfer hydrogenation of imines with formic acid: Chen, H.-Y. T.; Wang, C.; Wu, X.; Jiang, X.; Catlow, C. R. A.; Xiao, J.; Iridicyclic-catalysed imine reduction: An experimental and computational study of the mechanism[J]. *Chem. Eur. J.*, **2015**, 21(46), 16564–16577.
- [200] Although KBr and KCl also promote this reaction, their effect is much less significant than that of KI (Scheme 5.1), probably because the iodide is softer and a stronger nucleophile in protic solvents and hence is expected to bind to the iridium more easily.
- [201] Merrifield, J. H.; Gladysz, J. A.; Synthesis and decarboxylation mechanism of the chiral rhenium formate $(\eta\text{-C}_5\text{H}_5)\text{Re}(\text{NO})(\text{PPh}_3)(\text{OCHO})$ [J]. *Organometallics*, **1983**, 2 (6): 782–784.
- [202] Nova, A.; Taylor, D. J.; Blacker, A. J.; Duckett, S. B.; Perutz, R. N.; Eisenstein, O.; Computational studies explain the importance of two different substituents on the chelating bis(amido) ligand for transfer hydrogenation by bifunctional $\text{Cp}^*\text{Rh}(\text{III})$ catalysts[J]. *Organometallics*, **2014**, 33(13): 3433-3442.
- [203] Jones, W. D.; Feher, F. J.; Preparation and conformational dynamics of $(\text{C}_5\text{Me}_5)\text{Rh}(\text{PR}'_3)\text{RX}$. Hindered rotation about rhodium-phosphorus and rhodium-carbon bonds[J]. *Inorg. Chem.*, **1984**, 23(16): 2376-2388.

Appendixes

Appendix A

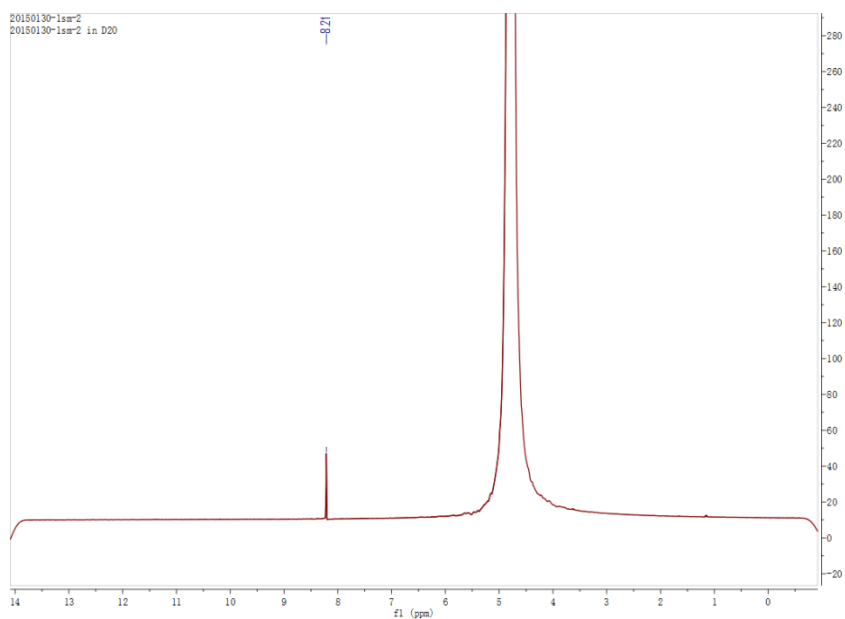


Scheme A.1 Detection of HCOOK and the determination of product amount with ^1H NMR. Reaction conditions: complex **3** ($3.0 \mu\text{mol}$), 1.0 M KOH MeOH solution (10.0 mL), $4.5 \text{ MPa CO}_2/\text{H}_2$ ($1:2$), $80 \text{ }^\circ\text{C}$, 16 h .



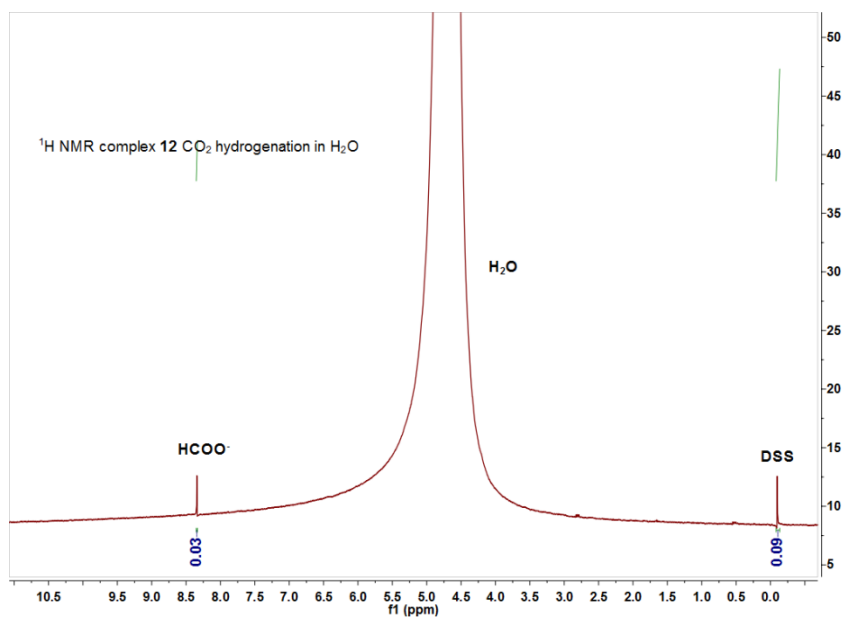
Scheme A.2 ^1H NMR spectrum ($400 \text{ MHz, D}_2\text{O}$) of reaction mixture Reaction conditions: complex **8** ($0.2 \mu\text{mol}$), $1.0 \text{ M KOH/MeOH/H}_2\text{O}$ ($1:1$) solution (10.0 mL), $5.0 \text{ MPa CO}_2/\text{H}_2$ ($1:1$), $40 \text{ }^\circ\text{C}$, 1 h .

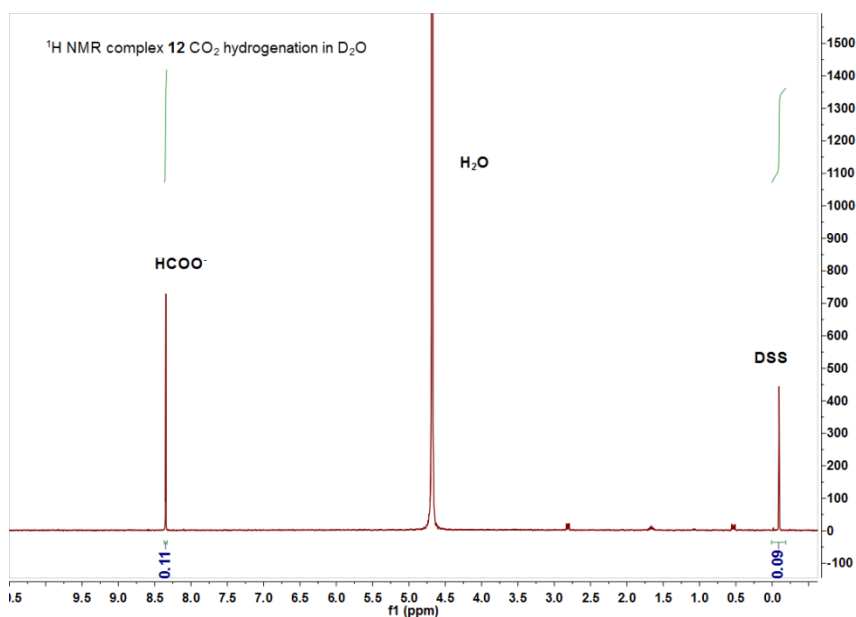
Appendix B



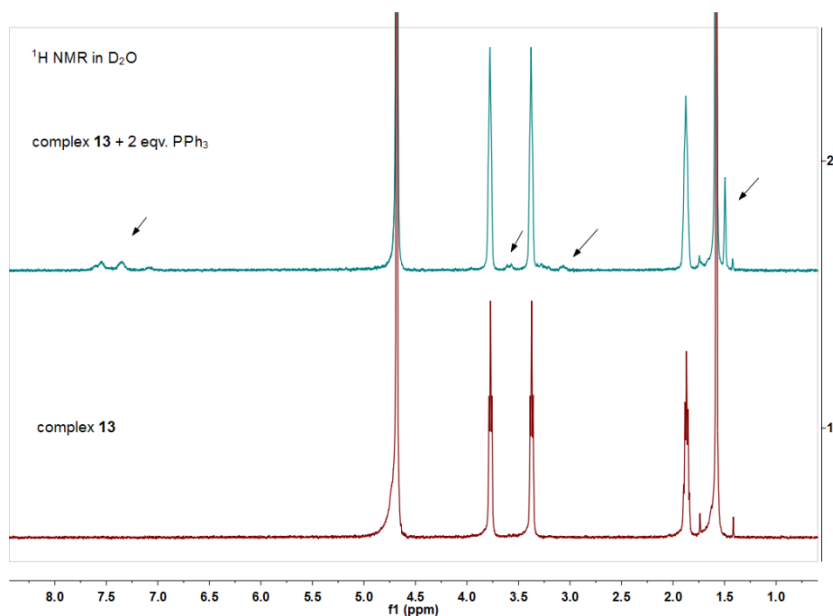
Scheme B.1 CO₂ hydrogenation product detection with ¹H NMR

Reaction conditions: complex **12** (0.25 μmol), H₂O (10.0 mL), CO₂/H₂ = 1/1 (5.0 MPa), 40 °C, 30 min.

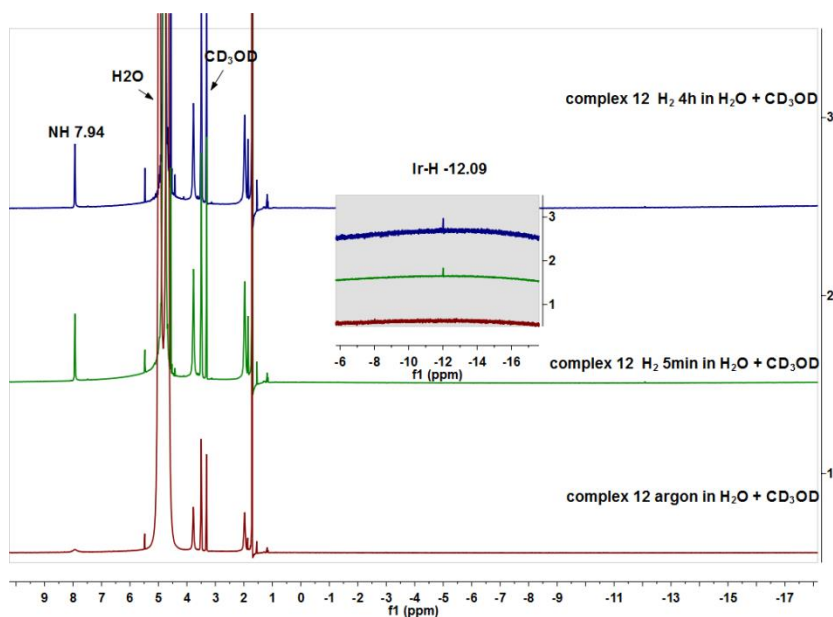




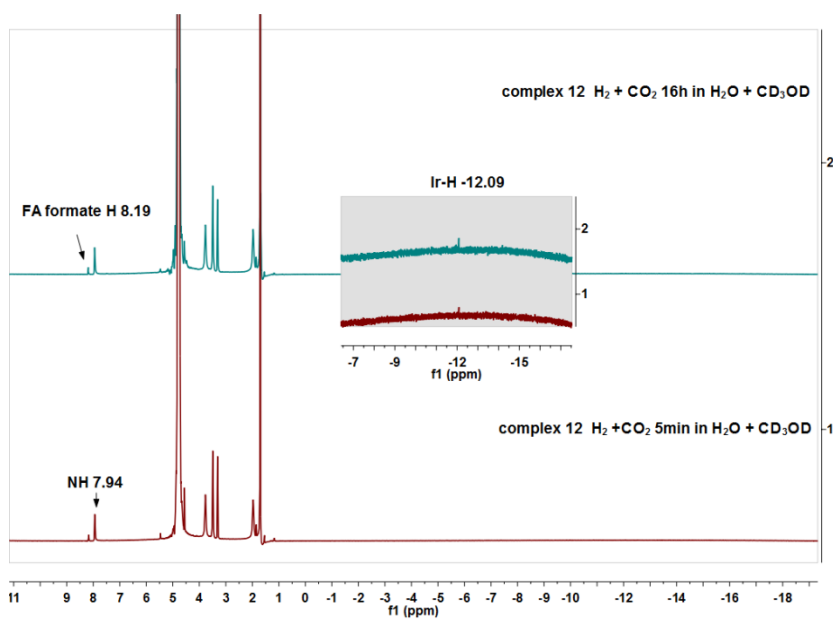
Scheme B.2 Product detection of CO₂ hydrogenation (H₂) performed in H₂O (a) and D₂O (b). Reaction conditions: complex **12** (0.25 μmol), 0.01 mmol of DSS (internal standard), H₂O or D₂O (10.0 mL), CO₂/H₂ = 1/1 (2.0 MPa); at 40 °C, 30 min. After reaction was cooled down in ice water, the autoclave was unsealed and 0.2 mmol of Na₂CO₃ was added into the solution. 0.5 mL of the product solution was taken out and submitted to the NMR machine.



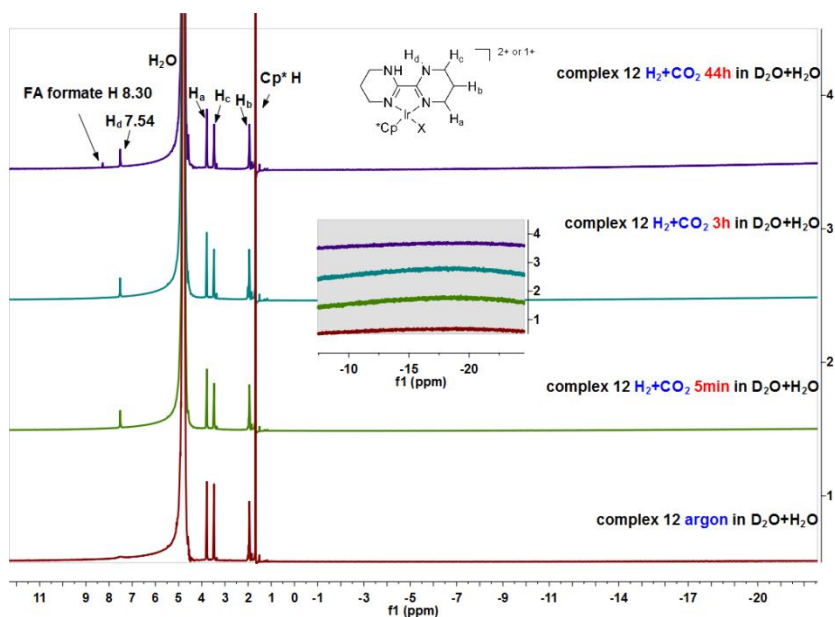
Scheme B.3 ¹H NMR spectra of complex **13** in the presence of PPh₃: the generation of new species indicates that the coordination of PPh₃ occurred.



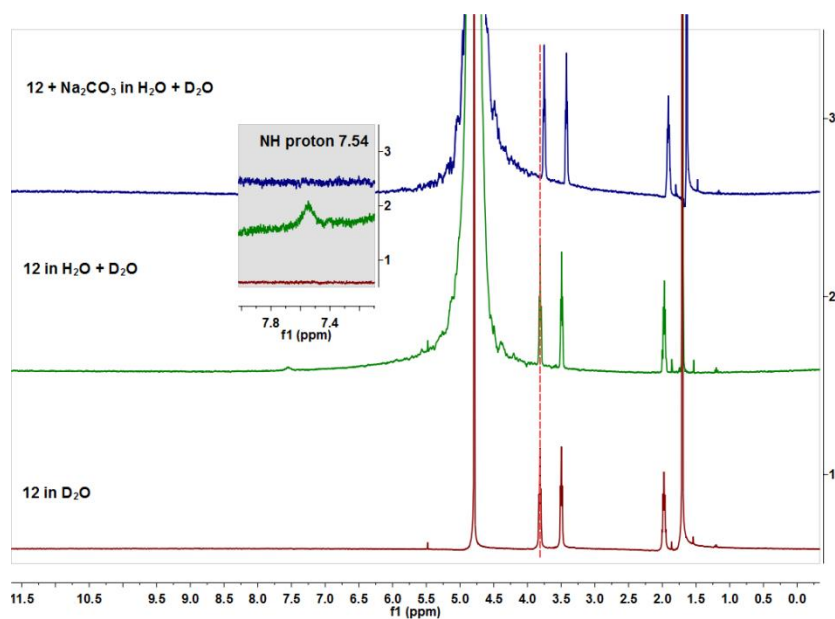
Scheme B.4 Reaction of complex **12** with H₂ (1.5 MPa) in CD₃OD/H₂O (0.1 mL CD₃OD + 0.03 mL H₂O) was tracked in Wilmad thick-wall NMR tube: Ir-H signal at $\delta = -12.09$ ppm appeared within 5 min.



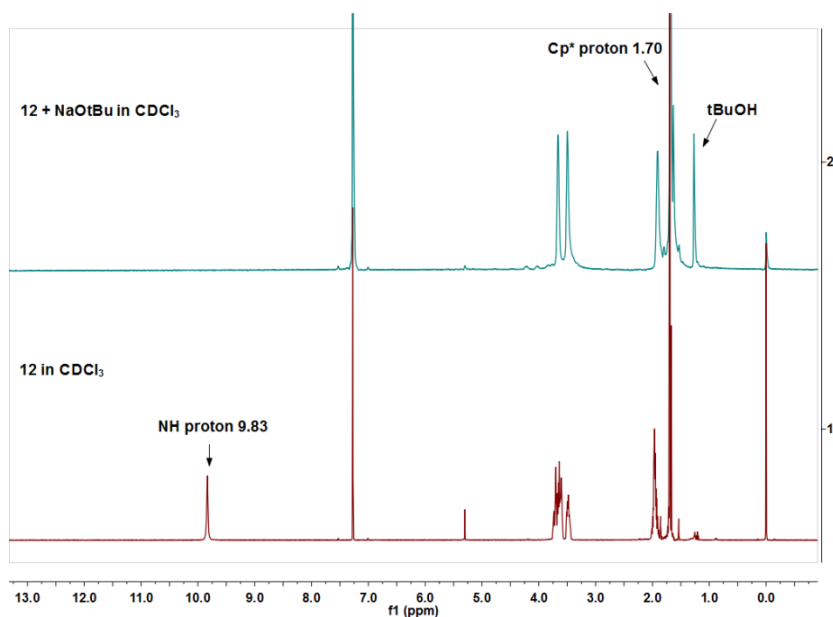
Scheme B.5 Reaction of complex **12** with H₂/CO₂ (1:1, total 1.2 MPa) in CD₃OD/H₂O (0.1 mL + 0.03 mL) was tracked: Ir-H signal at $\delta = -12.09$ ppm and H-COOH signal at $\delta = 8.19$ ppm appeared within 5 min.



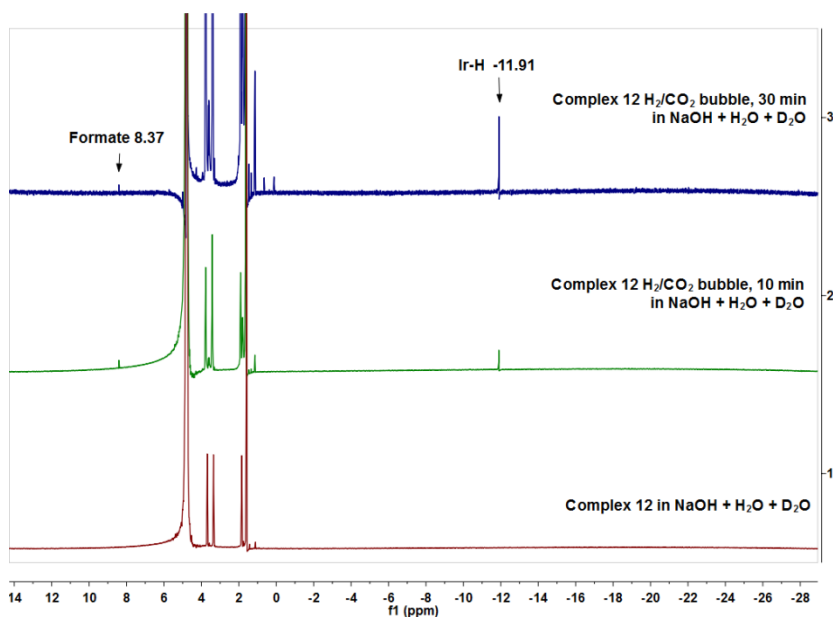
Scheme B.6 Reaction of complex **12** with H_2/CO_2 (1:1, total 1.2 MPa) in $\text{D}_2\text{O}/\text{H}_2\text{O}$ (0.05 mL + 0.15 mL) was tracked in Wilmad thick-wall NMR tube



Scheme B.7 Detection of NH protons on complex **12** and the disappearance of NH protons with the addition of base in water by ^1H NMR at room temperature: $\text{H}_2\text{O}/\text{D}_2\text{O}$ (0.2 mL + 0.3 mL); Na_2CO_3 (1.1 eqv.)



Scheme B.8 Detection of NH protons on complex **12** and the disappearance of NH protons with the addition of base in CDCl₃ by ¹H NMR at room temperature: NaO^tBu (2.2 eqv.).



Scheme B.9 Detection of Ir-H and HCOO⁻ with complex **12** under H₂/CO₂ bubbling in the presence of base at room temperature: 10.0 μmol of complex **12**, 20.0 mg NaOH, 0.4 mL D₂O + 0.1 mL H₂O.

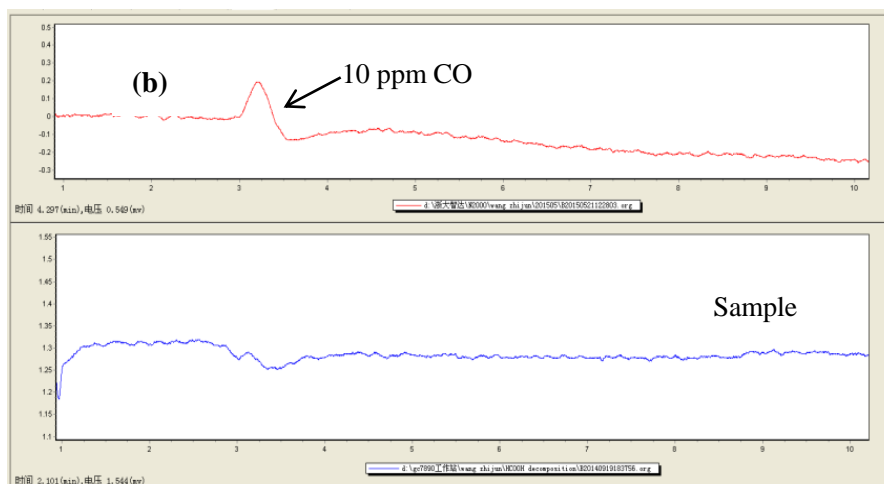
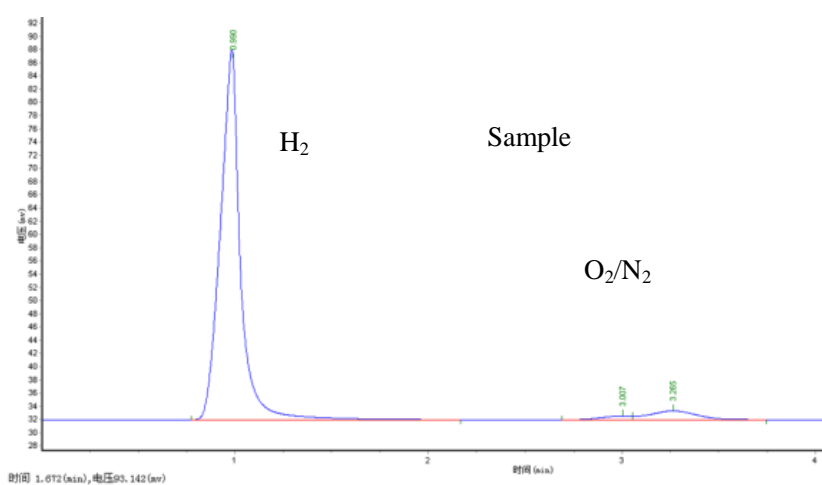
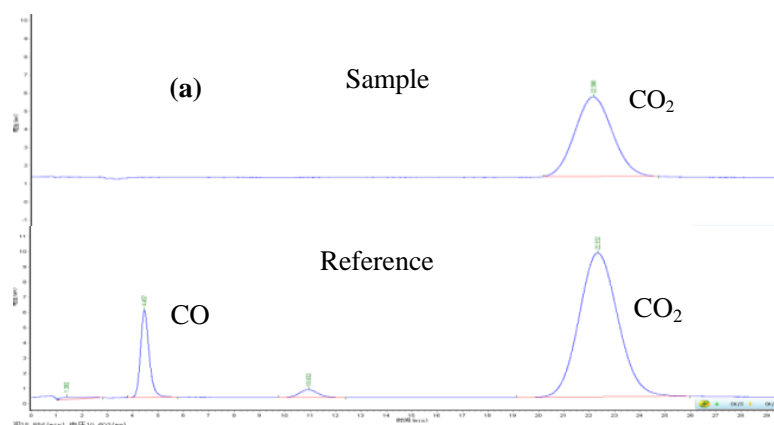
Appendix C

Table C.1 Dehydrogenation of FA in water with *in situ* formed catalyst from [IrCp*Cl₂]₂ and N₃N³ ligands^a

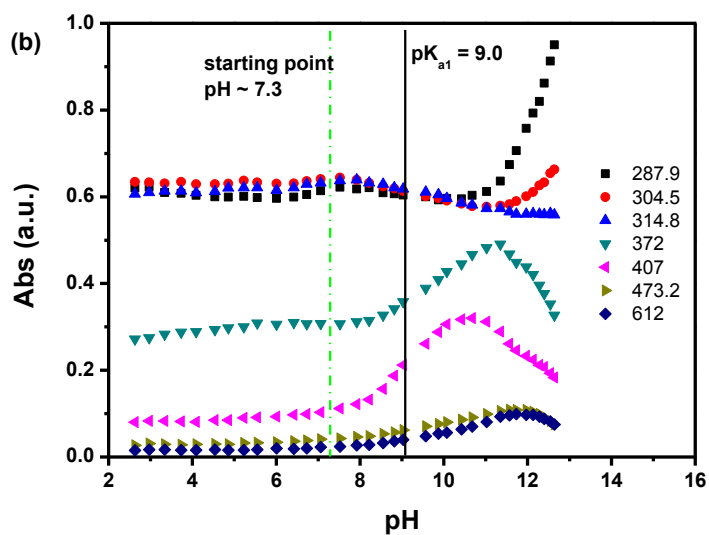
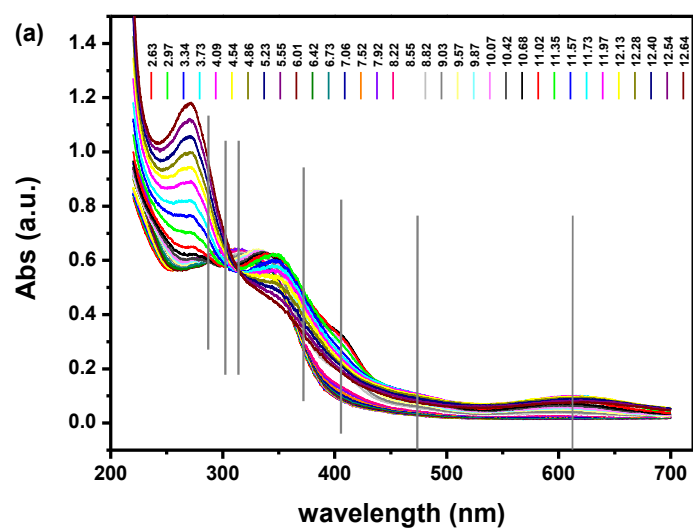
$$\text{HCO}_2\text{H} \xrightarrow[\text{H}_2\text{O}]{\text{Cat.}} \text{H}_2 + \text{CO}_2$$

Entry	Ligand	TOF _{initial} (h ⁻¹) ^b	H ₂ (mL) ^c	TON ^d
1	L13^e	0	4	167
2	L15	12188	82.5	3438
3	L16^e	0	1	42
4	L17	43750	204	8500
5	L18	31250	178	7438
6	L19	0	3.5	146

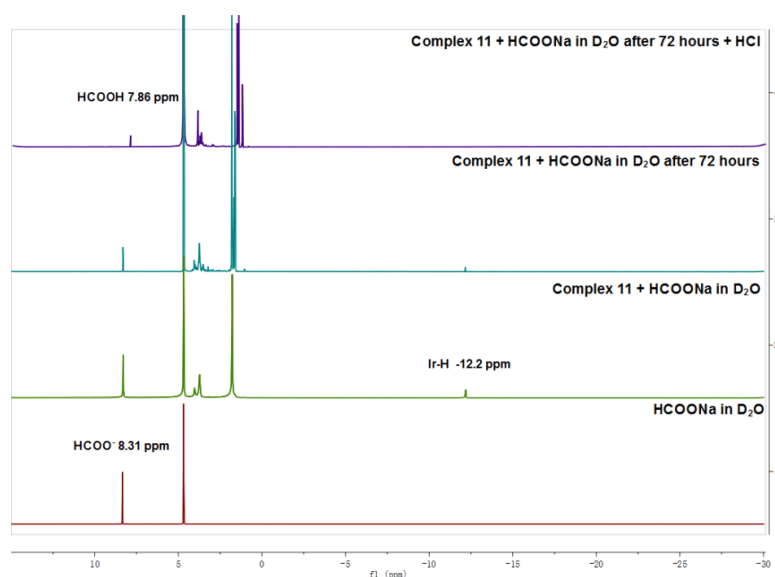
^a: [IrCp*Cl₂]₂ (0.5 μmol), **L** (5.0 μmol), HCO₂H (1.0 M, 10.0 mL), 60 °C; ^b: TOF was calculated in the first 2 minutes; ^c: Volume of H₂ evolved was recorded at 20 minutes; ^d: TON was calculated based on the H₂ amount; ^e: Good-quality complex may not be formed due to the insolubility of ligands in water.



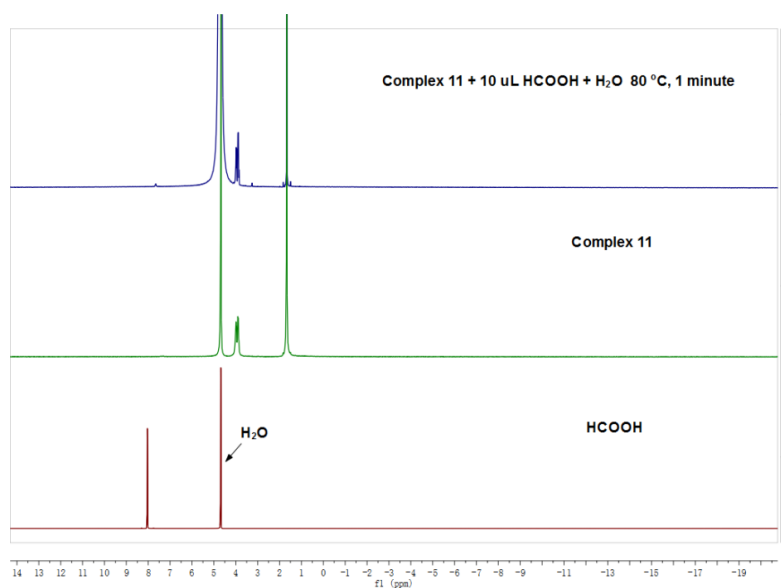
Scheme C.1 (a) Composition analysis of the evolved gas mixture by GC: 1.0 μmol of complex, FA (1.0 M, 10.0 mL), 60 $^{\circ}\text{C}$. (b) Detection limit for CO by GC



Scheme C.2 (a) The UV-Vis absorption spectra of complex **11** measured at pH varied from 2 to 13; (b) Absorbance at 287.9 nm, 304.5 nm, 314.8 nm, 372 nm, 407 nm, 473.2 nm and 612 nm as a function of pH.

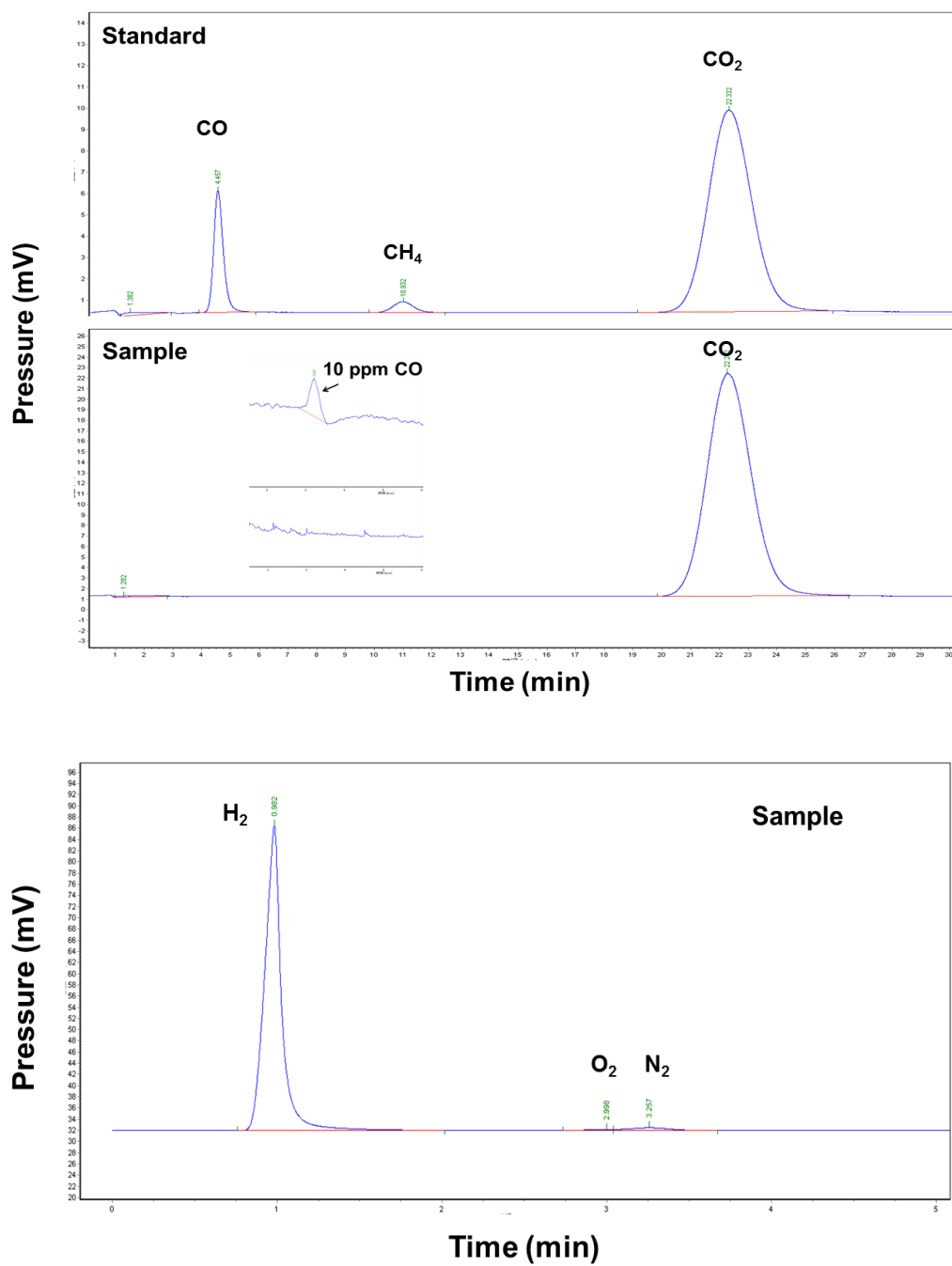


Scheme C.3 ¹H-NMR spectra of (a) HCO₂Na in D₂O (red line, bottom); (b) complex **11** was added to HCO₂Na in D₂O (green line); (c) complex **11** and HCO₂Na in D₂O after 72 h (blue line); (d) Hydrogen chloride acid (HCl) was added to the mixture of complex **11** and HCO₂Na in D₂O after 72 h (purple line, upper).



Scheme C.4 ¹H-NMR spectra of HCO₂H in D₂O (red line, bottom), complex **11** in D₂O before (green line, middle) and after (blue line, upper) reaction with HCO₂H. NMR test procedure: First, 4.0 mg of complex **11**, 0.2 mL H₂O and 1.0 mL D₂O were mixed together in an NMR tube to obtain the green line in Figure C.4. Subsequently, 10.0 μL HCO₂H was added, and the reaction was held at 80 °C for approximate 1 min until the bubbling stopped. The NMR tube was quickly sealed and submitted to obtain the blue line.

Appendix D

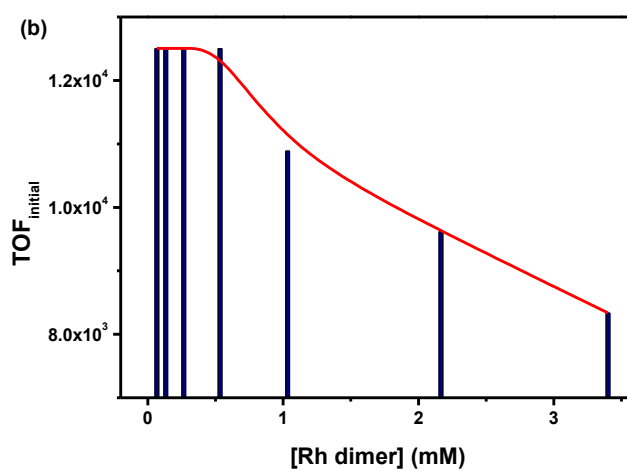
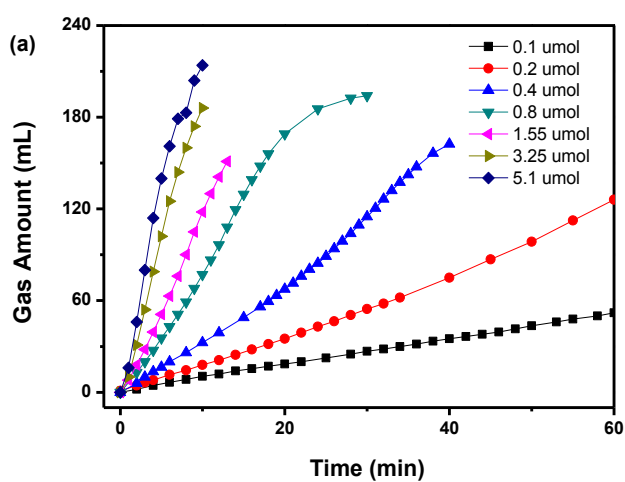


Scheme D.1 Composition analysis of the evolved gas mixture by GC using TCD and FID detector and the detection limit for CO

Table D.1 FA dehydrogenation using different catalyst precursors in combination with KI^a

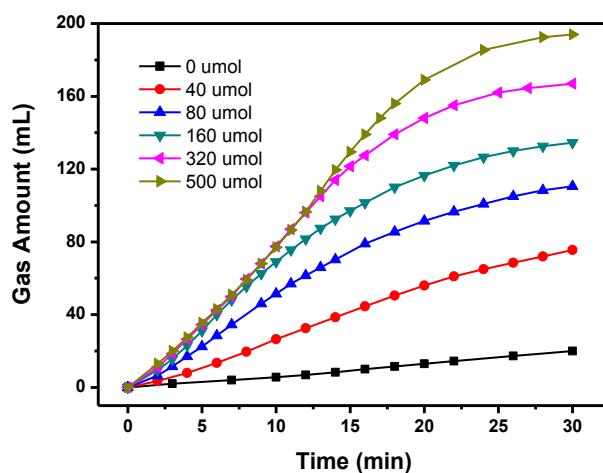
$\text{HCOOH} \xrightarrow[\text{TEA, 60}^\circ\text{C}]{\text{precatalyst, KI}} \text{H}_2 + \text{CO}_2$					
Entry	Precatalyst	TOF _{max} ^b /h ⁻¹	Volume of H ₂ ^c /mL	TON ^c	Con. (%)
1	[RhCp*Cl ₂] ₂	4375	144	600	37.5
2	[RuCl ₂ (p-cymene)] ₂	1500	50	208	13.0
3 ^d	[RuCl ₂ (p-cymene)] ₂	250	14	58	3.6
4	RhCl ₃ ·xH ₂ O	188	12	50	3.1
5	Rh(NBD) ₂ BF ₄	25	2	8	0.5
6 ^e	[Rh(COD) ₂]BF ₄	42	2	8	0.5
7 ^f	[IrCp*Cl ₂] ₂	125	7	29	1.8
8	[Rh(COD)Cl] ₂	25	1.5	6	0.4
9	[Rh(OAc) ₂] ₂	0	0	0	0

^a: Reaction conditions: 10.0 μmol of Rh or Ir (monomer), 1.0 mmol of KI, 1.5 mL of FT azeotrope, at 60 °C; ^b: Turnover frequencies were determined at the fastest reaction time interval, usually from 6 min to 10 min after reaction had started; ^c: Hydrogen volume was measured after 20 min, and TON was calculated in the same time zone; ^d: Reaction without KI; ^e: TON was measured after 30 min; ^f: TON was measured after 25 min.

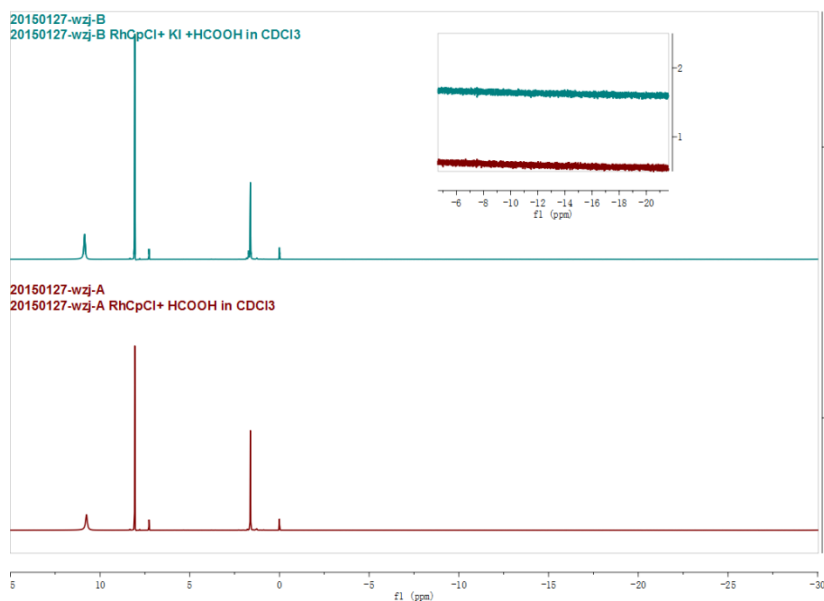


Scheme D.2 (a) Time course of gas evolution during the dehydrogenation of FA with different catalyst amount; (b) Initial TOFs at different catalyst concentrations.

Reaction conditions: 0.1 ~ 5.0 μmol of $[\text{RhCp}^*\text{Cl}_2]_2$, 500 μmol of KI, 1.5 mL of FT azeotrope, at 60 $^\circ\text{C}$.



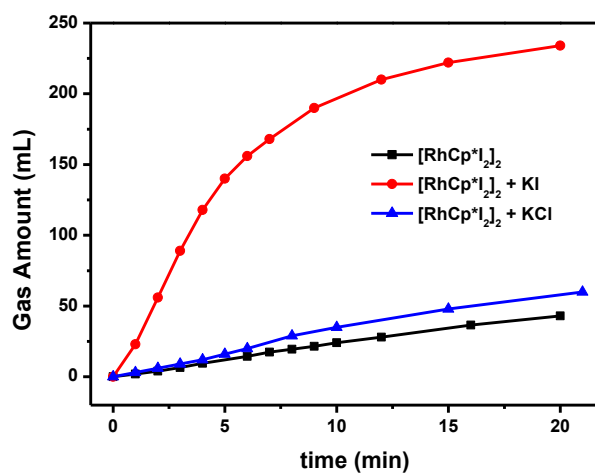
Scheme D.3 Time course of gas evolution during the dehydrogenation of FA with different KI amount: 0.8 μmol of $[\text{RhCp}^*\text{Cl}_2]_2$, 0 ~ 500 μmol of KI, 1.5 mL of FT azeotrope, at 60 $^\circ\text{C}$.



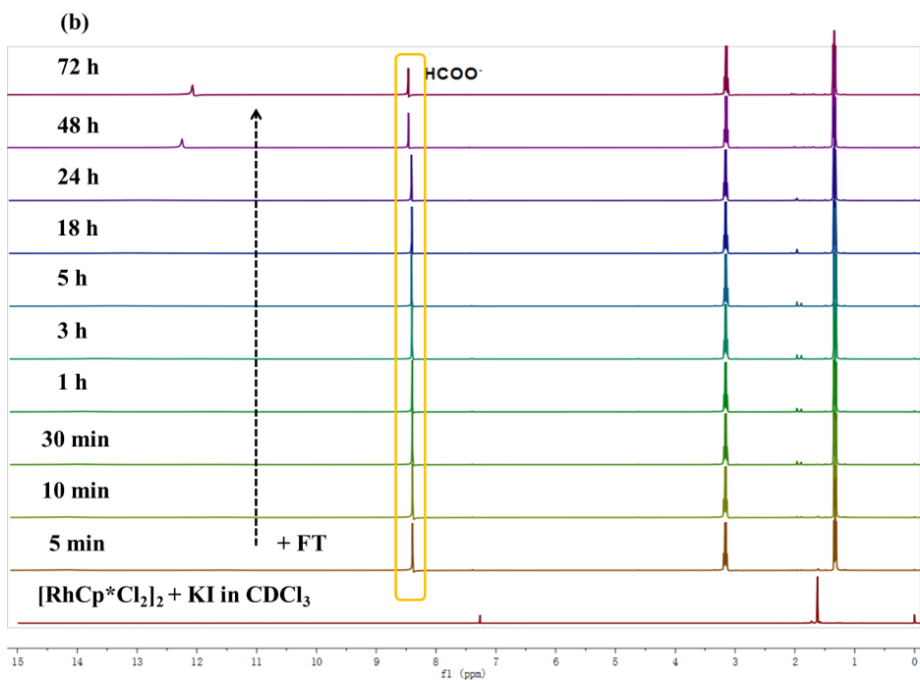
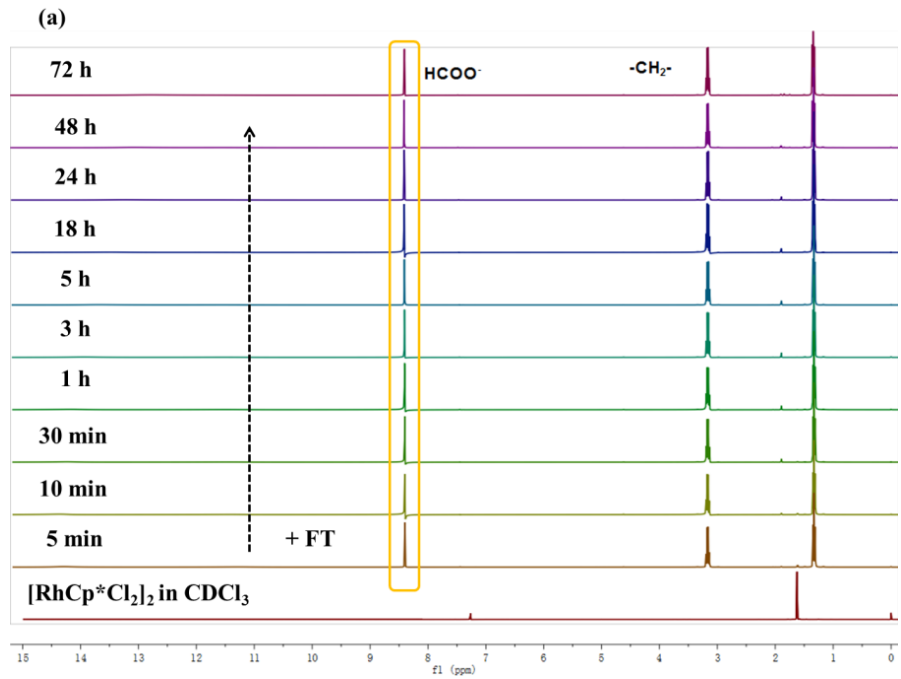
Scheme D.4 ^1H NMR spectra of FA dehydrogenation in neat FA with (upper blue line) and without KI (lower red line): 5.0 μmol of $[\text{RhCp}^*\text{Cl}_2]_2$, 250 μmol of KI, 0.1 mL of FA, 1.0 mL of CDCl_3 , at room temperature. No Rh-H hydride signal was observed in neat FA.

Table D.2 pKa values of the amines applied for FA dehydrogenation

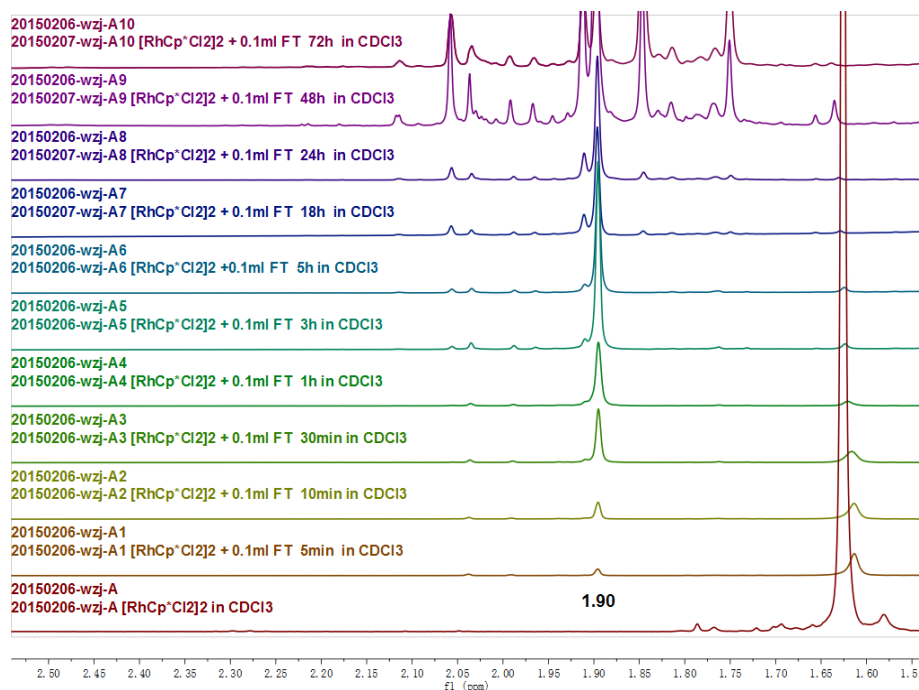
Amine	pKa	
triethylamine	10.65	3°
1-methylpiperidine	10.08	
piperidine	11.22	2°
dibutylamine	11.25	
octylamine	10.65	1°
cyclohexanamine	10.64	



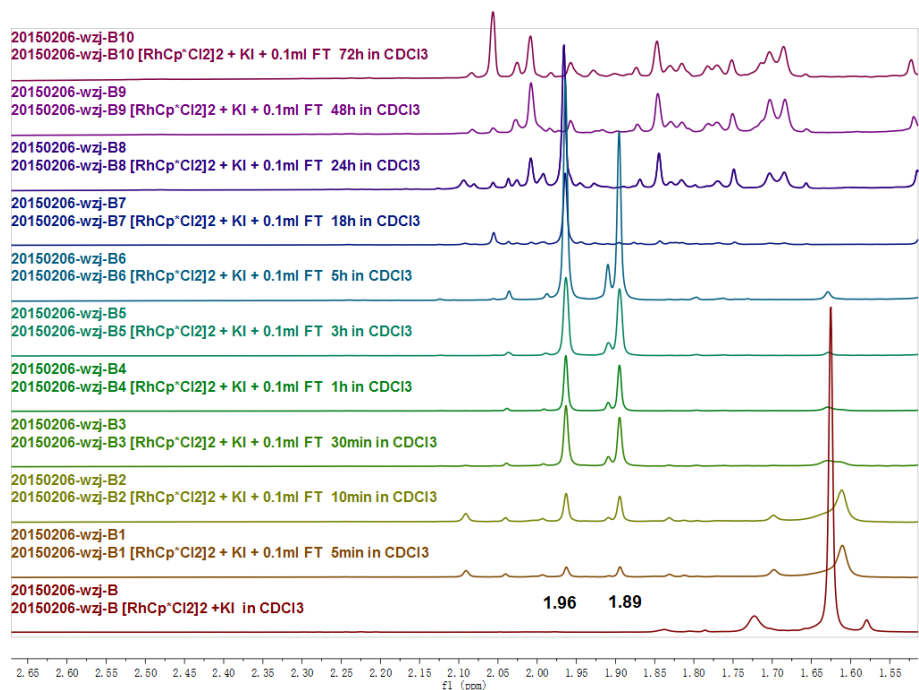
Scheme D.5 FA dehydrogenation using [RhCp*I₂]₂: 5.0 μmol of [RhCp*I₂]₂, 1 mmol of KI or KCl, 1.5 mL of FT azeotrope, at 60 °C

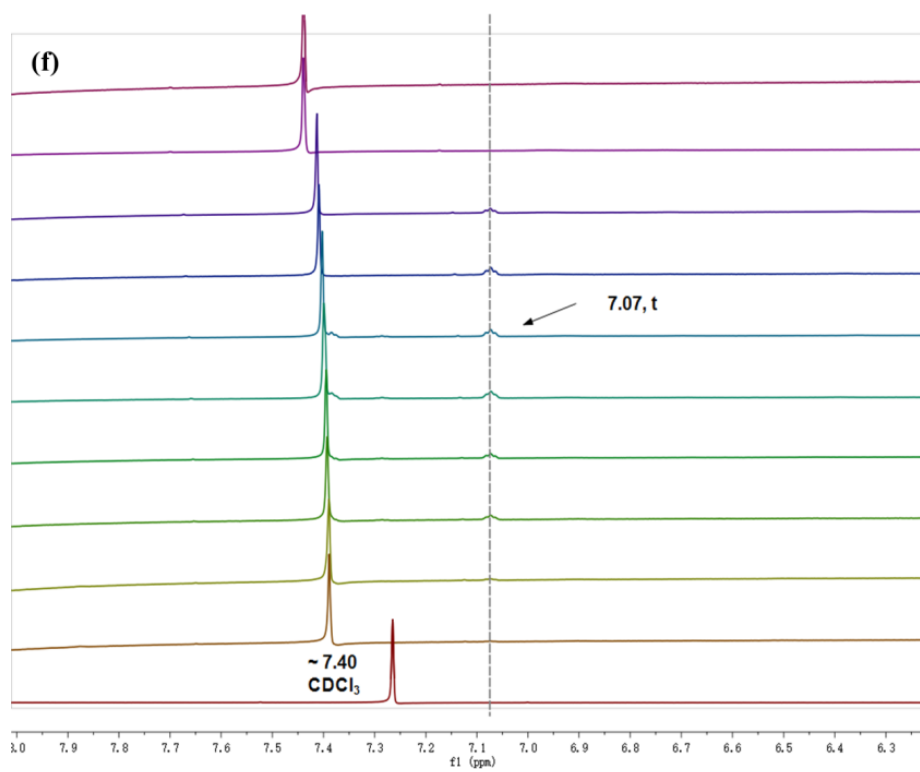
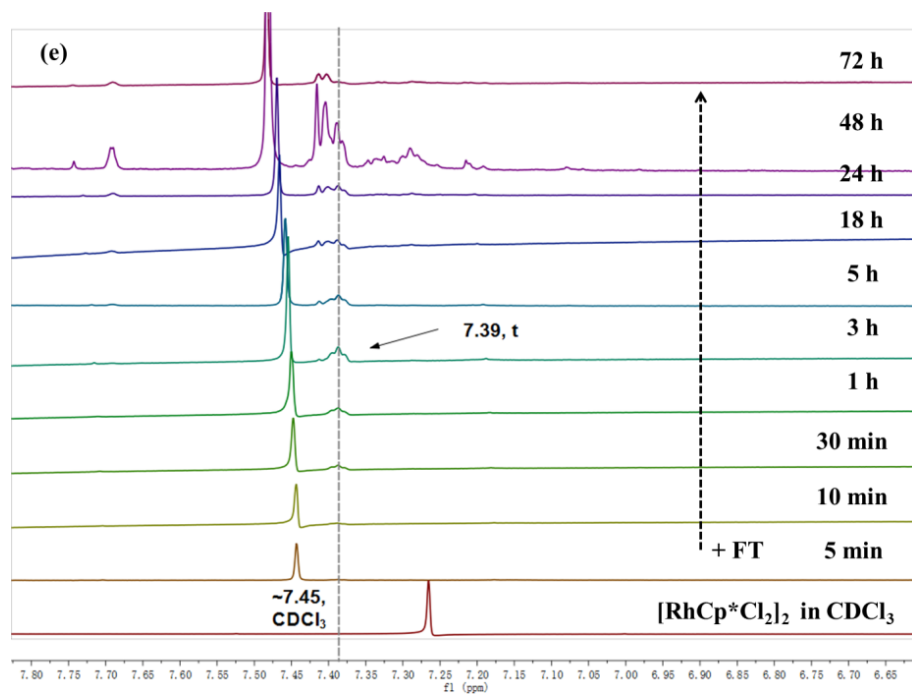


(c)

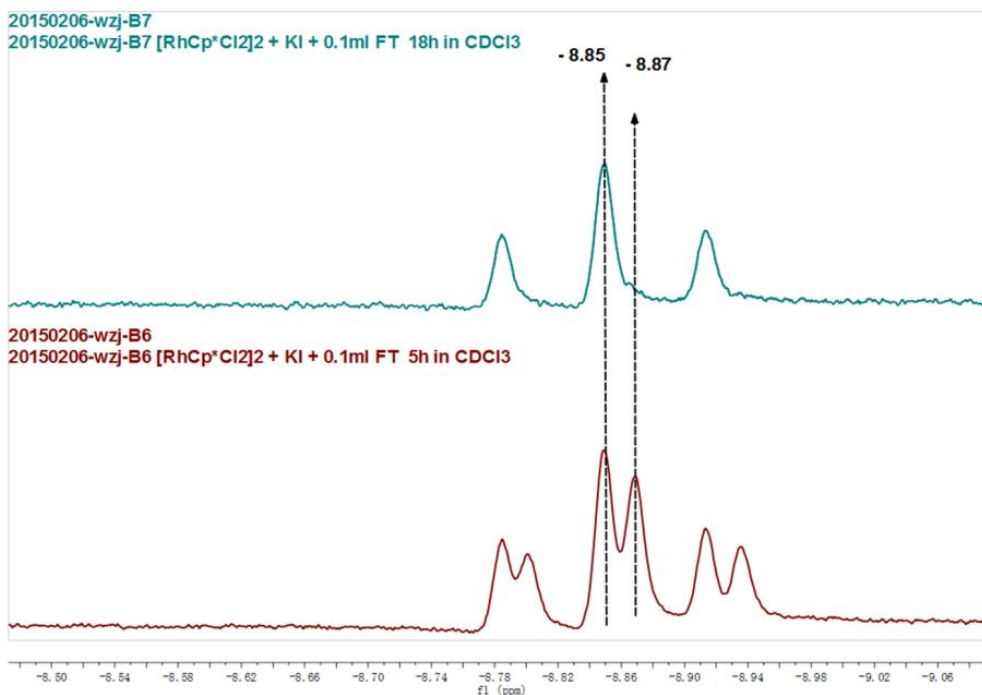


(d)

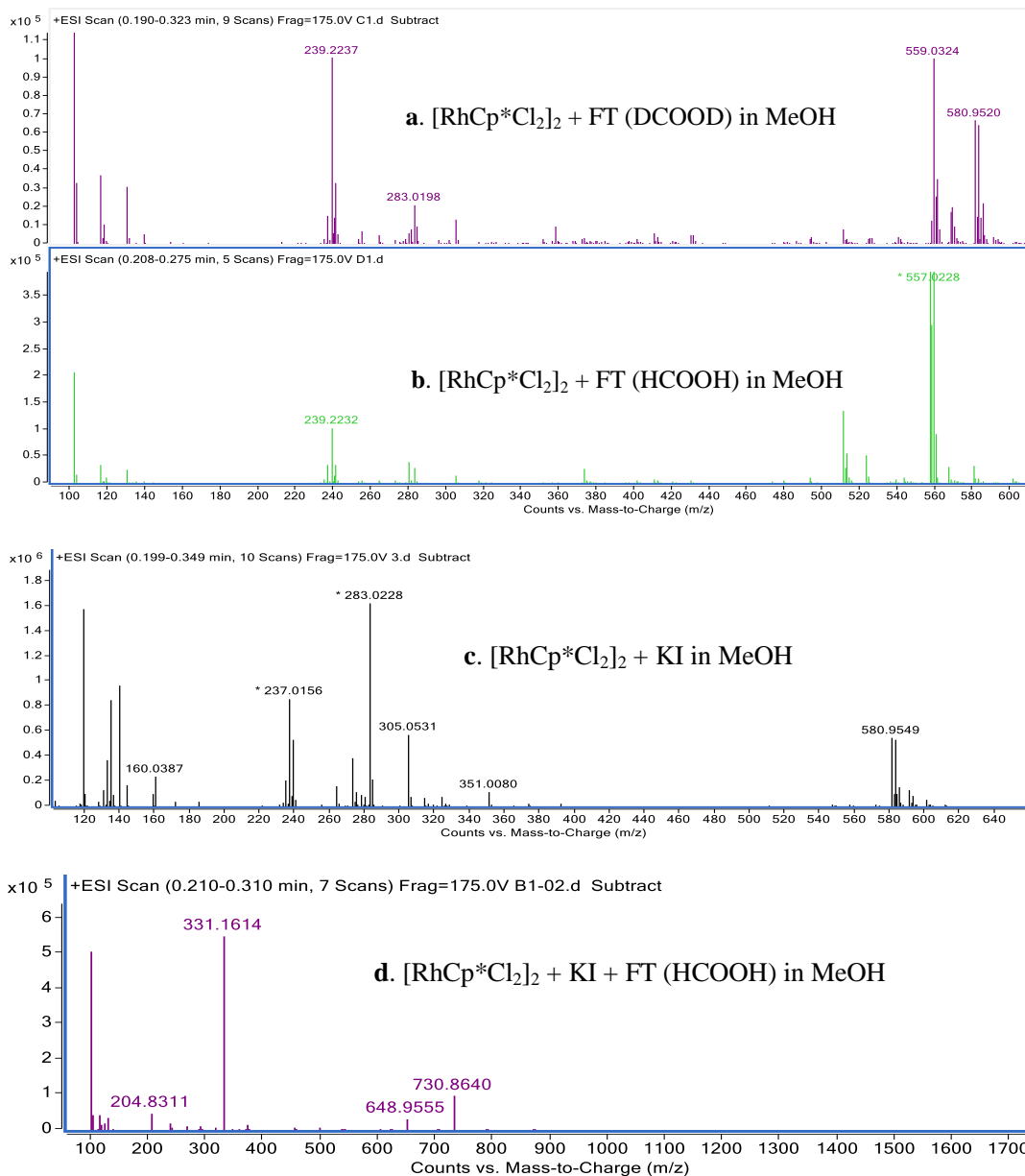




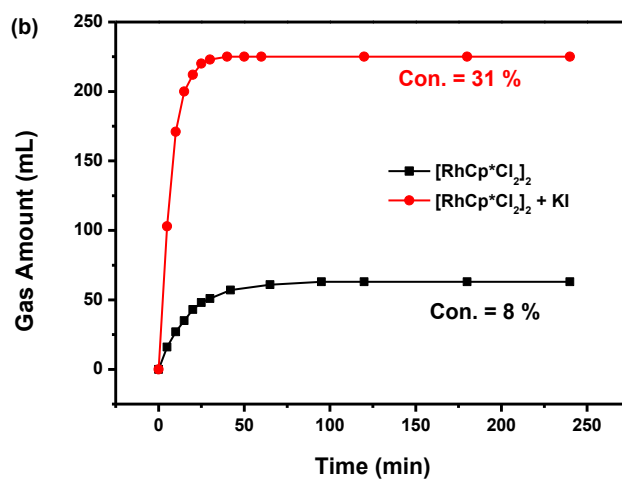
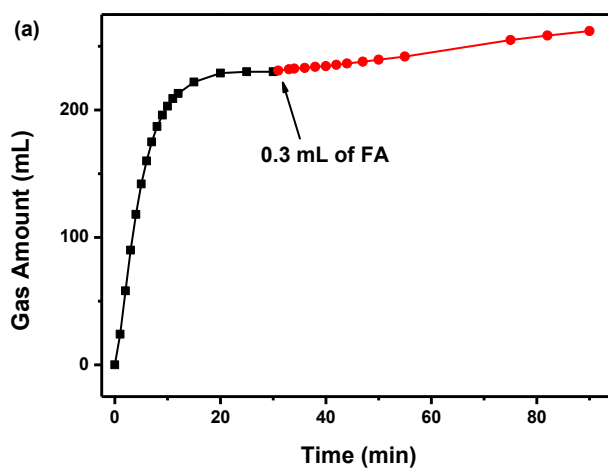
(g)



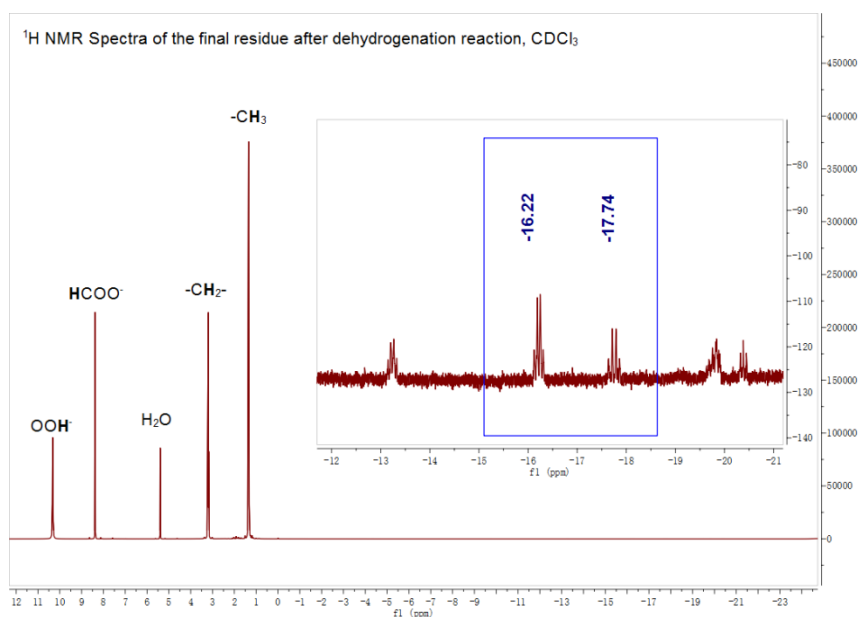
Scheme D.6 ¹H NMR spectra of FA dehydrogenation with and without KI: 5.0 μmol of [RhCp*Cl₂]₂, 250 μmol of KI, 0.1 mL of FT azeotrope, 1.0 mL of CDCl₃, room temperature. (a) FA formate proton signal without KI: Con. 18% using TEA as internal standard; (b) FA formate proton signal in presence of KI: Con. 54% using TEA as internal standard; (c) Cp* proton signal in the absence of KI; (d) Cp* proton signal in the presence of KI; (e) Bridging formate ligand proton signal of **d**; (f) Bridging formate ligand proton signal of **D**; (g) enlargement of Figure 5.8b. The time scale is the same for (a)-(f).



Scheme D.7 (a) & (b): Mass spectra of 1.6 μmol of $[\text{RhCp}^*\text{Cl}_2]_2$ reacting with 0.2 mL of FT azeotrope (DCOOD vs. HCOOH) in 1.0 mL of methanol at room temperature; (c): Mass spectrum of 1.6 μmol of $[\text{RhCp}^*\text{Cl}_2]_2$ mixed with 120 μmol of KI in 1.0 mL of methanol; (d): Mass spectrum of 1.6 μmol of $[\text{RhCp}^*\text{Cl}_2]_2$ reacting with 0.2 mL of FT azeotrope in presence of 120 μmol of KI in 1.0 mL of methanol. All these spectra were obtained at room temperature.



Scheme D.8 (a) FA dehydrogenation with the addition of FA at the end of a reaction: 5.0 μmol of $[\text{RhCp}^*\text{Cl}_2]_2$, 1.0 mmol of KI, 1.5 mL of FT azeotrope, at 60 $^\circ\text{C}$. The amount of added FA was roughly based on the evolved gas amount. (b) FA dehydrogenation at prolonged reaction time using $[\text{RhCp}^*\text{Cl}_2]_2$ in the presence and absence of KI under the same reaction conditions.



Scheme D.9 ¹H NMR spectra of the reaction residue after dehydrogenation.

Conditions and procedure: 16.2 μmol of [RhCp*Cl₂]₂, 3.0 mmol of KI, 5.0 mL of FT azeotrope, at 60 °C, 24 h. After the reaction cooled down, 2 mL of water was added and the organic layer was extracted with 2 mL of dichloromethane. After evaporating the solvent, the residue was submitted to NMR analysis in CDCl₃. Comparing the NMR spectra with Figure 5b suggesting that the new rhodium hydride species at -16.22 ppm (q) and -17.74 ppm (q) could possibly be deactivated species.

A list of publications arising from the thesis:

1. Shengmei Lu, **Zhijun Wang**, Jun Li, Jianliang Xiao, Can Li.* Base-free hydrogenation of CO₂ to formic acid in water with an iridium complex bearing a *N,N'*-diimine ligand. *Green Chem.*, **2016**, *18*, 4553-4558. (Chapter 3)
2. **Zhijun Wang**, Sheng-Mei Lu, Jun Li, Jijie Wang, Can Li.* Unprecedentedly high formic acid dehydrogenation activity on an iridium complex with an *N,N'*-diimine ligand in water. *Chem. Eur. J.*, **2015**, *21*, 12592-12595. (Chapter 4)
3. **Zhijun Wang**, Sheng-Mei Lu, Jianjun Wu, Can Li,* Jianliang Xiao.* Iodide-promoted dehydrogenation of formic acid on a rhodium complex. *Eur. J. Inorg. Chem.*, **2016**, *4*, 490-496. (Chapter 5)